Alma Mater Studiorum - Università di Bologna
Dipartimento di Elettronica, Informatica e Sistemistica

Dottorato di Ricerca in Ingegneria Elettronica, Informatica
e delle Telecomunicazioni - XXI Ciclo

Settore scientifico-disciplinare:
ING-INF/03 - Telecomunicazioni

Adaptive wireless multimedia communication systems

Tesi di:
Ing. Laura Toni

Coordinatore:
Chiar.mo Prof. Ing. Paola Mello

Relatore:
Chiar.mo Prof. Ing. Oreste Andrisano

Co-relatore:
Prof. Ing. Andrea Conti

Esame Finale Anno 2009

Chi non sa sedersi sulla soglia dell'attimo,
dimenticando tutto il passato,
chi non sa stare ritto su un punto senza vertigini
e paura come una dea della vittoria,
non saprà mai che cos'è la felicità e ancor peggio,
non farà mai qualcosa che renda felici gli altri.
- F. Nietzsche

Contents

Abstract **1**

1 Introduction **3**
1.1 Introduction 4
1.2 Outline of the work 5
1.3 System modeling 7
1.3.1 Wireless channel modeling 7
1.3.2 SIMO system - spatial diversity 10
1.3.3 Multicarrier systems - OFDM 13

2 Channel coding for progressive images **17**
2.1 Motivation and outline of the work 18
2.2 Progressive image and multiple description 20
2.3 Channel model and time-frequency channel coding 24
2.4 ICI and channel estimation errors 28
2.5 Problem formulation 31
2.6 Results and discussion 33
2.7 Conclusion 49

3 JSCC for MC-FGS Video **53**
3.1 Motivation and outline of the work 54
3.2 Motion-compensated FGS with leaky prediction 57
3.3 System model overview 60
3.3.1 Channel model 60
3.3.2 Time-frequency MD coding 60
3.4 Problem formulation 62
3.4.1 Drift management 62

3.4.2 Motion-compensated FEC-MD coding construction 64
3.4.3 Rate-Distortion curve 68
3.5 Results and discussion 72
3.6 Conclusion 84

4 Adaptive modulation techniques 85
4.1 Motivation and outline of the work 86
4.2 System model 88
4.2.1 Adaptive modulation 88
4.2.2 Channel estimation 91
4.3 Imperfect CSI at the transmitter 92
4.3.1 Mean throughput 94
4.3.2 Outage probability 96
4.4 Imperfect CSI at the receiver 97
4.4.1 Bit error probability 98
4.4.2 Mean throughput 99
4.5 Numerical results 101
4.5.1 Imperfect CSI at the transmitter 101
4.5.2 Imperfect CSI at the receiver 105
4.6 Conclusion 112

5 Adaptive modulation in the presence of... 113
5.1 Motivation and outline of the work 114
5.2 System model 115
5.3 Imperfect thresholds 117
5.4 Approximated BEP expressions 118
5.5 Co-channel interference 120
5.6 Numerical results 125
5.7 Conclusion 132

6 Conclusion 135

A Packet loss rate 137

B Canonical expression 141

C Approximation on BEP expressions **145**
C.1 Instantaneous BEP 145
C.2 Mean BEP 146

D Co Channel Interference **151**

Bibliography **156**

Thanks **169**

List of Figures

1.1 Simplified scheme of heterogenous scenarios. The same encoded bitstream is transmitted to different users, each of whose receives the image at its achievable data rate. . . 5

1.2 Combiner schemes at the receiver. a) A generic scheme, b) descriptions of a hybrid-selection/maximum ratio combiner. 12

1.3 OFDM implementation scheme at the transmitter and at the receiver. 14

2.1 Scheme of a Lena image transmission to two different users, with different data rates at the receiver, and indeed different qualities of the received image. 22

2.2 Illustration of the FEC-based multiple description coding technique for an embedded bistream with $n = 5$ descriptions. 23

2.3 Subcarrier spectrum assignment. 25

2.4 Transmission of the embedded bitstream over OFDM mobile wireless networks. The dark shaded area to the right of the RCPC coding boundary line represents the bits for CRC and RCPC coding. The lighter shaded area under the RS coding boundary staircase represents Reed-Solomon parity symbols. The unshaded area represents information symbols. Note that the CRC/RCPC parity symbols are interleaved with the RS symbols in the actual system. $N_t = N \times M$ total subcarriers and L_{RS} Reed-Solomon symbols are considered. For each (n, k) RS codeword, k information symbols are encoded into $n = N_t$ total symbols. 26

2.5 Pilot insertion scheme for systems with: (a) one correlated subcarrier; (b) M correlated subcarriers. 30
2.6 Profiles showing the optimal allocation of source and channel symbols for systems with $(N, M) = (4, 32)$, $f_{nd} = 10^{-3}$ and SNR = 16.0 dB for different choices of RCPC coding rates and for both perfect CSI and imperfect CSI. 34
2.7 Profiles showing the optimal allocation of source and channel symbols for systems with $R_{rcpc} = 8/24$ and SNR = 16.0 dB and imperfect CSI for systems with frequency diversity orders $N = 1, 4, 32, 128$, respectively. 36
2.8 Optimal R_{rs} vs. R_{rcpc} for systems with $(N, M) = (4, 32)$, $f_{nd} = 10^{-3}$ SNR = 16.0 and both perfect and imperfect CSI. 37
2.9 Optimized PSNR vs R_{rcpc} for different Doppler spreads in systems with $(N, M) = (4, 32)$, SNR = 16 dB and imperfect CSI. 38
2.10 Optimized PSNR vs. f_{nd} for systems with $(N, M) = (16, 8)$, SNR = 16 dB and $R_{rcpc} = 1$ for perfect and imperfect CSI systems. 40
2.11 Optimized PSNR vs R_{rcpc} for different coherence bandwidths. 41
2.12 Optimized PSRN vs. f_{nd} for systems with $(N, M) = (16, 8)$, SNR = 16 dB and different RCPC code rates. . . . 42
2.13 Optimal PSNR performances vs. both N and f_{nd} in systems with SNR = 16 dB for both perfect CSI systems (a) and imperfect CSI systems (b). 44
2.14 Optimized PSNR vs. f_{nd} for systems with SNR = 16 dB and both perfect and imperfect CSI. Two different frequency diversity order are considered: $(N, M) = (32, 4)$ and $(N, M) = (4, 32)$. 46
2.15 Image quality for a system with $f_{nd} = 10^{-1}$, $(N, M) = (32, 4)$, SNR = 16 dB, and imperfect CSI. We denote by R_{TX} the transmitted source rate and by R_{RX} the received source rate. . 51

3.1 Encoder structure of the FGS coding methodology based on MPEG-4. 57

3.2 Motion-compensated FGS hybrid coder with leaky prediction. 59

3.3 Transmission of the embedded bitstream over OFDM mobile wireless networks. (a) FGS embedded bitstream. (b) Motion-compensated MD coding. The white shaded area represents the parity symbols (both in time and frequency domain), the light-grey shaded area represents the EL-MCP symbols, and the dark-grey shaded area represents the EL-Extra symbols. Note that the CRC/RCPC symbols are interleaved with RS symbols in real systems. . . . 65

3.4 Rate-Distortion curve evaluation. 69

3.5 RD curve evaluation methods. 71

3.6 Rate-Distortion function for the MC-FGS with various MCP values (β), without leaky prediction ($\alpha = 1$), and with no time coding ($R_{rcpc} = 1$). 73

3.7 Comparison of the *off-line* and *on-line* method for the FEC level evaluation. 74

3.8 Rate-distortion function and optimal FEC profiles for both the *off-line* and the *on-line* method for systems with $f_{nd} = 10^{-3}$, $R_{rcpc} = 1$, $(N, M) = (2, 64)$. Note that the frame nr. 10 and nr. 30 are considered in the *on-line* method. 76

3.9 Optimal profile of the parity symbols for a system with $f_{nd} = 2.5 \times 10^{-4}$, $R_{rcpc} = 8/12$, and N variable for the transmission of sequences encoded with different α and β parameters. The profile for the 20-th frame is considered. . 77

3.10 Optimal profile of the parity symbols for a system with $f_{nd} = 2 \times 10^{-4}$,$(N, M) = (2, 64)$, and different R_{rcpc} values for the transmission of sequences encoded with $\alpha = 0.9$ and the optimal β parameter. The profile for the 20-th frame is considered, and the PSNR values are expressed in dB. 78

3.11 Optimum β vs. R_{rcpc} for systems with $f_{nd} = 2 \times 10^{-4}$, $(N, M) = (2, 64)$, and $\alpha = 1, 0.9,$ and 0.7. 80

3.12 PSNR performance for several orders of diversity available in the frequency domain in both slow and fast fading systems. 81

3.13 Expected PSNR-Y vs. f_{nd} for systems with $(N, M) = (4, 32)$, $\beta = 0.10$, and 0.35, $\alpha = 1.0$. Both optimal R_{rcpc} values and constant rates ($R_{rcpc} = 1$, and $8/14$) are employed. 82

3.14 PSNR-Y vs. number of frame for systems with $(N, M) = (4, 32)$, $f_{nd} = 10^{-4}$, and several β and α values. 83

4.1 Adaptive modulation technique. Starting from the bit error probability expression, the SNR thresholds are evaluated, and then, the optimal modulation level to be adopted is chosen. Note that if FAM (SAM) is considered, the bit error probability, P_{b}, considered is the instantaneous (mean) BEP, the SNR parameter, χ, is the instantaneous (mean) SNR, and the observed fluctuations variable with the time are hte small-scale (large-scale) fading. 89

4.2 Transmitted pilot scheme. 91

4.3 BEO vs. μ_{dB} for SAM system with maximum modulation size 256, $N = 4$, $P_{\mathrm{b}}^{\star} = 10^{-2}$, and $\sigma_{\mathrm{dB}} = 8$. A comparison between perfect and imperfect CSI is reported. 102

4.4 BEO vs. $N_{\mathrm{p}}\varepsilon$ for SAM systems with imperfect CSI, maximum modulation size 256, $N = 2, 4$, and 8, $P_{\mathrm{b}}^{\star} = 10^{-2}$, $\mu_{\mathrm{dB}} = 35$ and $\sigma_{\mathrm{dB}} = 8$. 102

4.5 Effective throughput vs. μ_{dB} for SAM systems with MRC ($N = 4$), maximum constellation size 256, maximum outage 5%, $P_{\mathrm{b}}^{\star} = 10^{-2}$, and $\sigma_{\mathrm{dB}} = 8$. Results are evaluated for both perfect and imperfect CSI, considering several channel estimation quality levels. 103

4.6 Comparison between effective throughout in SAM and in FAM systems with imperfect CSI, maximum modulation level 256, maximum outage 5%, $P_{\mathrm{b}}^{\star} = 10^{-2}$, and $\sigma_{\mathrm{dB}} = 8$. . 104

4.7 BEO vs. μ_{dB} for a non adaptive scheme with $P_{\mathrm{b}}^{\star}$, $\sigma_{\mathrm{dB}} = 8$, $N = 4$ (MRC), different constellation sizes M ($M = 4$, $M = 64$) and both perfect and imperfect CSI systems. . . 105

4.8 Effective throughput vs. μ_{dB} for adaptive and non-adaptive scheme with $P_{\text{b}}^{\star}$, $\sigma_{\text{dB}} = 8$, $N = 4$ (MRC), $\varepsilon = 1$, maximum modulation $M_{\max} = 256$, and $N_{\text{tot}} = 180$. 106

4.9 Effective throughput vs. μ_{dB} for SAM systems with $P_{\text{b}}^{\star}$, $\sigma_{\text{dB}} = 8$, H-S/MRC (L/N=2/8) and MRC (L/N=8/8), $\varepsilon = 1$, maximum modulation $M_{\max} = 64$, and $N_{\text{tot}} = 180$. . 107

4.10 Effective throughput vs. μ_{dB} for SAM systems with $P_{\text{b}}^{\star} = 10^{-2}$, Nakagami$-m$ channels with $m = 0.5$ and $m = 4$, $\sigma_{\text{dB}} = 8$, MRC (N=8), $\varepsilon = 1$, maximum modulation $M_{\max} = 64$, and $N_{\text{tot}} = 180$. 107

4.11 Effective throughput vs. N_{p} for SAM systems with $P_b^{\star}$, $\sigma_{\text{dB}} = 8$, MRC ($N = 8$), $\varepsilon = 1$, and maximum modulation $M_{\max} = 256$. Several median values μ_{dB} are considered, $\mu_{\text{dB}} = 25, 30, 40$. $N_{\text{tot}} = 180$. 109

4.12 Effective throughput vs. N_{p} for SAM systems with $P_b^{\star} = 10^{-2}$, $\sigma_{\text{dB}} = 8$, MRC (N=4), maximum modulation $M_{\max} = 256$. Several median values μ_{dB} ($\mu_{\text{dB}} = 25, 30, 40$) and ε values ($\varepsilon = 0.5, 1, 3$) are considered. $N_{\text{tot}} = 100$. 110

4.13 SNR outage penalty and Mean throughput penalty vs. ϵ for SAM systems with $P_b^{\star}$, $\sigma_{\text{dB}} = 8$, MRC (N=4), and several values of pilot symbols ($N_{\text{p}} = 1, 2, 4$,and 6). In the throughput penalty plot(b), $\mu_{\text{dB}} = 15$. 111

5.1 Approximated and Exact threshold lines for a system with $N_d = 1$, $N_{\text{I}} = 2$, and M ranging from 4 to 256. 124

5.2 Outage probability vs. μ_{dB} for SAM systems with maximum modulation size $64, 256, 1024$, no diversity at the receiver, $P_{\text{b}}^{\star} = 10^{-2}$, $\sigma_{\text{dB}} = 8$. To evaluate SNR thresholds, the BEP approximation A3 is adopted. 126

5.3 Mean SE vs. μ_{dB} for SAM systems with maximum modulation size $64, 256, 1024$, MRC with $N = 1, 2, 8$, maximum outage 5%, $P_{\text{b}}^{\star} = 10^{-2}$, and $\sigma_{\text{dB}} = 8$. The mean SE is evaluated with both perfect and imperfect BEP expressions. 127

5.4 BEP vs. $\overline{\gamma}_{\mathrm{dB}}$ for M-QAM systems with modulation size $M = 16$, maximum outage 5%, $P_{\mathrm{b}}^{\star} = 10^{-2}$, and $\sigma_{\mathrm{dB}} = 8$. The bit error probability, conditioned to SIR, is evaluated for several N and N_{I} values. 128
5.5 $\Delta_{j,\mathrm{dB}}$ vs. $\overline{\gamma}_{\mathrm{I,dB}}$ for SAM systems with $M_{\max} = 256$, maximum outage 5%, $P_{\mathrm{b}}^{\star} = 10^{-2}$, $\sigma_{\mathrm{dB}} = 8$, and several N and N_{I} values. The analysis is conditioned to the SIR value. . . 129
5.6 Mean throughput (conditioned to SIR) vs. μ_{dB} for SAM systems with $M_{\max} = 256$, maximum outage 5%, $P_{\mathrm{b}}^{\star} = 10^{-2}$, $\sigma_{\mathrm{dB}} = 8$, $N_{\mathrm{I}} = 6$, and number of antennas equals to 2 and 4. 130
5.7 BEP vs. $\overline{\gamma}_{\mathrm{dB}}$ for M-QAM systems with $M = 4$, $N = 1$, $N_{\mathrm{I}} = 4$. 131
5.8 SNR thresholds vs. INR thresholds for SAM systems with $M_{\max} = 256$, $N = 1$, $N_{\mathrm{I}} = 2$. 132
5.9 Mean throughput vs. μ_{dB} SAM systems with $M_{\max} = 64$, $N = 1$, and $N_{\mathrm{I}} = 2$. 133

A.1 Simulation and analytic results for the packet success rate for an uncoded system with different f_{nd} with SNR(R_{th}) = 9 dB. 139

C.1 Exact and approximated BEP vs. instantaneous SNR for a 4-QAM and 1024-QAM system. 147
C.2 Exact and approximated BEP vs. averaged SNR for 1024-QAM system. 148

List of Tables

2.1 Factors affecting the application layer quality-of-service (QoS) in a fast fading environment. 28
2.2 Optimal PSNR, R_{rcpc}, R_{rs}, and R_{tot} for a system with perfect CSI, SNR = 16dB and different diversity order in both time and frequency domains. 48
2.3 Optimal PSNR, R_{rcpc}, R_{rs}, and R_{tot} for a system with imperfect CSI, SNR = 16dB and different diversity order in both time and frequency domains. 49

5.1 $\Delta_{j,\mathrm{dB}}$ for SAM and FAM techniques for different modulation levels when no diversity is considered ($N = 1$). 119
5.2 $\Delta_{j,\mathrm{dB}}$ for SAM technique for different modulation levels and orders of diversity when the approximation (A1) is considered. 120

Abbreviations

QoS	Quality of Service
OFDM	Orthogonal Frequency Division Multiplexing
SIMO	Single Input Multiple Output
MIMO	Multiple Input Multiple Output
PDF	Probability Density Function
CDF	Cumulative Density Function
MGF	Moment-Generating Function
FEC	Forward Error Correction
MDS	Maximum Distance Separable
RS	Reed-Solomon
RCPC	Rate-Compatible Punctured Convolutional
CRC	Cyclic Redundancy Check
RB	Resource Block
AWGN	Additive White Gaussian Noise
SNR	Signal-to-Noise Ratio
SINR	Signal-to-Interference-plus-Noise Ratio
INR	Interference-to-Noise Ratio
FFT	Fast Fourier Transform
IFFT	Inverse Fast Fourier Transform
MMSE	Minimum Mean Square Error
MRC	Maximum Ratio Combining
H-S/MRC	Hybrid- Selection/Maximum Ratio Combining
ECG	Equal-Gain Combining
SC	Selection Combining
OC	Optimum Combining
AGC	Automatic Gain Control
PSAM	Pilot Symbol Assisted Modulation
CSI	Channel State Information
ICI	Inter-Carrier Interference
ISI	Inter-Symbol Interference

SPIHT	Set Partitioning In Hierarchical Trees
EZW	Embedded Zerotrees Wavelet
MD	Multiple Description
PET	Priority Encoding Transmission
UEP	Unequal Error Protection
EEP	Equal Error Protection
JSSC/D	Joint Source and Channel Coding/Decoding
MPEG	Moving Pictures Experts Group
BL	Base Layer
EL	Enhanced Layer
FGS	Fine Granularity Scalable
MCP	Motion-Compensated Prediction
VLC	Variable Length Coding
BSC	Binary Symmetric Channel
DCT	Discrete Cosine Transform
RD	Rate-Distortion
SAM	Slow Adaptive Modulation
FAM	Fast Adaptive Modulation
SE	Spectral Efficiency
SSD	Subset Diversity
BEP	Bit Error Probability
BEO	Bit Error Outage
QAM	Quadrature Amplitude Modulation

Abstract

In recent years, due to the rapid convergence of multimedia services, Internet and wireless communications, there has been a growing trend of heterogeneity (in terms of channel bandwidths, mobility levels of terminals, end-user quality-of-service (QoS) requirements) for emerging integrated wired/wireless networks. Moreover, in nowadays systems, a multitude of users coexists within the same network, each of them with his own QoS requirement and bandwidth availability. In this framework, embedded source coding allowing partial decoding at various resolution is an appealing technique for multimedia transmissions. This dissertation includes my PhD research, mainly devoted to the study of embedded multimedia bitstreams in heterogenous networks, developed at the University of Bologna, advised by Prof. O. Andrisano and Prof. A. Conti, and at the University of California, San Diego (UCSD), where I spent eighteen months as a visiting scholar, advised by Prof. L. B. Milstein and Prof. P. C. Cosman. In order to improve the multimedia transmission quality over wireless channels, joint source and channel coding optimization is investigated in a 2D time-frequency resource block for an OFDM system. We show that knowing the order of diversity in time and/or frequency domain can assist image (video) coding in selecting optimal channel code rates (source and channel code rates). Then, adaptive modulation techniques, aimed at maximizing the spectral efficiency, are investigated as another possible solution for improving multimedia transmissions. For both slow and fast adaptive modulations, the effects of imperfect channel estimation errors are evaluated, showing that the fast technique, optimal in ideal systems, might be outperformed by the slow adaptive modulation, when a real test case is considered. Finally, the effects of co-channel interference and approximated bit error probability (BEP) are evaluated in adaptive modulation techniques, providing new decision regions concepts, and showing how the widely used BEP approximations lead to a substantial loss in the overall performance.

Chapter 1

Wireless multimedia transmission overview

Only those who dare may fly.
- Luis Sepúlveda

The high demand of high quality multimedia applications has promoted a significant development in multimedia transmissions at high data rate. In this framework, great interest is reposed in cross-layer optimization for joint source and channel coding/decoding (JSCC/D) as well as in adaptive modulation algorithms, aimed at optimizing the transmitting parameters taking into account both the physical and the application layer conditions. Moreover, in multiuser networks, where requirements from different users must be met at the same time, a multi-rate (i.e., multi-quality) transmission is needed. With this aim, an enormous simplification in the transmission overhead is represented by the progressive image and video bitstreams. The combination of source and channel coding and modulation parameters optimization in systems transmitting progressive multimedia bitstreams is therefore an appealing technique, able to provide a system that is robust enough to the channel impairments, still satisfying the multiusers constraints. In the following thesis, several optimized multimedia wireless transmissions will be discussed. In the introductory chapter, we provide an outline of the thesis mainly focusing on the contributions of this work as compared to existing literature. Next, we provide a basic overview of the system model adopted

in the thesis.

1.1 Introduction

In recent years, due to the rapid convergence of multimedia services, Internet and wireless communications, there has been a growing trend of heterogeneity (in terms of channel bandwidths, mobility levels of terminals, end-user quality-of-service (QoS) requirements) for emerging integrated wired/wireless networks. In multi-services multi-users networks, different users need different QoS requirements due to the multitude of applications and scenario coexisting within the modern networks. The quality required for a real-time video played on a PAD, for example, is lower than the one reproduced on a laptop. The heterogeneity comes not only from different data rates and QoS requirements, but also from different scenarios, as the PAD might be for example connect to a wireless networks with an high level of mobility, and the latpot to a wired connection. Embedded source coding [1], allowing partial decoding at various resolution and quality levels from a single compressed bitstream, is a promising technology for multimedia communications in heterogeneous environments. Thanks to the progressive image features, in a multi-user networks, each user is able to decode the same transmitted bitstream at the desired data rate. A typical case can be the one represented in Fig. 1.1, where only one transmitter can provide embedded progressive bitstream to a multitude of users. Although a single progressive bitstream can be decoded at different data rates, providing a multitude of decoded quality levels, an error in the bitstream would make the subsequent bit useless. Thus, a single error can cause an unrecoverable loss in synchronization between encoder and decoder, and produce substantial quality degradation. It follows that embedded source coders are usually extremely sensitive to channel impairments which can be severe in mobile wireless links due to multipath signal propagation, delay and Doppler spreads, and other effects. In order to cope with the channel, it is therefore clear the importance of making the signal as reliable as possible, introducing redundancy in the bitstream [2–4], or optimizing the trans-

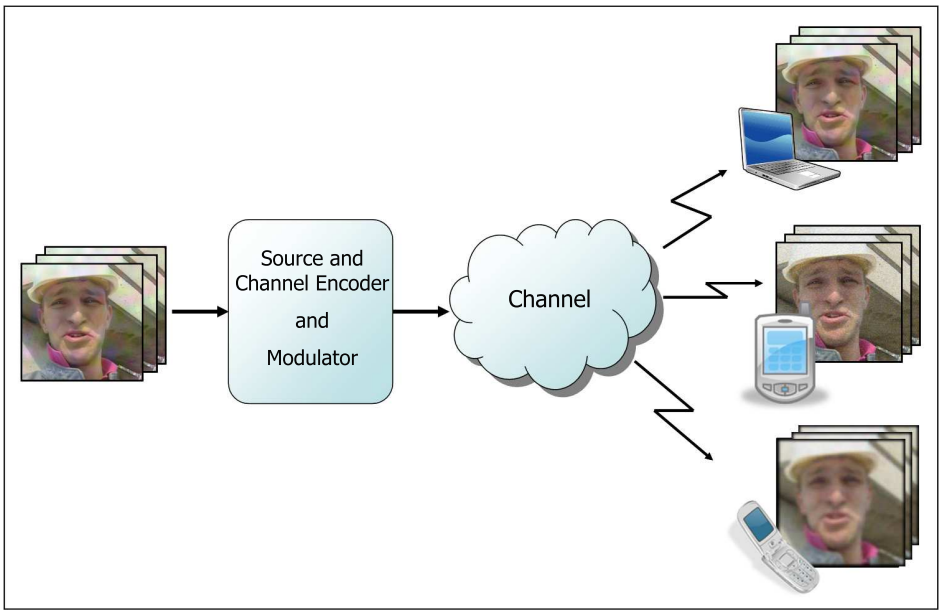

Figure 1.1: Simplified scheme of heterogenous scenarios. The same encoded bitstream is transmitted to different users, each of whose receives the image at its achievable data rate.

mitting parameters [5–7]. The suitable level of redundancy introduced by the channel coding depends on the channel conditions. The optimization of joint source and channel coding able to exploit both the physical and application layer diversity is investigated in this thesis. Beyond JSSC, another solution to improve robustness in multimedia wireless transmission is the adaptive modulation technique. Here, the modulation parameters are adapted to the channel conditions, leading to an improvement of the received throughput, and thus of the decodable data rate. In this thesis, adaptive modulation techniques in real systems are investigated, taking into account all the possible effects impairing the performance, i.e., channel estimation errors or co-channel interference.

1.2 Outline of the work

Aimed at maximizing the performance for multimedia wireless systems, the following work is focused on the optimization of the trans-

mission parameters (at physical level), such as code rates or modulation levels. First, the design of channel coding is investigated in image transmissions applications. In addiction to the physical layer gain, an application layer diversity [8] can be exploited by adopting a multiple description encoding. Thus a symmetric n-channel forward error correction (FEC)-based multiple description is investigated, with the FEC level based on channel conditions. Then, this study has been extended to video transmissions. Due to the high complexity of a video bitstream, the channel coding is optimized in conjunction with the source coding parameters. It follows that the JSSC design is investigated, aimed at evaluating the optimal channel code rate together with the suitable compression rate to be employed for the transmission over a given wireless channel.

Since, in embedded bitstreams, the quality of the decoded image is proportional to the data-rate to be decoded, adaptive modulation techniques, aimed at maximizing the received throughput, can also be employed. In perfect systems, adaptive modulation techniques allow a substantial improvement on the averaged received throughput, without compromising the outage probability [5, 6]. In this thesis, adaptive modulation techniques are investigated for real systems, i.e., systems experiencing imperfect channel estimations or the presence of interference or other issues that might compromise the bit error probability performance. The remainder of the Thesis is organized as follows.

In Chapter 2, channel coding in both time and frequency domain is optimized for progressive images transmission. The topic is investigated for OFDM systems and several Doppler values of the channels. It has been demonstrated that the optimization of the FEC protection in both the domains provides a system that results to be robust to channel impairments, for channels with both fast and slow variations.

In Chapter 3, the embedded video transmission is investigated. A JSSC is considered, and the channel coding is optimized in conjunction with the source coding in OFDM systems experiencing several orders of diversity in both time and frequency domain. Important results are reported for the rate distortion curve evaluation. The method we propose achieves worthy quality transmissions, optimizing the transmitting

scheme, and satisfying the imposed temporal constraints.

Chapter 4 investigates adaptive modulation techniques in systems with imperfect channel estimation. Both the cases of imperfect channel estimation at the transmitter and at the receiver are considered, for both slow and fast adaptive modulation techniques. Pilot symbols insertion is considered for the channel estimation, and the design of the optimal pilot scheme is optimized, based on the tradeoff *estimation quality-throughput reduction*. The results show that the fast technique, optimal in ideal systems, might be outperformed by the slow adaptive modulation technique.

In Chapter 5, adaptive modulation techniques are investigated for more general systems, experiencing a shift in the SNR thresholds. Some applicative examples are considered, as systems experiencing co-channel interference and/or the employment of the bit error probability approximated expression. Depending on the channel configurations, the median SNR values that achieve satisfactory performance can be evaluated in all the applicative examples. Moreover, we highlight the lost of performance in terms of mean throughput that the system experiences when the widely used exponential bit error probability approximation is employed.

In Chapter 6, concluding remarks and future directions are reported.

1.3 System modeling

In this section, the system model has been described in details. In particular, starting from basic concepts on wireless channels, the assumption employed in the analysis of the thesis are described. The characterization of the wireless channels, the descriptions of SIMO and OFDM systems are here presented.

1.3.1 Wireless channel modeling

It is well known that the additive white gaussian noise is not the only issue affecting the performance in wireless systems [9–12]. Because of reflection, diffusion and refraction of signals through scattering objects, a short impulse transmitted over the channel is received as a sum of multiple impulses, each of whose with its own amplitude and delay. These

amplitude and phase fluctuations, varying with the time, are named fading, and they can be modeled statistically, as described in the following. Moreover, for long distance communications, the signal suffer of a power reduction due to the path loss.

The equivalent low-pass response of the channel at time t to an impulse at time $t - \tau$ can be represented as

$$h(t, \tau) = \sum_{n=1}^{N(t)} \alpha_n(t) e^{j2\pi f_0 \tau_n(t)} \delta(\tau - \tau_n(t)),$$

where we denote by $\alpha_n(t)$ the possibly time-variant attenuation factor of the $N(t)$ multipath propagation and by $\tau_n(t)$ the corresponding time delays. For stationary channels, the channel response results in a function of only τ. Knowing the correlation function in the time and frequency domain, the channel can be characterized as follows.

Frequency-flat or frequency-selective channel. The coherence bandwidth Δf_c, defined as the frequency range in which the fading process results correlated, can be expressed as $\Delta f_c = 1/\tau_{\max}$, where $\tau_{\max}$ is the maximum delay spread. When the system bandwidth is smaller than the coherence bandwidth (for example, narrow band systems), the channel is defined a flat-frequency channel, and the frequency components are affected in similar manner. Conversely, when the system bandwidth exceeds Δf_c (for example, wide band systems), the channel is frequency-selective.

Slow or fast fading channel. Defining the coherence time T_c as the period over which the fading process is correlated, it can be related to the maximum Doppler spread, f_D, as $T_c \simeq 1/f_D$.

In general, the multipath fading, characterizing the short-term signal fluctuation, is usually too complex for an exact physical analysis, thus, it is considered statistically distributed. Assuming the fading h zero-mean complex Gaussian distributed, its phase is uniform distributed between 0 and 2π, and the envelope is Rayleigh distributed. It follows that the channel power has the following probability density function (PDF)

$$f_{|h|^2}(x) = \frac{1}{\Omega} \exp\left[-\frac{x}{\Omega}\right] \qquad x \geq 0, \tag{1.1}$$

where $\mathbb{E}\{|h|^2\} = \Omega$. The corresponding moment-generating function is $M_{|h|^2}(s) = [1 - \Omega s]^{-1}$. Another fading distribution adopted throughout the thesys is the Nakagami-m distribution, that usually arises when the dimension of the cluster of scatters is comparable to the signal wavelength. In the case of a Nakagami-m channel, the PDF of the channel power is given by

$$f_{|h|^2}(x) = \frac{m^m x^{m-1}}{\Omega^m \Gamma(m)} \exp\left[-\frac{mx}{\Omega}\right] \qquad m \geq \frac{1}{2} \tag{1.2}$$

One sided Gaussian can be modeled for $m = 1/2$, while $m = 1$ corresponds to Rayleigh fading, as it can be observed from (1.1) and (1.2).

As briefly mentioned before, the signal suffers of a power reduction due to the path-loss (large-scale fading), that is typically assumed *log-normal distributed*. Denoting by $\overline{\gamma}$ the log-normal SNR averaged over the small-scale fading, $\overline{\gamma}_{\text{dB}} = 10\log_{10}(\overline{\gamma})$ is Gaussian distributed with mean μ_{dB} and variance σ^2_{dB}, i.e., $\overline{\gamma}_{\text{dB}} \sim \mathcal{N}(\mu_{\text{dB}}, \sigma^2_{\text{dB}})$. Note that the effects of the shadowing in adaptive systems are considered only in Chapter 4 and Chapter 5.

Jakes model or block fading assumption. When the symbol period is lower than the coherence time, the fading is said to be slow. In particular, a possible assumption, that can be made in case of slow fading, is the *block fading* channel. In this case, the fading channel coefficients are assumed constant within the transmitted packet period, T_p. Note that the block fading assumption implies that $T_p \ll T_c$. A block fading channel for both Rayleigh and Nakagami-m fading channels is assumed in Chapter 4 and Chapter 5. Conversely, in the Chapter 2 and Chapter 3, a Rayleigh fading channel without the block fading assumption is considered. In the literature, many different approaches have been used for modeling mobile radio channels, as the well known mathematical model due to Clarke [13] and its simplified model due to Jakes [14]. However, the Jakes' simulator is a deterministic model, leading to a complicated implementation of uncorrelated fading waveforms for frequency-selective fading channels, or multiple-input multiple-output (MIMO) channels. Thus, the model we consider in the thesis is a modified Jakes' model, described in [15].

1.3.2 SIMO system - spatial diversity

In order to overcome the performance reductions due to the presence of fading, the adoption of diversity-combining of independently fading signal paths is one of the most powerful technique [9, 10, 12, 16, 17]. The basic idea is to send the same message x over independent channels, that are less likely to experience deep fades simultaneously. A spatial diversity is exploited when multiple antennas are considered at the receiver, (i.e., antenna array)[1]. In this case, the receiver combines the independent fading paths to obtain a resultant signal which is then passed through a standard demodulator. In particular, the received signal on each k-th branch, after the receiver filter and sampling, is weighted with a given value, w_k, and then it is combined to the other weighted received signals. It follows that the decision variable can be expressed as

$$z = \mathbf{w}^{\mathrm{H}}\mathbf{h}\sqrt{P}x + \mathbf{w}^{\mathrm{H}}\mathbf{n},$$

where $\mathbf{h} = [h_1, \ldots, h_N]^{\mathrm{H}}$ is the channel coefficient vector and h_k is the channel experienced by the signal received on the k-th branch; $\mathbf{n} = [n_1, \ldots, n_N]^{\mathrm{H}}$ is the noise vector, and $\mathbf{w}$ is the $N \times 1$ weight vector. The combining can be done in several ways which vary in complexity and overall performance. In the following, a brief description of the most common techniques is reported.

Minimum Mean Square Error (MMSE). MMSE addresses both problems of multipath fading of the desired signal and the presence of co-channel interference. With MMSE, or optimum combining (OC), the signals received by several antenna elements are weighted and combined to maximize the output signal-to-interference-plus-noise ratio (SINR) [18]. The weight vector $\mathbf{w}$ is given by

$$\mathbf{w} = \left[\mathbf{R}_{\mathrm{I}} + \sigma_N^2\mathbf{I}\right]^{-1}\mathbf{h},$$

where $\mathbf{R}_{\mathrm{I}} = \mathbf{H}_{\mathrm{I}}\mathbf{H}_{\mathrm{I}}{}^{H}$ is the covariance matrix of the interfence signals. It follows that the SINR at the output of the combiner is given by

$$\gamma_{\mathrm{T}} = \mathbf{h}^{H}\left[\mathbf{R}_{\mathrm{I}} + \sigma_N^2\mathbf{I}\right]^{-1}\mathbf{h}.$$

[1] In order to have a spatial diversity available, the distance between each antennas has to be so that the signal on each branch can be not correlated from each other.

Maximum Ratio Combining (MRC). MRC is the optimum linear combining technique for coherent reception with independent fading at each antenna element in the presence of spatially white Gaussian noise. The complex weight at each element compensates for the phase shift in the channel and is proportional to the signal strength. The weight vector $\mathbf{w}$ is given by

$$\mathbf{w} = \frac{\mathbf{h}}{||\mathbf{h}||},$$

At the cost of the knowledge of channel coefficients, the MRC allows to maximize the instantaneous SNR at the combiner output, given by

$$\gamma_{\mathrm{T}} = \sum_{i=1}^{N} \gamma_i.$$

It is well known that γ_{T} is a chi-square distributed with $2N$ degrees of freedom [9, 10] and its MGF can be easily derived. In particular, assuming the channel coefficients independent from each other, the MGF of γ_{T} can be derived as the product of the MGF of the single SNR on each branch, γ_i. Thus, $M_{\gamma_{\mathrm{T}}}(j\nu) = (1 + j\nu\overline{\gamma})^{-N}$. MRC mitigates fading, however, it ignores co-channel interference.

Equal-Gain Combining (EGC). To overcome the high complexity of the MRC, the equal-gain combining technique can be adopted, which is essentially a maximal-ratio combiner with all of the weight $w_i = 1$. In practice, EGC is often limited to coherent modulations with equal energy symbols (M-ary PSK signals). Indeed, for signals with unequal energy symbols such as M-QAM, estimation of the path amplitudes is needed anyway for automatic gain control (AGC) purposes, and thus for these modulations MRC should be used to achieve better performance.

Selection Combining (SC). In contradiction with the previous combiners, the SC do not combine all the branches and it does not require the channel knowledge. In particular, in SC techniques, the branch signal with the largest amplitude (or signal-to-noise ratio) is selected for demodulation. Therefore, the SC scheme can be used in conjunction with differentially coherent and noncoherent modulation techniques since it does not require knowledge of the signal phases on each branch as would be needed to implement MRC or EGC in a coherent system. Clearly, SC

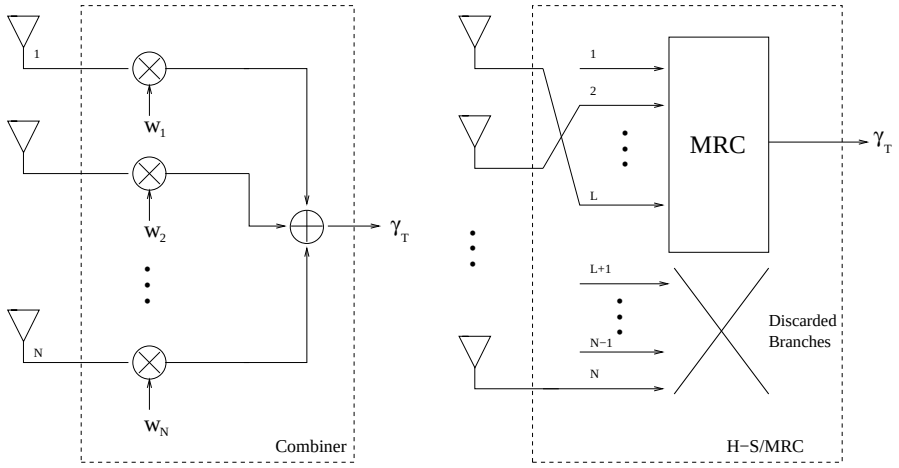

Figure 1.2: Combiner schemes at the receiver. a) A generic scheme, b) descriptions of a hybrid-selection/maximum ratio combiner.

and MRC (or EGC) represent the two extremes in diversity combining strategy with respect to the number of signals used for demodulation.

Hybrid-Selection/ Maximum Ratio Combining (H-S/MRC). This hybrid combining technique processes a subset of the available diversity branches, reducing the system complexity, but achieving better performance than SC. The H-S/MRC selects the L branches (over N) with the largest SNR at each instant, and then combines these branches to maximize the instantaneous output. It means, that the L most powerful branches are processed by a MRC, as it can be observed from Fig. 1.2. Here, the model scheme of a hybrid-selection/maximum ratio combiner , together with the scheme of a general combiner receiver, is reported. The main issue in the H-S/MRC, from an analytical point of view, is that after the reordering, the branches are not independent from each other. An enormous simplification can be derived by adopting the virtual branches technique, introduced in [19]. In particular, the instantaneous SNR of the ordered diversity branches, $\gamma_{[N]}$, are transformed into a new set of virtual branch instantaneous SNRs, V_ns, by using the following relation

$$\gamma_{[N]} = \mathcal{T}_{\mathrm{VB}} V_N,$$

where $\mathcal{T}_{\mathrm{VB}}$ is an upper triangular virtual branch transformation matrix,

defined in [19]. The gain in adopting this transformation matrix is that the virtual branches SNRs are independent and identically-distributed random variables, with characteristic function given by $\psi_{V_n}(j\nu) = (1 - j\nu)^{-1}$.

1.3.3 Multicarrier systems - OFDM

The basic idea of multicarrier systems is to split the bitstream into multiple substreams transmitted over multiple channels, overcoming the performance degradation due to frequency selective channels. When the subchannels are orthogonal, the multicarrier technique is defined as orthogonal frequency division multiplexing (OFDM). Considering a system with baseband bandwidth B and desired data rate R, we assume the channel divided into N subchannels, each of those will have a baseband bandwidth equals to $B_N = B/N$. Usually, N is set sufficiently large so that B_N is smaller than the coherence bandwidth, i.e., $B_N \ll (\Delta f)_c$. It follows that the flat fading assumption in each subcannel can be considered, leading to a reduction of the ISI generated by the fading channels. Moreover, in the discrete implementation of OFDM[2], the ISI can be completely eliminated by inserting a cyclic prefix. It is worth noting that each substream will have a data rate equals to $R_N = R/N$, but the total data rate will equal $NR_N = R$, and also the total bandwidth will be $NB_N = B$. The discrete OFDM baseband model is reported in Fig. 1.3 and it can be easily implemented by adopting the fast fourier transform (FFT), and the inverse fast fourier transform (IFFT). Considering $X_{i,j,n}$ the i-th constellation point of the j-th symbol transmitted in the n-th subcarrier, the vector $\{X_{i,j,n}\}_{n=0}^{N-1}$ is processed by the IFFT. Then, after the serial-to-parallel (S/P) converter, the cyclic prefix is added to the signal, that is processed by a D/A converter and a band-limiting filter before the transmission. The transmitted signal reads as

$$y(t) = \sum_i \sum_j \sum_{n=0}^{N-1} X_{i,j,n} \mathrm{e}^{j2\pi nt/T} g(t - jT),$$

[2]Note that, in the following, only the discrete implementation will be described in details, being the model considered in the next chapters.

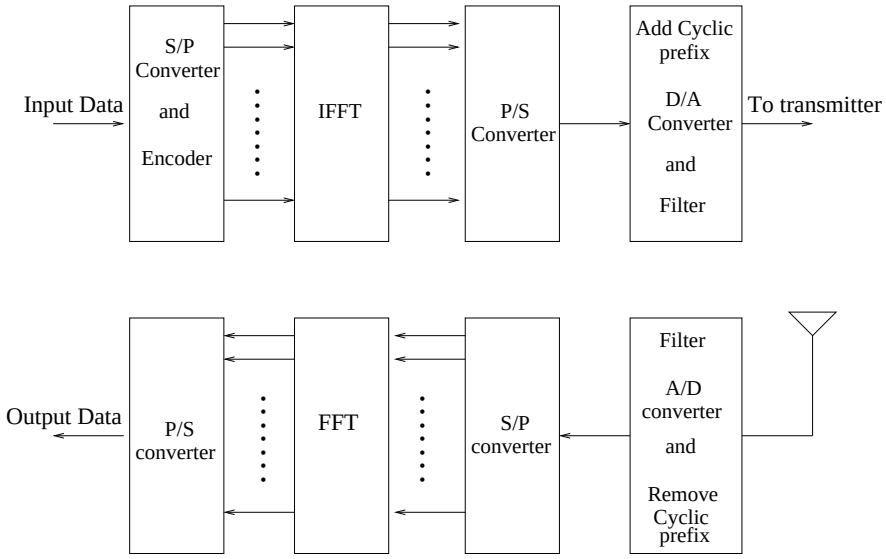

Figure 1.3: OFDM implementation scheme at the transmitter and at the receiver.

where T is the OFDM symbol period, comprehensive of the guard time added in the cyclic prefix, and $g(t)$ is the rect function of period T. At the receiver, after the filter and the A/D converter, the cyclic prefix is removed and the signal is reported to the frequency domain by the FFT. In order to better understand the ISI cancellation due to the cyclic prefix, let consider the signal $y(t)$ sampled at the rate T/N and let assume that the channel has a maximum time delay spread equal to pT/N. It follows that, in the first p received samples, the current signal might be interfered from the previous one (ISI), and the insertion of a cyclic prefix with duration greater than pT/N provides an ISI free system.

In order to combact channel errors caused by multipath, due to the frequency selectivity of multiple parallel channels, the system can experience frequency diversity, by adding redundancy across the subcarriers. The same information, for example, can be sent over multiple subchannnels, so that multiple independently faded replicas of the information symbol can be obtained and a more reliable reception can be achieved. This gain comes at the cost of a data rate reduction. On the opposite, in order to maximize the data rate, a different message can be

sent over each subchannels, leading to an higher transmitted data rate, but a lower reliability of the information. It is worth noting, therefore, the tradeoff between diversity gain and information rate in OFDM systems experiencing frequency selectivity. It will be observed in the next chapters, for example, that an important parameter in this tradeoff is the channel coherence bandwidth. In particular, the diversity gain can be roughly evaluated as $(\Delta f)_c/N$, and the optimal tradeoff can be found depending on the diversity naturally offered by the channels.

Chapter 2

Channel coding for progressive images

In this chapter, the optimization of channel encoder for image transmissions is addressed. The transmission of progressive image bitstreams using channel coding in a 2-D time-frequency resource block in an OFDM network, employing time and frequency diversities simultaneously is investigated. The physical channel conditions arising from various different coherence bandwidths and coherence times, leading to various orders of diversities available in the time and frequency domains, are considered in the optimization. We investigate the effects of different error patterns on the delivered image quality due to various fade rates. We also study the tradeoffs and compare the relative effectiveness associated with the use of erasure codes in the frequency domain and convolutional codes in the time domain under different physical environments.

The remainder of this chapter is organized as follows: In Section 2.1 a description of progressive images, together with a brief overview of the multiple description coding are provided. In Section 2.2, progressive image transmissions are deeply explained and further details on MD coding is reported. In Section 2.3, we give a description of the OFDM system and the channel model. We also describe the proposed transmission system and discuss some of the issues associated with the use of channel coding in a time-frequency block. In Section 2.5, we describe the optimization problem. In Section 2.6, we provide simulation results and discussion. Finally, in Section 2.7, we provide a summary and conclusion.

2.1 Motivation and outline of the work

In recent years, with the rapid convergence of multimedia, Internet and wireless communications, there is a growing trend of heterogeneity (in terms of channel bandwidths, mobility levels of terminals, enduser quality-of-service (QoS) requirements) for emerging integrated wired/wireless networks. Embedded source coding, allowing partial decoding at various resolution and quality levels from a single compressed bitstream, is a promising technology for multimedia communications in heterogeneous environments. Early study of embedded transmission includes [20, 21]. Both papers studied the transmission of a progressively compressed bitstream employing the Set Partitioning in Hierarchical Trees (SPIHT) source coder combined with rate-compatible punctured convolutional (RCPC) codes. Coding and diversity are very effective techniques for improving the transmission reliability in a mobile wireless environment. However, time diversity achieved by channel coding plus intra-packet interleaving in a single carrier communication system becomes less effective in a slow fading environment where correlated and prolonged deep fades often result in the erasure of the whole packet or even several contiguous packets. Hence, although improvement could still be achieved due to the coding gain associated with the use of RCPC codes, the performance was not satisfactory [21].

To improve the performance against deep fades in a wireless environment, two approaches have been proposed to exploit diversity in the time domain at the physical layer for SC communication systems. One was to add systematic Reed-Solomon (RS) codes across multiple packets [22]. Specifically, channel codes consisted of a concatenation of RCPC and CRC codes as the row codes and RS codes as the column codes. With the addition of RS codes across multiple packets, lost packets might still be recoverable due to independently faded time slots [22].

Another approach [23–26] uses contiguous information symbols from the progressive bitstreams, which, instead of being packed in the same packets [20, 22], are spread across multiple packets (descriptions). The information symbols are protected against channel errors using systematic RS codes with the level of protection depending on the relative im-

portance of the information symbols. This coding scheme is sometimes referred to as symmetric n-channel FEC-based multiple description (MD) coding. Due to the individually decodable nature of the multiple packets, the source can be recoverable despite packet loss, although at a lower fidelity that depends on the number of successfully received packets. Analogous to the physical layer diversity techniques offered by channel coding, this has sometimes been referred to as *application layer diversity* [8].

While both approaches perform well in slow fading environments, the order of diversity of the physical channel is vital to the selection of system parameters (e.g., choice of channel codes and corresponding channel code rates) as shown in [27]. Despite their importance, such factors are usually overlooked in the literature. More importantly, studies of these channel coding techniques have been limited to 1-D time domain coding in a slow fading environment [22, 26]. For fast fading, rapid channel variations due to high mobility can potentially provide a high diversity gain and significantly improve the effectiveness of channel coding in the time domain. Unfortunately, rapid channel variation also poses a significant challenge for channel estimation [28–30]. The accuracy of this channel state information (CSI) is particularly important in optimizing channel coding. In particular, it has been shown that imperfect CSI due to estimation errors affects the performance of communications systems designed to take advantage of the diversity opportunities [31–33].

In recent years, orthogonal frequency division multiplexing (OFDM) has drawn intense interest. OFDM differentiates itself from an SC communications system in many ways, such as robustness against frequency-selective fading. Frequency diversity by adding redundancy in the frequency domain can combat channel errors due to multipath fading and achieve a more reliable overall system performance. In other words, OFDM offers a unique opportunity to improve system efficiency by employing both time and frequency domain channel coding depending on the propagation environment and user's mobility. A highly scattered environment may make the frequency domain coding more effective. A highly mobile user will probably make time domain coding more compelling. Although there have been some works investigating transmission

of embedded bitstreams over OFDM networks [34–36], none has explicitly characterized the time and frequency domains independently and jointly optimized the coding scheme based on these different physical environments.

In this work, we study the transmission of progressively coded image bitstreams using channel coding in a 2-D time-frequency resource block in an OFDM network under different physical environments. By properly decoupling the time domain and frequency domain channel variations, we propose a 2-D channel coding scheme which employs time and frequency diversities simultaneously. In particular, in the frequency domain, based on the order of diversity, we construct FEC-based multiple descriptions using channel erasure codes combined with embedded source coding. In the time domain, concatenated RCPC codes and CRC codes protect individual descriptions. Both the effects of inter-carrier interference (ICI) and channel estimation errors, which may become severe in a fast fading environment, are taken into consideration. We use pilot symbol assisted modulation (PSAM) with pilot symbol density depending on the channel selectivities in both time and frequency. As diversity is the primary factor determining the performance of a wireless system, the results presented can provide some design criteria for other progressive transmission coding schemes over mobile wireless networks.

2.2 Progressive image and multiple description

Progressive images coding has interrupted the well known simultaneous progression of efficiency and complexity in multimedia transmissions. Thanks to a progressive nature of the encoded bitstream, the same transmitted image can be reconstructed at different quality levels. In particular, progressive images have many attractive features. First, the quality of the decoded image is proportional to the received data rate, it means that the more the bits used for the decoding, the higher the quality of the reconstructed image. Second, the decoding process can be stopped as soon as a target bit rate or a target distortion metric is met, and

the quality will be the best possible for that bit rate. Third, as a consequence of the previous properties, one bitstream can be truncated at different data rates, providing several qualities. Thus, progressive images are suitable for heterogeneous networks. For Internet image applications, for example, embedded coding is desirable because the server can easily partition a scalable bit stream into layers to accommodate clients with different bandwidth. This can be observed also in Fig. 2.1, where the same encoded bitstream is transmitted to two different users, each with different received data rate. It is obvious that the user with lower data rate will experience a higher distortion of the received image. Extensive research has shown that the images obtained with wavelet-based methods yield very good visual quality; even simple coding methods produced good results when combined with wavelets. One of the pioneristic work for embedded encoding was introduced by Shapiro [37], who attempted to design a wavelet image encoder, *embedded zerotrees wavelet* (EZW). The algorithm introduced was able to encode the bits in the bitstream accordingly with their importance, inherent of progressive images, with no apparent sacrifice in image quality. In addition to producing a fully embedded bitstream, EZW consistently produced compression resulting competitive with all known compression algorithms on standard test images. The Shapiro's algorithm has been significantly improved by Said and Pearlman [1], by introducing the *set partitioning in hierarchical trees* (SPIHT). The zerotrees method is still exploited in SPIHT, but the tree structure is slightly different. Moreover, it has been observed that this algorithm is capable of providing good quality levels without arithmetic coding. In this work, we adopt the SPIHT algorithm as source coding.

Since in progressive image bitstreams an error generally renders the subsequent bit useless, embedded images results highly sensible to channel impairments. In order to make the system more robust, the insertion of unequal error protection (UEP) is desirable. In particular, mapping the encoded bitstream in multiple descriptions system with redundancy achieves a quality improvement in the system. Early study of embedded transmission was due to Sherwood and Zeger who considered transmission of a progressively compressed bitstream employing the SPIHT source

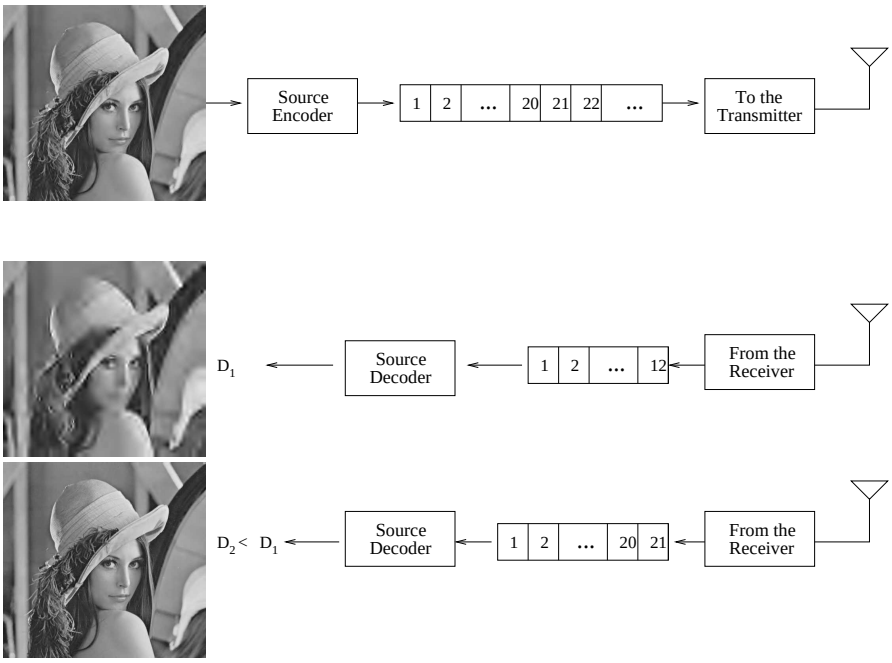

Figure 2.1: Scheme of a Lena image transmission to two different users, with different data rates at the receiver, and indeed different qualities of the received image.

coder over a binary symmetric channel (BSC) [20]. In particular, the authors considered a concatenation of outer cyclic redundancy check (CRC) codes for error detection and inner rate-compatible punctured (RCPC) codes for error correction in the transmission of the SPIHT-coded embedded bistream. The joint source channel image coder was shown to outperform previously reported techniques at that time. Unfortunately, the performance of this scheme was not satisfactory for certain physical channels, commonly observed in a mobile wireless environment. To improve the performance against deep fades in wireless channels, systematic Reed-Solomon (RS) codes across multiple packets were added [22]. The main weakness of this algorithm is that contiguous information symbols from the bitstream are packed in the same packets, leading to substantial lost in terms of quality if the first packets are not correctly received.

This high sensibility to packet loss was overcame by Sach et al. [26]. Although the authors still considered a CRC/RCPC time encoder and

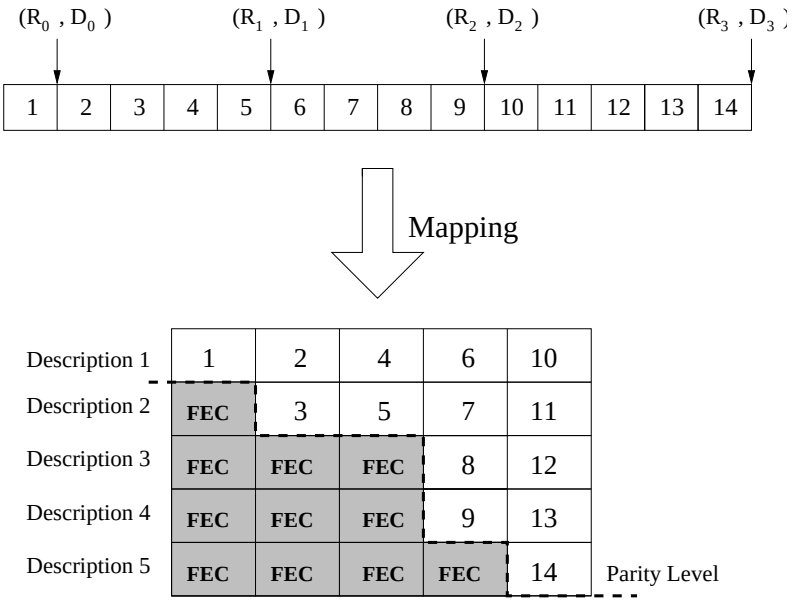

Figure 2.2: Illustration of the FEC-based multiple description coding technique for an embedded bistream with $n = 5$ descriptions.

RS codes across the packets, contiguous symbols from the bitstream were here spread across the packets rather than being distributed in the same packets. A priority encoding transmission (PET)-like model is assumed for the evaluation of the RS code rates. Since the first symbols are more important than the others, they required a lower code rate. This coding scheme is sometimes referred to as symmetric *n-channel FEC-based multiple description* (MD) coding. The basic concept of multiple description (MD) source coder is the generation of multiple bitstreams of the source such that each description individually describes the source with a certain level of fidelity. The main features of the MDs is that each description can be individually decoded and then combined with the other received and decoded MDs. It follows that, the more descriptions are correctly received, the higher is the quality of the decoded image, and also, the corruption of one description does not jeopardize the decoding of the correctly received descriptions. It is worth noting that in this algorithm, and also in the one proposed in the next sections, maximum distance separable (MDS) (n, k) erasure codes are considered, where k information

symbols are encoded into n channel symbols. In MDS codes, the minimum distance $d_{\min}$ equals $n-k+1$. Knowing that in each (n,k) codes, the reception of each $(n-d_{\min}+1)$ channel symbols allows to recover the k information symbols, in MDS codes, the k information symbols are recovered if any k channel symbols are correctly received. In Fig. 2.2, a general mechanism for converting an embedded bitstream from a source encoder into multiple descriptions is considered. In this example, $n=5$ descriptions are considered, and an UEP is assumed. Considering the first RS codeword, that is a $(5,1)$ codeword, the single information symbols can be reconstructed if up to 4 descriptions are lost. Is is worth noting that assuming all the descriptions equally important is an approximation, leading to a lower bound of the expected distortion. For example, receiving the first g out of n descriptions provides a lower distortion than the reception of the last g descriptions. In the MD scheme in Fig. 2.2, for example, receiving correctly the first three descriptions rather than the last three allows to recover up to eight information symbols rather than up to five. Anyway, since increasing the number of the descriptions the probability of a particular combination of the received packets is less likely, the descriptions are usually assumed *equally important*.

2.3 Channel model and time-frequency channel coding

As already mentioned in Section 1.3.3, the basic principle of OFDM is to split a high-rate data stream into a number of lower rate streams that are transmitted over overlapped but orthogonal subcarriers. Since the symbol duration increases for the lower rate parallel subcarriers, the relative amount of dispersion in time caused by multipath delay spread is decreased. Depending on the propagation environment and the channel characteristics, the resource block in an OFDM system can be used to exploit time and/or frequency diversities through channel coding. For time diversity, channel coding plus interleaving can be used in the time domain. However, for the technique to be effective, the time frame has to be greater than the channel coherence time $(\Delta t)_c$. The maximum time-

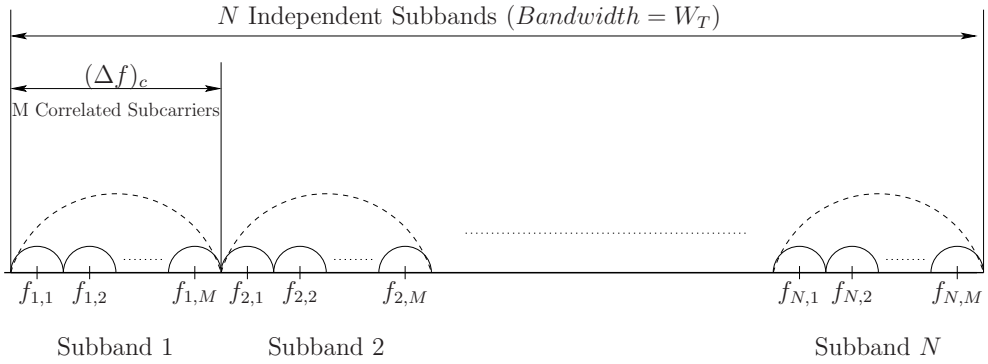

Figure 2.3: Subcarrier spectrum assignment.

diversity gain $\mathcal{D}_t$ is given by the ratio between the duration of a time frame and $(\Delta t)_c$.

In addition to time diversity, frequency diversity by adding redundancy across the subcarriers can be applied to combat channel errors. Generally, the maximum achievable frequency diversity $\mathcal{D}_f$ is given by the ratio between the overall system bandwidth W_T and the coherence bandwidth $(\Delta f)_c$.

In this chapter, we consider a frequency-selective environment and use a block fading channel model to simulate the frequency selectivity [38]. In this model, the spectrum is divided into blocks of size $(\Delta f)_c$. Subcarriers in different blocks are considered to fade independently; subcarriers in the same block experience identical fades. As illustrated in Fig. 2.3, we assume an OFDM system with an overall system bandwidth W_T, such that we can define N independent subbands. Each subband consists of M correlated subcarriers spanning a total bandwidth of $(\Delta f)_c$. The total number of subcarriers in the OFDM system is NM. In the time domain, we assume the channel experiences Rayleigh fading. We use the modified Jakes' model [39] to simulate different fading rates, resulting in different time diversity orders.

Fig. 2.4 illustrates the proposed scheme for transmission of an embedded bitstream over a mobile channel characterized by a doubly selective environment. In the frequency domain, $S_{tot} = NM$ symmetric descriptions of approximately equal importance are constructed in which

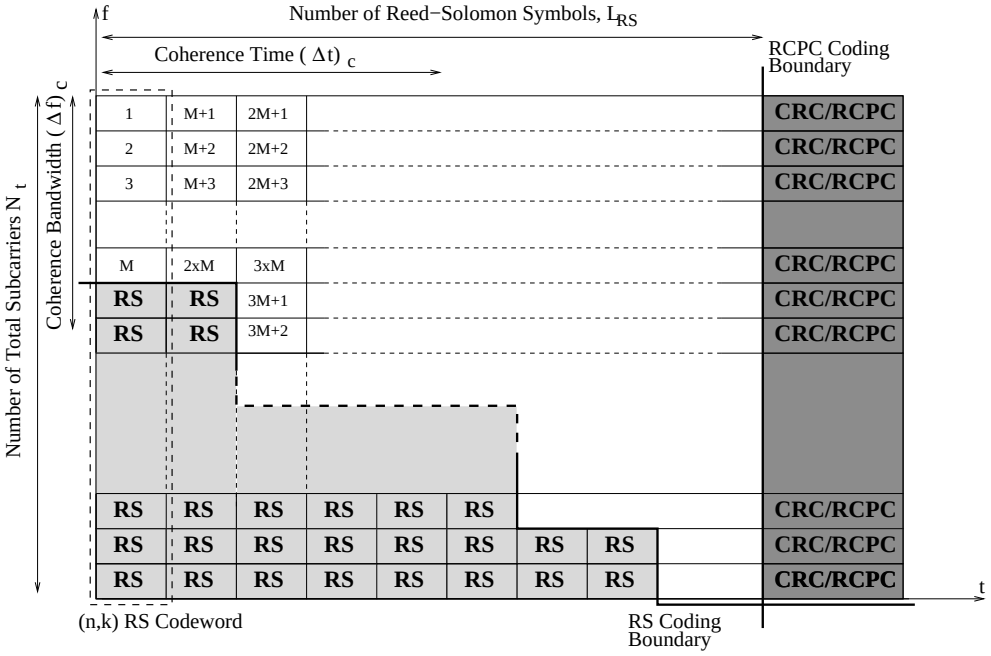

Figure 2.4: Transmission of the embedded bitstream over OFDM mobile wireless networks. The dark shaded area to the right of the RCPC coding boundary line represents the bits for CRC and RCPC coding. The lighter shaded area under the RS coding boundary staircase represents Reed-Solomon parity symbols. The unshaded area represents information symbols. Note that the CRC/RCPC parity symbols are interleaved with the RS symbols in the actual system. $N_t = N \times M$ total subcarriers and L_{RS} Reed-Solomon symbols are considered. For each (n, k) RS codeword, k information symbols are encoded into $n = N_t$ total symbols.

contiguous information from the embedded bitstream is spread across the multiple descriptions/packets [23, 24]. The algorithm adopted for the MD encoding is the one presented in [24]. In particular, because of the progressive nature of the encoded bitstream, MD encoding based on the priority of the bits in the bitstream is adopted, and the optimization of the FEC allocation in the frequency domain is designed to minimize the expected distortion. Specifically, the information symbols are protected by systematic (n, k) RS codes[1], with the level of protec-

[1]In each (n, k) RS codeword, k information symbols are encoded into n total symbols. While k is variable, n is constant in each codeword and equals N_t.

tion depending on the relative importance of the information symbols, as well as on the order of diversity available in the frequency domain. Generally, an (n, k) MDS erasure code can correct up to $n - k$ erasures. Hence, if *any* g out of n descriptions are received, those codewords with minimum distance $d_{min} \geq n - g + 1$ can be decoded. As a result, decoding is guaranteed at least up to distortion $D(R_g)$, where $D(R_g)$ refers to the distortion achieved with R_g information symbols.

The individual descriptions are then mapped to the $S_{tot} = NM$ subcarriers. A concatenation of CRC codes and RCPC codes, for possible diversity and coding gains in the time domain, are applied to each description. Since the descriptions are approximately equally important, RCPC codes with the same channel code rate can be applied to protect each individual description. This results in a vertical boundary (RCPC coding line), as illustrated in Fig. 2.4. The L_{RS} symbols on the left of the boundary are the RS symbols, while those on the right are CRC/RCPC parity symbols. It should be noted that the multiple description RS symbols and RCPC parity symbols would be interleaved in an actual system. However, for illustration, we show the de-interleaved version throughout the paper so that the relative amounts of RCPC parity symbols and RS symbols can be clearly indicated.

Since both forms of diversity are not necessarily simultaneously available at any given instant of time, the channel coding scheme should be designed to synergistically exploit the available diversity. For example, in a slow fading environment, channel coding plus interleaving is usually ineffective, especially for delay-sensitive applications such as real-time multimedia services. Hence, in this case, frequency diversity techniques may be more effective than time diversity techniques.

As stated previously, traditional studies of progressive transmission have concentrated on slow fading channels. In fact, in addition to the performance differences in channel coding efficiencies and channel estimation accuracies, the error patterns for different fade rates also affects the application layer throughputs and hence the end-user delivered quality. In particular, in a fast fading environment, the errors are more scattered among multiple packets due to the higher level crossing rate which mea-

Pros	Cons
Higher orders of time domain diversity	Larger channel estimation errors
⇒ higher coding gain	⇒ Lower channel decoding efficiency
⇒ higher diversity gain	Higher level crossing rates
	⇒ Errors scattered across multiple packets
	⇒ Lower application layer throughput

Table 2.1: Factors affecting the application layer quality-of-service (QoS) in a fast fading environment.

sures how often the fading crosses some threshold [40]. However, for a slow fading environment, the errors appear more bursty. Consequently, the application layer throughput, measured by the number of successively transmitted packets, of a fast fading environment can be dramatically lower than that of a slow fading system. In Table 2.1, we summarize the factors affecting the selection of an optimal channel coding scheme and end-user performance due to different fading rates.

On the other hand, information on frequency diversity can assist a source-channel codec in selecting a more robust source-cannel coding scheme [27]. For example, while unequal error protection (UEP) is considered as primarily important for robustness for some of the progressive transmission schemes proposed in the literature (e.g., [26]), it was shown that in a highly frequency selective environment, UEP only provides marginal improvement over equal error protection (EEP), while in a frequency diversity deficient system, UEP can greatly improve the performance of progressive transmission over an OFDM system.

2.4 ICI and channel estimation errors

The assumptions of perfect channel estimation and orthogonality between subcarriers cannot be considered accurate for fast fading environments. Rapid channel variations may cause severe ICI [41–43] and channel estimation errors, thereby degrading overall system performance. In this work, we model the ICI as in [41], i.e., a zero mean Gaussian random

process with variance σ^2_{ICI} expressed as

$$\sigma^2_{ICI} = E_s - \frac{E_s}{N_t^2}\left\{N_t + 2\sum_{i=1}^{N_t-1}(N_t - i)J_0(2\pi f_{nd} i)\right\} \tag{2.1}$$

where E_s is the modulated symbol energy, N_t is the number of subcarriers in the OFDM system, f_{nd} is the normalized Doppler spread and $J_0(\cdot)$ is the zero-order Bessel function of the first kind. The ICI varies directly with the Doppler frequency.

In addition to ICI, channel variations in the time domain may also increase the difficulty in channel estimation. The accuracy of this channel state information (CSI) is particularly important for coherent demodulation and channel decoding. We adopt pilot symbol assisted modulation (PSAM), commonly used in practical OFDM networks [29,30,44–48]. We refer the reader to [44] for details of PSAM and the analysis of channel estimation errors.

In this work, as shown in Fig. 2.5(a), pilot symbols are periodically inserted in the transmitted data symbols with a spacing equal to L modulated symbols. At the receiver, a linear minimum mean square error (MMSE) channel estimator [49] is adopted to estimate the fading coefficient using the following procedures: First, pilot symbols are extracted from the received sequence and the associated channel coefficients are evaluated. Then, the channel coefficient at the l-th data time ($l \neq jL$) is estimated by interpolating the K nearest pilot symbols with a Wiener filter. In particular, we consider $K = 2$, i.e., each channel parameter is estimated by interpolating the two closest pilot samples. Let us denote the received pilot symbol of the generic i-th slot[2] as $\widetilde{h}[iL]$ and assume that the l-th data symbol is transmitted in this i-th slot. Hence $\widetilde{\boldsymbol{h}} = [\widetilde{h}[iL], \widetilde{h}[(i+1)L]]^T$ is the set of two pilot symbols interpolated to estimate the l-th channel coefficient $h[l]$. Defining $\hat{h}[l]$ as the estimator of $h[l]$, the channel estimation errors can be expressed as

$$\varepsilon[l] = h[l] - \hat{h}[l], \quad l = iL \ldots (i+1)L - 1. \tag{2.2}$$

[2]The transmitted bitstream is divided into slots of length equal to the pilot spacing, i.e., L symbols. The first symbol of each slot is a pilot symbol, the other (L-1) symbols are data, as shown in Fig. 2.5.

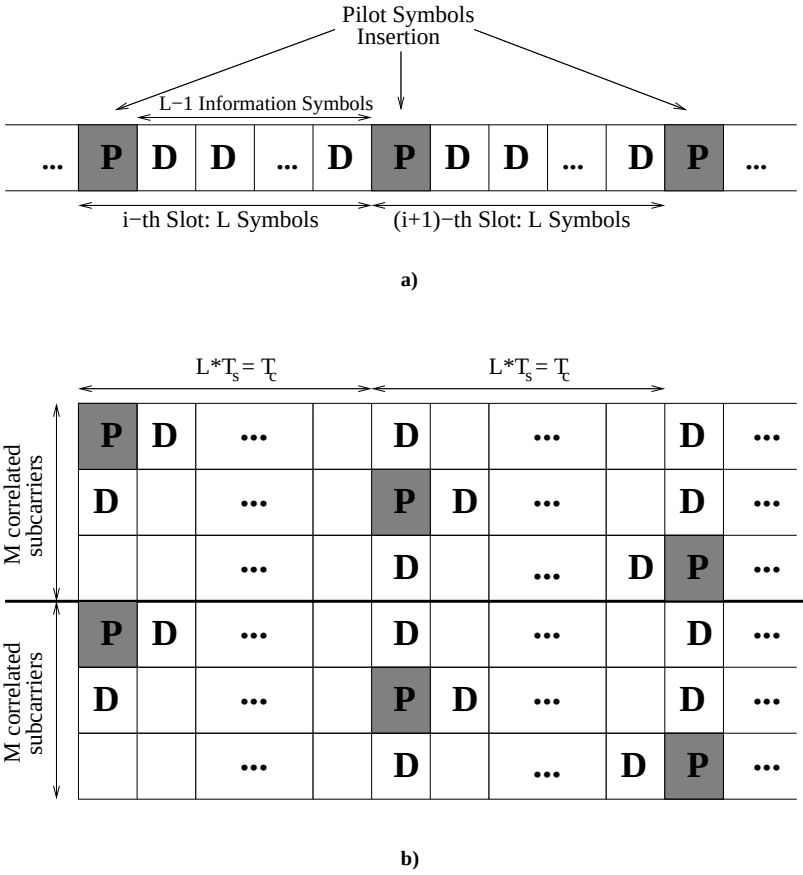

Figure 2.5: Pilot insertion scheme for systems with: (a) one correlated subcarrier; (b) M correlated subcarriers.

The quality of the estimation is expressed in terms of the mean square error $\sigma_e^2 = E[\varepsilon^2]$, where $E[\cdot]$ denotes the expectation operator. Defining $\boldsymbol{w}[l] = E[\widetilde{\boldsymbol{h}}h^*[l]]$ and $\boldsymbol{R} = E[\widetilde{\boldsymbol{h}}\widetilde{\boldsymbol{h}}^\dagger]$, the variance of the channel estimation errors can be expressed as [44] [30][3]

$$\sigma_e^2[l] = 1 - \boldsymbol{w}^\dagger[l]\boldsymbol{R}^{-1}\boldsymbol{w}[l], \tag{2.3}$$

where superscripts *, ^{T} and † stand for conjugate, transpose and transpose conjugate respectively. From (2.3), it can be seen that the estimation error variance depends on the channel correlation function.

[3]A multiplicative coefficient (the total average power of the channel impulse response) has been set equal to 1 and therefore ignored.

Recalling that we use a Jakes' model, the time correlation function is $r[n] = E[h[l]h^*[l+n]] \propto J_0(2\pi n f_{nd})$. This means that both the correlation function and the estimation error variance depend on the normalized Doppler frequency (f_{nd}). In particular, the channel estimation gets worse when the Doppler frequency increases. It is worthwhile to notice that the variance $\sigma_e^2[l]$ depends also on the received pilot samples $\widetilde{\boldsymbol{h}}$, and thus on the signal-to-noise-ratio (SNR).

In this work, the pilot and data symbols are transmitted at the same power level. Since a frequent pilot insertion improves channel estimation, at the cost of reduced throughput, a fixed pilot scheme for different Doppler frequency environments is not the best solution. Thus, we consider a pilot spacing equal to the coherence time. It follows that for a slow fading channel, the number of pilot symbols is negligible, leading to a high transmitted throughput. In high Doppler systems, to achieve good channel estimation, we have to reduce significantly the number of transmitted data symbols in each packet. Since under the block fading model, correlated subcarriers experience the same fading channel in the frequency domain, pilot symbols inserted once every coherence time are distributed among correlated subcarriers, as shown in Fig. 2.5(b). Thanks to this pilot scheme, the number of inserted pilot symbols decreases drastically in systems with low frequency diversity order.

2.5 Problem formulation

In this section, we describe the optimization problem to be solved. Consider N i.i.d. subbands, each with M subcarriers and packet size equal to L_{RS} code symbols before channel coding using RCPC/CRC codes. Since each vertical column corresponds to one RS codeword, there are altogether L_{RS} RS codewords. The constraint on the bit budget/packet can then be written as

$$(L_{RS} \times S_{tot} \times B_{RS} + B_{CRC})/R_{rcpc} \leq B_{tot}, \tag{2.4}$$

where B_{CRC} is the bit budget allocated for the CRC codes and R_{rcpc} is the channel code rate of the RCPC codes. B_{RS} is the number of bits-per-RS symbol and B_{tot} is the total bit budget of the RB.

We assume that for RS codeword l, where $l \in [1, L_{RS}]$, c_l code symbols are assigned to information data symbols. Hence, the number of RS parity symbols assigned to codeword l is

$$f_l = S_{tot} - c_l \qquad l \in [1, L_{RS}]. \tag{2.5}$$

Let ϕ_{th} be the minimum number of descriptions that a decoder needs to reconstruct the source, and g be the number of correctly received packets. The reception of any number of packets $g \geq \phi_{th}$ leads to improving image quality $D(R_g)$, where R_g is the allocated bit budget for the information symbols,

$$R_g = \sum_{\{l:c_l \leq g\}} c_l \times B_{RS}. \tag{2.6}$$

Hence, the overall RS channel code rate equals $R_{rs} = R_{S_{tot}}/(S_{tot} \times L_{RS} \times B_{RS})$. Given the source code rate-distortion curve $D(R_g)$ and the packet loss probability mass function $P_{\mathcal{J}}(j)$, where $j = S_{tot} - g$ is the number of lost packets, we can minimize the expected distortion as follows:

$$E^*[D] = \min_{\{c_l, R_{rcpc}\}} \left\{ \sum_{j=0}^{S_{tot}-\phi_{th}} P_{\mathcal{J}}(j) D(R_{S_{tot}-j}) + \sum_{j=S_{tot}-\phi_{th}+1}^{S_{tot}} P_{\mathcal{J}}(j) D_0 \right\} \tag{2.7}$$

subject to the constraint on the overall bit budget

$$\frac{R_{S_{tot}}/R_{rs} + B_{CRC}}{R_{rcpc}} \leq B_{tot} \tag{2.8}$$

where D_0 corresponds to the distortion when fewer than ϕ_{th} descriptions are received and so the decoder must reconstruct the source without being able to use any of the transmitted information. For a still image, this typically means reconstructing the entire image at the mean pixel value.

The packet loss probability mass function $P_{\mathcal{J}}(j)$ depends on $(\Delta f)_c$, $(\Delta t)_c$ and R_{rcpc}. Although $P_{\mathcal{J}}(j)$ can be found analytically for uncorrelated fading channels, due to the correlated fading in both time and frequency domains of the mobile environment considered here, we use simulations to find $P_{\mathcal{J}}(j)$. We use the iterative procedure described in [24] to solve the optimization problem (2.7).

2.6 Results and discussion

We carried out simulations on the 512×512 gray-scale images Lena, Peppers and Goldhill. Similar results were obtained for all three. Hence, in this paper, we only present the results using the Lena image. The image was encoded using the SPIHT [1] algorithm to produce an embedded bitstream. The serial bitstream was converted into 128 parallel bitstreams using the FEC-based multiple description encoder. The 128 descriptions were mapped to the OFDM system with 128 subcarriers. We used RS codes in the frequency domain and there were 8 bits per RS symbol. The packet size was set equal to 512 bits. We used QPSK modulation and considered both perfect and imperfect CSI. It should be noted that more sophisticated modulation schemes could be used to further improve the system performance, such as the one discussed in [50]. However, for the sake of simplicity and better understanding of the fundamental impact of the time and frequency diversities on the construction of the 2-D OFDM block, a fixed modulation scheme using QPSK was chosen. The RCPC codes of rates $R_{rcpc} = \frac{8}{9}, \frac{8}{10}, \ldots, \frac{8}{24}$, were obtained by puncturing an $R_c = 1/3$ mother code with $K = 7$, $p = 8$ and generator polynomials $(133, 165, 171)_{octal}$ with the puncturing table given in [51].

In the following figures, we illustrate the proposed channel coding scheme under different fading environments and study the effects of channel estimation on the selection by comparing performance of systems with perfect CSI to systems with imperfect CSI and ICI. From here onwards, for systems with imperfect CSI and ICI, ICI is omitted from the notation for sake of brevity, although it is considered as well. We begin by studying the optimized construction of RS information and parity symbols for

- Different values of RCPC coding rate,
- Both perfect and imperfect CSI, and
- Different frequency diversity orders and different fading rates.

Then we study how the received image PSNR varies for different Doppler spreads, for perfect and imperfect CSI, and for different frequency diversity orders.

In Fig. 2.6, we show the optimized construction of RS information symbols, RS parity symbols and RCPC parity symbols for different R_{rcpc}'s

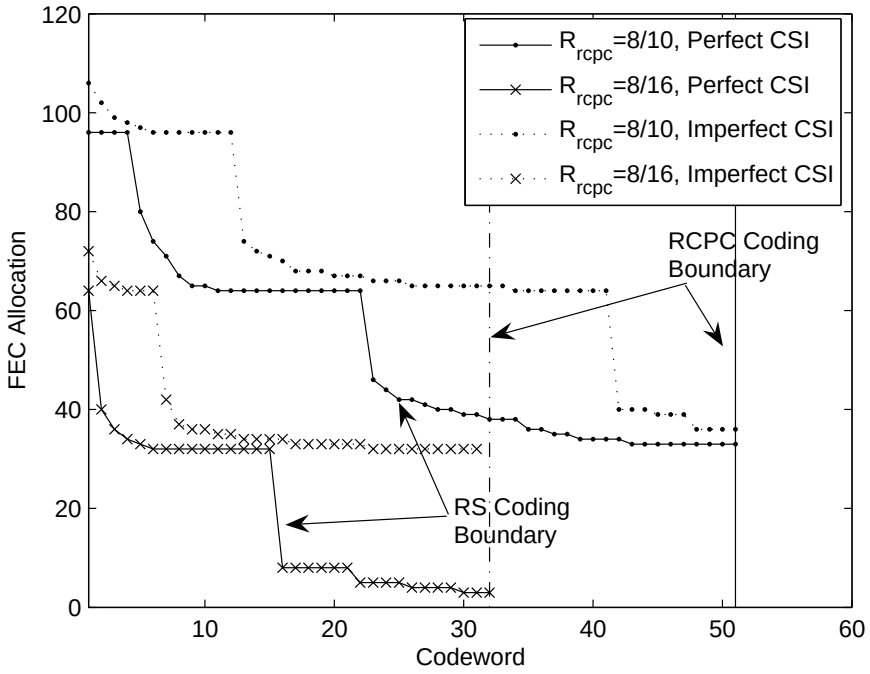

Figure 2.6: Profiles showing the optimal allocation of source and channel symbols for systems with $(N, M) = (4, 32)$, $f_{nd} = 10^{-3}$ and SNR = 16.0 dB for different choices of RCPC coding rates and for both perfect CSI and imperfect CSI.

for $(N, M) = (4, 32)$ and normalized Doppler spread $f_{nd} = 10^{-3}$ at SNR = 16 dB for systems with perfect CSI and imperfect CSI. The maximum order of diversity achieved in the frequency domain is $\mathcal{D}_f = 4$, while the maximum order of diversity in the time domain is $\mathcal{D}_t = 1$. In other words, no diversity can be exploited by using RCPC codes, although coding gain can still be obtained. In general, lower code rates in the time domain improve the packet loss performance, thus reducing the number of RS parity symbols required for minimizing the expected distortion $E[D]$, as can be noticed from the figures. Moreover, since for a fixed code rate in the time domain the perfect-CSI system outperforms the imperfect-CSI system, the latter system requires more protection in the frequency domain than does the perfect system.

As can be seen from Fig. 2.6, the RS code boundaries exhibit similar degree of tilting for both R_{rcpc} rates, and for both the perfect CSI and imperfect CSI systems for the same diversity order. As discussed in [27], the degree of tilt of the RS boundary indicates the importance of unequal error protection (UEP) relative to equal error protection (EEP) which has a horizontal RS boundary line. Hence, the results demonstrate that although the packet loss performance of an individual subcarrier can be improved by using a lower channel coding rate, the degree of UEP, represented by the tilt of the RS boundaries, mainly depends on the frequency diversity order of the system, and is relatively insensitive to the selection of the channel code rate in the time domain. In addition to the similar degree of tilting, the curves also show similar stepwise behavior. In particular, the RS boundaries show similar leveling behavior at approximately the same FEC value with step-size roughly equal to the coherence bandwidth. This observation agrees with the simulation results shown in [27] which is mainly due to, in addition to the same diversity order, the perfectly correlated fading within a subband in the frequency domain, which results in, with high probability, the simultaneous loss of the correlated subcarriers when a subband is under a deep fade.

In general, as the frequency diversity order increases, the variation of the number of lost packets decreases and thus reduces the need and hence the relative advantages of UEP, as shown in Fig. 2.7. In particular, in Fig. 2.7, we show the optimal allocation of source and channel symbols for imperfect CSI systems with different frequency diversity orders ($N = 1, 4, 32, 128$) in an environment with $f_{nd} = 10^{-2}$. The time domain channel code rate R_{rcpc} is fixed at $8/24$. As can be seen, in spite of significant difference in the time domain channel conditions due to the effect of fast fading and the time domain channel coding, similar behavior of the RS boundaries can still be observed when compared with the slow fading system reported in Fig.12 of [27]. Specifically, the amount RS code rate increases with the increasing frequency diversity order while the degree of UEP decreases with increasing frequency diversity order. Observe that at $N = 128$, the RS boundary is almost flat.

The tradeoff between RCPC codes and RS codes for both perfect and

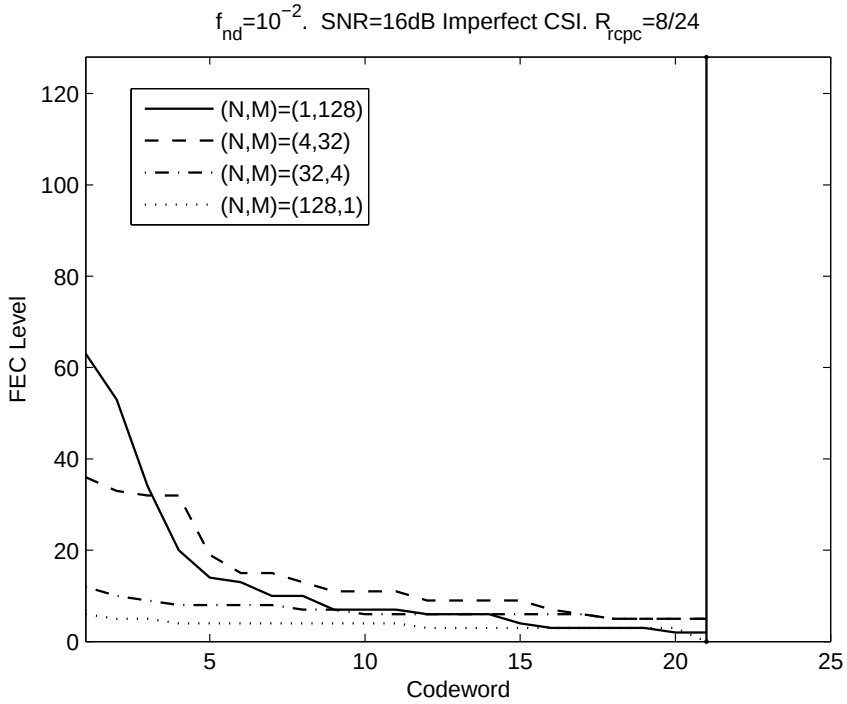

Figure 2.7: Profiles showing the optimal allocation of source and channel symbols for systems with $R_{rcpc} = 8/24$ and SNR = 16.0 dB and imperfect CSI for systems with frequency diversity orders $N = 1, 4, 32, 128$, respectively.

imperfect CSI is further illustrated in Fig. 2.8, where the optimal R_{rs} vs. R_{rcpc} is shown. By lowering the RCPC code rates, better packet loss performance is achieved due to the coding gain, and less protection in the frequency domain is required.

In Fig. 2.9, we plot the optimal peak-signal-to-noise ratio (PSNR) performances against R_{rcpc} for selected normalized Doppler spreads in systems with $(N, M) = (4, 32)$, SNR = 16 dB and imperfect CSI at the receiver. In the figure, for each selection of the time domain channel coding rate R_{rcpc}, the RS boundary is optimally constructed to maximize the delivered PSNR based on the frequency diversity order of the system. For comparison, in the plot, we also include the curves for the normalized Doppler spread with $f_{nd} = 10^{-1}$ and 10^{-4} with perfect CSI, representing

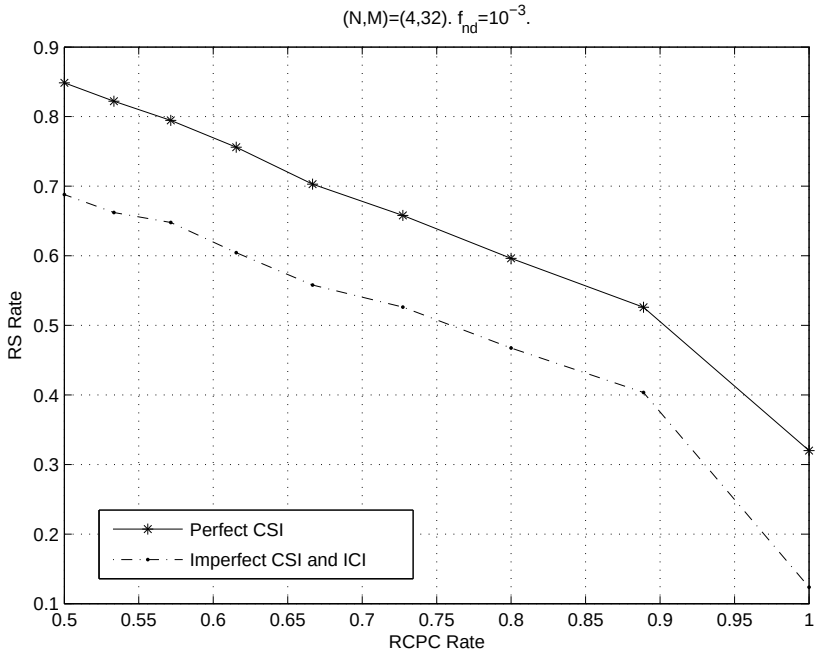

Figure 2.8: Optimal R_{rs} vs. R_{rcpc} for systems with $(N, M) = (4, 32)$, $f_{nd} = 10^{-3}$ SNR $= 16.0$ and both perfect and imperfect CSI.

the fast fading and slow fading scenarios with ideal channel estimation. As can be observed, the curve corresponding to of $f_{nd} = 10^{-4}$ with perfect CSI tracks the performance of the system with imperfect CSI closely, with minor degradation due to channel estimation errors. However, the curve corresponding to $f_{nd} = 10^{-1}$ and imperfect CSI deviates significantly from the system with perfect CSI due to the high channel estimation errors in a fast fading environment. It is worth mentioning that for the fast fading $f_{nd} = 10^{-1}$ environment and high signal-to-noise ratio, the system with imperfect CSI performs close to the perfect CSI system, indicating that extra redundancy can effectively compensate for channel estimation errors in a highly mobile scenario. Note that if the signal-to-noise ratio is low, even the lowest channel code rate in the time domain cannot sufficiently compensate for the effects of channel estimation errors.

Perhaps the more interesting observation is the crossovers among the curves with different fade rates. To explain crossovers, we look at the

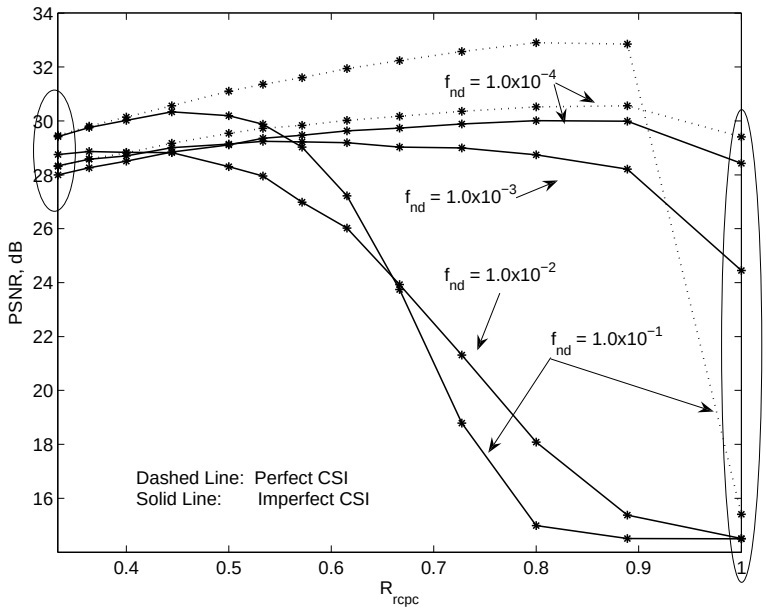

Figure 2.9: Optimized PSNR vs R_{rcpc} for different Doppler spreads in systems with $(N, M) = (4, 32)$, SNR = 16 dB and imperfect CSI.

two extremes of the plot, i.e., the highest and lowest time domain channel code rate $R_{rcpc} = 1$ and $R_{rcpc} = 0.333$. For the selected fade rates, at $R_{rcpc} = 0.333$, the PSNR performance increases monotonically with the fade rate, while the PSNR performance at $R_{rcpc} = 1$ shows a monotonic decreasing behavior with increasing fade rate. The different behaviors are due to the two countering effects on the system performance as a result of increasing fade rate. As stated previously, on the one hand, the increase in fade rate increases the diversity order in the time domain and hence the efficiency of the RCPC channel coding. However, on the other hand, due to the higher level crossing rate in a fast fading system, errors are scattered across multiple packets rather than being bursty. For systems with little or no channel coding in the time domain, this scattered nature of the error pattern can significantly increase the packet loss rate and reduce the application layer throughput. Consequently, the PSNR performance drops drastically, as can be noticed by the significant performance degradation for $f_{nd} = 10^{-1}$ and 10^{-2}. As we shall see below, due to the higher level crossing rate associated with fast fading environments,

the correct selection of an RCPC rate is more important for a fast fading system than for a slow fading system.

To further illustrate the effect of the error pattern on the PSNR performance, in Fig. 2.10, we plot the optimized PSNR performance vs. the normalized fading speed (f_{nd}) for $R_{rcpc} = 1$ for a system with a frequency diversity order $N = 16$ and SNR = 16 dB. We include the PSNR performance curves for both perfect CSI and imperfect CSI. As expected, the performance difference between perfect CSI and imperfect CSI widens as the fade rate increases due to the increasing channel estimation errors. However, more importantly, both curves show a monotonic decreasing behavior with an increasing fade rate due to the increasingly scattered error pattern. In the Appendix A, we provide some further analysis for the packet error rates due to the effects of error patterns resulting from different fading rates on the application layer throughput. In particular, by combining the threshold model [52] and the analysis on fade duration distribution [53, 54], we provide a simple analytic solution showing that for an uncoded system, the application layer throughput decreases exponentially with increasing fade rates due to the fact that deep fading events are shorter but occur more frequently.

In Fig. 2.11, we illustrate the effects of the frequency and time diversity orders on the selection of optimal coding schemes. In Fig. 2.11(a), we show the optimal PSNR performance vs. R_{rcpc} for different diversity orders ($N = 1, 2, \ldots, 128$) in a system with $f_{nd} = 10^{-3}$, SNR = 16 dB and imperfect CSI. In the figure, we also mark with a circle ($\circ$) the optimal R_{rcpc}. As the system experiences low Doppler spread with $\mathcal{D}_t = 1$ and channel estimation becomes more accurate, the selection of optimal coding schemes is dominated by the frequency diversity order of the system. As can be observed, generally a better performance can be achieved with a higher diversity order. More importantly, as the diversity order N increases, the optimal R_{rcpc} increases and the delivered image quality improves accordingly. Notice also that, except for the case $N = 1$, the PSNR performance curves are relatively flat around the optimal R_{rcpc}. To give a specific example, consider the PSNR performance curve for $N = 8$. Although $R_{rcpc} = 0.62$ gives the optimal performance, if $R_{rcpc} = 0.5$ or

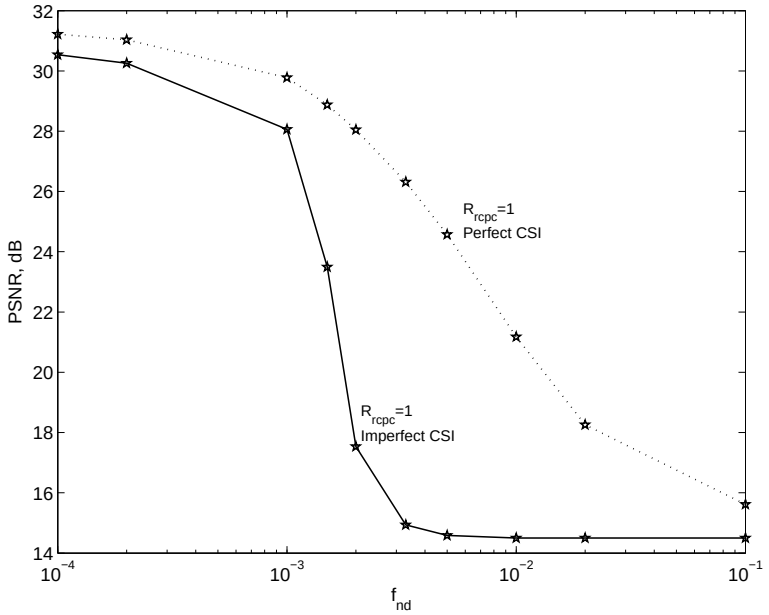

Figure 2.10: Optimized PSNR vs. f_{nd} for systems with $(N, M) = (16, 8)$, SNR = 16 dB and $R_{rcpc} = 1$ for perfect and imperfect CSI systems.

0.87 is selected instead, only minor degradation is suffered. This is because, in a slow fading environment, the performance loss due to the non-optimal selection of R_{rcpc} is partly compensated by the RS coding in the frequency domain. The results indicate that in a slow fading environment, by using the proposed 2D coding scheme, the results are relatively insensitive to the selection of R_{rcpc}, which can be selected on a broad range. The sub-optimal approach only sacrifices marginal performance degradation. The case $N = 1$ represents a flat fading environment, in which RS coding across the subcarriers becomes ineffective. The imperfect CSI system can now be compared to the perfect CSI system, reported in Fig. 2.11(b). As expected, since a slow fading channel is considered, the effects of ICI and estimation errors are negligible.

In Fig. 2.11(c), instead of a slow fading environment, we study the performance of under fast fading conditions. Specifically, we plot the optimal PSNR performance vs. R_{rcpc} for different frequency diversity orders for a fast fading system with $f_{nd} = 10^{-1}$, SNR = 16 dB and im-

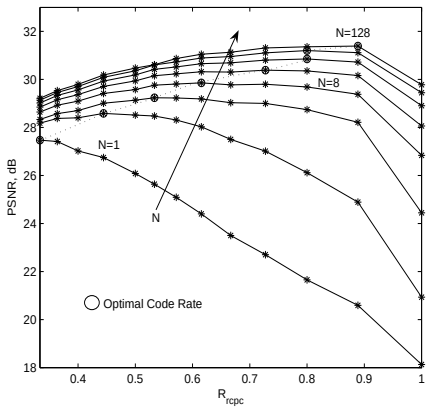

(a) $f_{nd} = 10^{-3}$, SNR = 16 dB and imperfect CSI.

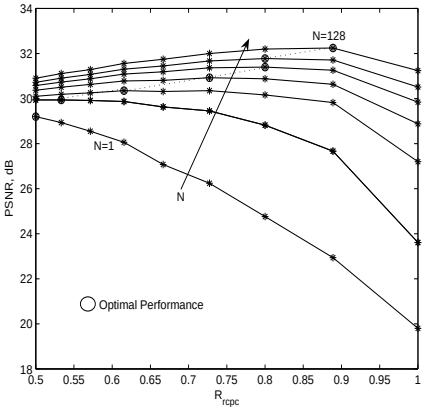

(b) $f_{nd} = 10^{-3}$, SNR = 16 dB and perfect CSI.

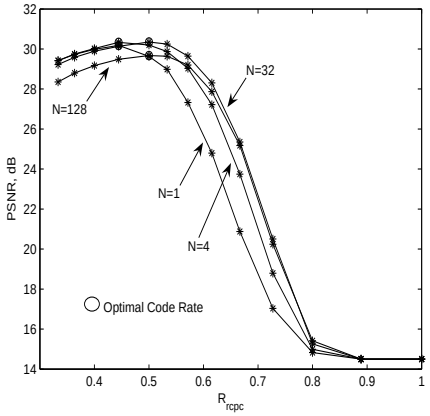

(c) $f_{nd} = 10^{-1}$, SNR = 16 dB and imperfect CSI.

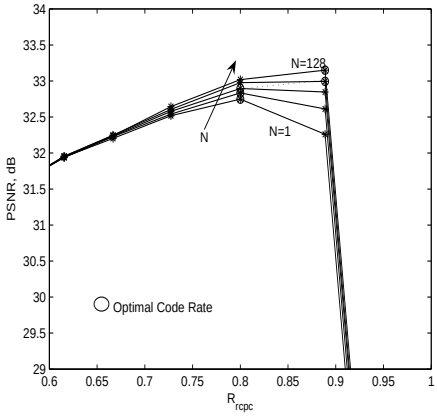

(d) $f_{nd} = 10^{-1}$, SNR = 16 dB and perfect CSI.

Figure 2.11: Optimized PSNR vs R_{rcpc} for different coherence bandwidths.

perfect CSI. As can be easily noticed, by comparing Fig. 2.11(c) with Fig. 2.11(a), the performance of a fast fading system is drastically different from that of a slow fading system due to a combination of higher diversity, more scattered errors and poorer channel estimation accuracy associated with fast fading environments. In particular, the system experiences a relatively flat region at low R_{rcpc} rates and a drastic drop in PSNR as it moves towards high R_{rcpc}. Observe that, although the system with a higher frequency diversity order generally provides a better perfor-

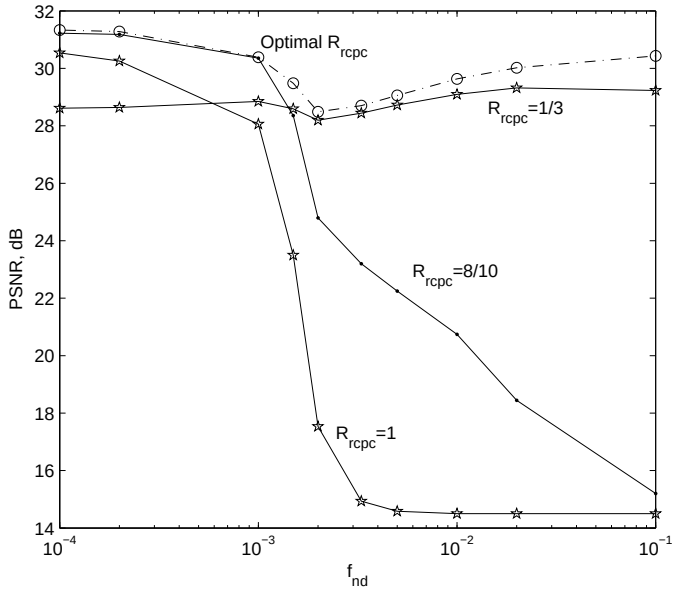

Figure 2.12: Optimized PSRN vs. f_{nd} for systems with $(N, M) = (16, 8)$, SNR = 16 dB and different RCPC code rates.

mance, unlike the slow fading systems, the optimal R_{rcpc}'s are relatively insensitive to the frequency diversity order. This is because in the time domain, the performance is dominated by the high time diversity gain, and thus PSNR depends only slightly on the frequency diversity order. Moreover, it is worth noting that, due to the high time diversity order, the time domain channel coding is very effective and the optimal channel code rate in the time domain is dominated by the channel estimation errors and ICI.

This can be illustrated by comparing Fig. 2.11(c) with Fig. 2.11(d). In Fig. 2.11(d), we plot the corresponding system with perfect CSI as opposed to the system with imperfect CSI shown in Fig. 2.11(c). Observe that, generally, high R_{rcpc}'s are preferred for better system performance. However, the performance is relatively insensitive to the frequency diversity order. Moreover, both systems exhibit precipitous drops in PSNR performance due to a more dispersed error pattern, leading to poor application layer throughput if the system is under-protected.

Now that the effects of slow or fast channel impairments has been observed, the motivation of this works can be better understand observing Fig. 2.12. Here, the PSNR as a function of the normalized Doppler is reported for a system with $(N, M) = (16, 8)$ for different RCPC code rates. In particular, systems with fixed RCPC code rates are compared to the system adopting the optimal code rates in both time and frequency domain. It is worth noting that a low temporal code rate (i.e. $R_{rcpc} = 1/3$) achieves good performance for fast fading systems, but it represent a waste of resources for low Doppler values. Note that, since the constraint (2.8) is imposed, by lowering the RCPC code rate, the maximum number of information symbols that can be transmitted decreases. Conversely, the system experiencing a high code rate (i.e., $R_{rcpc} = 1, 8/10$) is robust to the channel impairments in slow channel systems. As well as the Doppler increases, a drop of the overall performance occurs. Hence, the good performance of the system adopting the optimal RCPC code rate can be observed. Although the normalized doppler varies, the system is able to sufficiently protect the transmitted packets over wireless channel, without wasting information symbols.

In Fig. 2.13(a) and Fig. 2.13(b), we show the optimized PSNR vs. both normalized Doppler spread f_{nd} and the number of independent subbands (N) using the proposed coding scheme for a 2D time-frequency OFDM resource block with perfect and imperfect CSI, respectively. The SNR is set to 16 dB. As can be observed from Fig. 2.13(a), without channel estimation errors, systems with greater diversity opportunities in time and/or frequency domains generally give better performance. However, more importantly, observe the relatively stable performance under different physical environments. Only for both low Doppler and flat fading environments does the system perform poorly. For other values of frequency and time diversity, the PSNR provided is always more than 30dB, even in the case of systems with low time or low frequency diversity order.

In Fig. 2.13(b), we plot the corresponding system with imperfect CSI. Complicated by the effects of channel estimation errors, the optimal performance becomes more irregular. While in general systems with higher

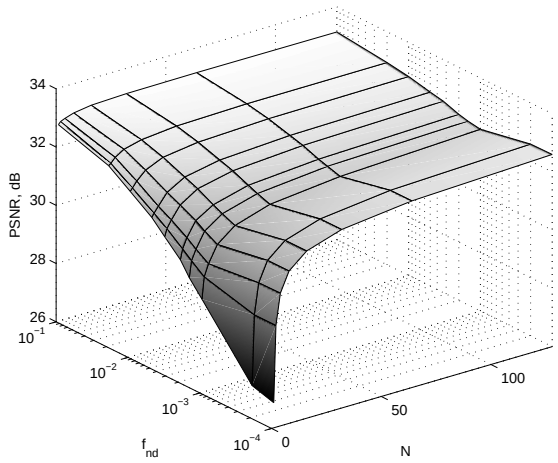

(a)

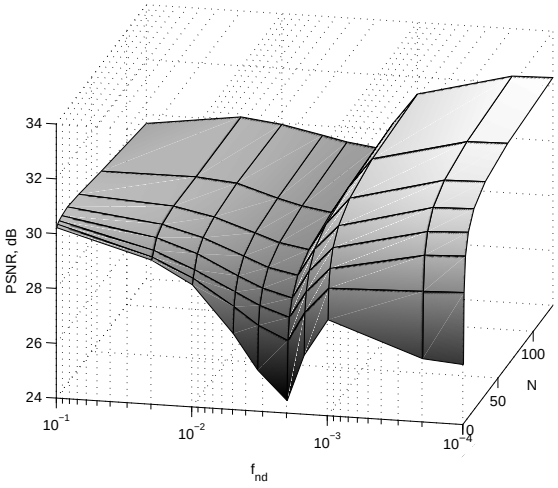

(b)

Figure 2.13: Optimal PSNR performances vs. both N and f_{nd} in systems with SNR = 16 dB for both perfect CSI systems (a) and imperfect CSI systems (b).

frequency diversity orders outperform systems with lower frequency diversity orders, some irregularities are observed in the time domain. In particular, the PSNR drops with decreasing fade rate and starts to rise

again at fade rates around 10^{-2} and 10^{-3}. To have a better understanding of the optimal behavior, in Fig. 2.14 we show the optimal PSNR performance vs. f_{nd} for systems with two different frequency diversity orders, $\mathcal{D}_f = 4$ and $\mathcal{D}_f = 32$. The SNR is set to 16 dB. The OFDM resource block is constructed with optimal RS profiles and RCPC rates based on the proposed scheme. For comparison, systems with both perfect and imperfect CSI are considered. By first looking at the slow fading section, i.e., the region with $f_{nd} < 10^{-3}$, it can be observed that the optimal PSNR performances are relatively flat, with some degradation in the systems with imperfect CSI due to channel estimation errors. The performance gap between the perfect CSI and imperfect CSI in this region is relatively small due to better channel estimation accuracy in a slow fading environment. At the middle section, i.e., $(10^{-3} < f_{nd} < 10^{-2})$, the drops in PSNR performance are steepened for systems with imperfect CSI, due to the combined effects of low time diversity gain, increasing channel estimations errors, and the impact of the more scattered nature of the error pattern. For $f_{nd} > 10^{-2}$, the large channel variations provide significant time diversity gain which improves the efficiency of the RCPC codes and partly compensate for the performance loss due to the channel estimation errors.

Finally, results in terms of reconstructed images in Fig. 2.15 for systems with $f_{nd} = 10^{-1}$, $(N, M) = (32, 4)$, and imperfect CSI, provide some subjective comparisons. Here, the advantage of the proposed scheme and the effect of channel impairments under a fast fading environment can be observed by comparing the reconstructed images with the original one. The five reconstructed images (Fig. 2.15(b)-(f)) represent 5 different simulated results based on 5 different RCPC code rates. In each of the cases, the corresponding RS boundary is optimally selected based on the chosen RCPC code rate. Fig. 2.15(c) shows the result for optimal channel coding for the 2D time-frequency OFDM block. It can be shown that the choice of the optimal 2D channel coding which includes the proper selections of RCPC codes in the time domain and RS boundary in the frequency domain turns out to be critical. As can be observed, RCPC code rates higher than 0.66 do not provide sufficient protection against the degra-

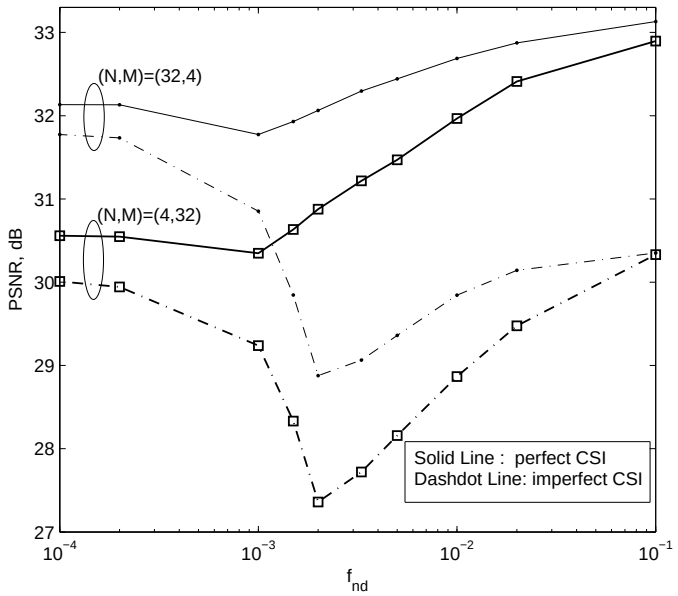

Figure 2.14: Optimized PSNR vs. f_{nd} for systems with SNR = 16 dB and both perfect and imperfect CSI. Two different frequency diversity order are considered: $(N, M) = (32, 4)$ and $(N, M) = (4, 32)$.

dation caused by the imperfect channel estimation and the intercarrier interference that the system experiences at high Doppler. Conversely, when an extremely low code rate is chosen, the system might be over protected, leading to too low a source rate.

In Table 2.2 and Table 2.3, by defining the total/combined channel code rate as $R_{tot} = R_{rcpc} \cdot R_{rs}$ and the total system diversity order available as $\mathcal{D}_{tot} = \mathcal{D}_f \cdot \mathcal{D}_t$, we provide further analysis regarding the proposed 2D channel coding scheme. In particular, in Table 2.2, the optimal PSNR, R_{rcpc}, R_{rs}, and R_{tot} are presented for a system with SNR = 16dB[4], perfect CSI and different diversity orders in both the time and frequency domains. In each row, we keep $\mathcal{D}_{tot}$ fixed and investigate the corresponding performance for different combinations of $\mathcal{D}_f$ and $\mathcal{D}_t$. To provide a specific comparison, consider systems with $\mathcal{D}_{tot}$ equal to 4. Obviously,

[4]Although only SNR = 16dB is reported, we also considered other SNR values and behavior similar to the one for SNR = 16dB were observed.

this can be achieved with three different combinations: $(\mathcal{D}_f = 4, \mathcal{D}_t = 1)$, $(\mathcal{D}_f = 2, \mathcal{D}_t = 2)$, and $(\mathcal{D}_f = 1, \mathcal{D}_t = 4)$. Generally, as expected, the higher the total diversity, the better is the quality of the received image, and the less is the required redundancy, which is reflected by the increase in combined channel coding rate R_{tot}. Comparing a system with no diversity to a system with $\mathcal{D} = 2$, a substantial gain in terms of PSNR can be observed (at least 2dB), although the gain diminishes with increasing diversity orders. This is because, although the error rate of a wireless communication system is generally a strictly decreasing function of the order of diversity, the gain diminishes with increasing order of diversity [55]. What is worth noting from the table is the behavior of optimal PSNR and R_{tot} for a constant total diversity order. Specifically, it can be seen that for a given $\mathcal{D}_{tot}$, with perfect CSI, both the optimal PSNR and the R_{tot} are roughly constant for all the possible combinations of $\mathcal{D}_f$ and $\mathcal{D}_t$, independent of whether the diversity gain comes from the frequency domain or time domain.

In Table 2.3, we provide a similar study for a system with imperfect CSI. Similarly to the observation above, we see an enhancement of the performance with an increase of the total diversity. However, for a fixed $\mathcal{D}_{tot}$, moving from slow fading to fast fading results in a decrease of the optimal PSNR, because of the channel estimation errors. Thus, for a fixed total order of diversity, the system with maximum frequency diversity order performs better than the system with maximum time diversity order.

Table 2.2: Optimal PSNR, R_{rcpc}, R_{rs}, and R_{tot} for a system with perfect CSI, SNR = 16dB and different diversity order in both time and frequency domains.

DIVERSITY ORDER=1: $(N = 1, f_{nd} = 10^{-4})$			
psnr = 27.28 dB $R_{rcpc} = 0.36$, $R_{rs} = 0.91$ $R_{tot} = 0.33$			
DIVERSITY ORDER $= 2$			
$\mathcal{D}_f = 2, \mathcal{D}_t = 1 \quad (N = 2, f_{nd} = 10^{-4})$ psnr = 29.49 dB $R_{rcpc} = 0.73$, $R_{rs} = 0.69$ $R_{tot} = 0.50$	$\mathcal{D}_f = 1, \mathcal{D}_t \sim 2 \quad (N = 1, f_{nd} = 3, 3 \cdot 10^{-3})$ psnr = 30.71 dB $R_{rcpc} = 0.53$, $R_{rs} = 0.95$ $R_{tot} = 0.51$		
DIVERSITY ORDER $= 4$			
$\mathcal{D}_f = 4, \mathcal{D}_t = 1$ $(N = 4, f_{nd} = 10^{-4})$ psnr = 30.55 dB $R_{rcpc} = 0.89$, $R_{rs} = 0.60$ $R_{tot} = 0.54$	$\mathcal{D}_f = 2, \mathcal{D}_t \sim 2$ $(N = 2, f_{nd} = 3, 3 \cdot 10^{-3})$ psnr = 30.96 dB $R_{rcpc} = 0.61$, $R_{rs} = 0.89$ $R_{tot} = 0.54$	$\mathcal{D}_f = 1, \mathcal{D}_t \sim 4$ $(N = 1, f_{nd} = 8 \cdot 10^{-3})$ psnr = 31.38 dB $R_{rcpc} = 0.67$, $R_{rs} = 0.92$ $R_{tot} = 0.61$	
DIVERSITY ORDER $= 8$			
$\mathcal{D}_f = 8, \mathcal{D}_t = 1$ $(N = 8, f_{nd} = 10^{-4})$ psnr = 31.23 dB $R_{rcpc} = 0.90$, $R_{rs} = 0.65$ $R_{tot} = 0.58$	$\mathcal{D}_f = 4, \mathcal{D}_t \sim 2$ $(N = 4, f_{nd} = 3.3 \cdot 10^{-3})$ psnr = 31.22 dB $R_{rcpc} = 0.73$, $R_{rs} = 0.78$ $R_{tot} = 0.57$	$\mathcal{D}_f = 2, \mathcal{D}_t \sim 4$ $(N = 2, f_{nd} = 8 \cdot 10^{-3})$ psnr = 31.59 dB $R_{rcpc} = 0.73$, $R_{rs} = 0.83$ $R_{tot} = 0.60$	$\mathcal{D}_f = 1, \mathcal{D}_t \sim 8$ $(N = 1, f_{nd} = 1.5 \cdot 10^{-2})$ psnr = 32.01 dB $R_{rcpc} = 0.73$, $R_{rs} = 0.92$ $R_{tot} = 0.67$
DIVERSITY ORDER $= 16$			
$\mathcal{D}_f = 16, \mathcal{D}_t = 1$ $(N = 16, f_{nd} = 10^{-4})$ psnr = 31.75 dB $R_{rcpc} = 0.89$, $R_{rs} = 0.70$ $R_{tot} = 0.62$	$\mathcal{D}_f = 8, \mathcal{D}_t \sim 2$ $(N = 8, f_{nd} = 3.3 \cdot 10^{-3})$ psnr = 31.64 dB $R_{rcpc} = 0.73$, $R_{rs} = 0.82$ $R_{tot} = 0.60$	$\mathcal{D}_f = 4, \mathcal{D}_t \sim 4$ $(N = 4, f_{nd} = 8 \cdot 10^{-3})$ psnr = 31.82 dB $R_{rcpc} = 0.73$, $R_{rs} = 0.88$ $R_{tot} = 0.64$	$\mathcal{D}_f = 1, \mathcal{D}_t \sim 16$ $(N = 1, f_{nd} = 3 \cdot 10^{-2})$ psnr = 32.37 dB $R_{rcpc} = 0.73$, $R_{rs} = 0.95$ $R_{tot} = 0.69$
DIVERSITY ORDER $= 32$			
$\mathcal{D}_f = 32, \mathcal{D}_t = 1$ $(N = 32, f_{nd} = 10^{-4})$ psnr = 32.13 dB $R_{rcpc} = 0.89$, $R_{rs} = 0.75$ $R_{tot} = 0.67$	$\mathcal{D}_f = 16, \mathcal{D}_t \sim 2$ $(N = 16, f_{nd} = 3.3 \cdot 10^{-3})$ psnr = 32.03 dB $R_{rcpc} = 0.80$, $R_{rs} = 0.81$ $R_{tot} = 0.64$	$\mathcal{D}_f = 8, \mathcal{D}_t \sim 4$ $(N = 8, f_{nd} = 8 \cdot 10^{-3})$ psnr = 32.16 dB $R_{rcpc} = 0.80$, $R_{rs} = 0.83$ $R_{tot} = 0.66$	$\mathcal{D}_f = 4, \mathcal{D}_t \sim 8$ $(N = 4, f_{nd} = 1.5 \cdot 10^{-2})$ psnr = 32.23 dB $R_{rcpc} = 0.73$, $R_{rs} = 0.93$ $R_{tot} = 0.68$

Table 2.3: Optimal PSNR, R_{rcpc}, R_{rs}, and R_{tot} for a system with imperfect CSI, SNR = 16dB and different diversity order in both time and frequency domains.

DIVERSITY ORDER=1: $(N = 1, f_{nd} = 10^{-4})$			
psnr = 26.15 dB $R_{rcpc} = 0.33$, $R_{rs} = 0.90$ $R_{tot} = 0.30$			
DIVERSITY ORDER = 2			
$\mathcal{D}_f = 2, \mathcal{D}_t = 1 \quad (N = 2, f_{nd} = 10^{-4})$ psnr = 28.75 dB $R_{rcpc} = 0.61$, $R_{rs} = 0.67$ $R_{tot} = 0.41$	$\mathcal{D}_f = 1, \mathcal{D}_t \sim 2 \quad (N = 1, f_{nd} = 3, 3 \cdot 10^{-3})$ psnr = 25.47 dB $R_{rcpc} = 0.33$, $R_{rs} = 0.72$ $R_{tot} = 0.24$		
DIVERSITY ORDER = 4			
$\mathcal{D}_f = 4, \mathcal{D}_t = 1$ $(N = 4, f_{nd} = 10^{-4})$ psnr = 30.00 dB $R_{rcpc} = 0.80$, $R_{rs} = 0.58$ $R_{tot} = 0.47$	$\mathcal{D}_f = 2, \mathcal{D}_t \sim 2$ $(N = 2, f_{nd} = 3, 3 \cdot 10^{-3})$ psnr = 27.06 dB $R_{rcpc} = 0.33$, $R_{rs} = 0.70$ $R_{tot} = 0.23$	$\mathcal{D}_f = 1, \mathcal{D}_t \sim 4$ $(N = 1, f_{nd} = 8 \cdot 10^{-3})$ psnr = 28.13 dB $R_{rcpc} = 0.33$, $R_{rs} = 0.87$ $R_{tot} = 0.28$	
DIVERSITY ORDER = 8			
$\mathcal{D}_f = 8, \mathcal{D}_t = 1$ $(N = 8, f_{nd} = 10^{-4})$ psnr = 30.74 dB $R_{rcpc} = 0.89$, $R_{rs} = 0.59$ $R_{tot} = 0.52$	$\mathcal{D}_f = 4, \mathcal{D}_t \sim 2$ $(N = 4, f_{nd} = 3.3 \cdot 10^{-3})$ psnr = 27.72 dB $R_{rcpc} = 0.36$, $R_{rs} = 0.66$ $R_{tot} = 0.24$	$\mathcal{D}_f = 2, \mathcal{D}_t \sim 4$ $(N = 2, f_{nd} = 8 \cdot 10^{-3})$ psnr = 28.48 dB $R_{rcpc} = 0.36$, $R_{rs} = 0.82$ $R_{tot} = 0.29$	$\mathcal{D}_f = 1, \mathcal{D}_t \sim 8$ $(N = 1, f_{nd} = 1.5 \cdot 10^{-2})$ psnr = 28.94 dB $R_{rcpc} = 0.36$, $R_{rs} = 0.90$ $R_{tot} = 0.33$
DIVERSITY ORDER = 16			
$\mathcal{D}_f = 16, \mathcal{D}_t = 1$ $(N = 16, f_{nd} = 10^{-4})$ psnr = 31.33 dB $R_{rcpc} = 0.89$, $R_{rs} = 0.65$ $R_{tot} = 0.58$	$\mathcal{D}_f = 8, \mathcal{D}_t \sim 2$ $(N = 8, f_{nd} = 3.3 \cdot 10^{-3})$ psnr = 28.22 dB $R_{rcpc} = 0.36$, $R_{rs} = 0.71$ $R_{tot} = 0.26$	$\mathcal{D}_f = 4, \mathcal{D}_t \sim 4$ $(N = 4, f_{nd} = 8 \cdot 10^{-3})$ psnr = 28.75 dB $R_{rcpc} = 0.36$, $R_{rs} = 0.83$ $R_{tot} = 0.30$	$\mathcal{D}_f = 1, \mathcal{D}_t \sim 16$ $(N = 1, f_{nd} = 3 \cdot 10^{-2})$ psnr = 29.79 dB $R_{rcpc} = 0.44$, $R_{rs} = 0.88$ $R_{tot} = 0.39$
DIVERSITY ORDER = 32			
$\mathcal{D}_f = 32, \mathcal{D}_t = 1$ $(N = 32, f_{nd} = 10^{-4})$ psnr = 31.77 dB $R_{rcpc} = 0.89$, $R_{rs} = 0.70$ $R_{tot} = 0.62$	$\mathcal{D}_f = 16, \mathcal{D}_t \sim 2$ $(N = 16, f_{nd} = 3.3 \cdot 10^{-3})$ psnr = 28.70 dB $R_{rcpc} = 0.44$, $R_{rs} = 0.66$ $R_{tot} = 0.29$	$\mathcal{D}_f = 8, \mathcal{D}_t \sim 4$ $(N = 8, f_{nd} = 8 \cdot 10^{-3})$ psnr = 29.23 dB $R_{rcpc} = 0.44$, $R_{rs} = 0.75$ $R_{tot} = 0.33$	$\mathcal{D}_f = 4, \mathcal{D}_t \sim 8$ $(N = 4, f_{nd} = 1.5 \cdot 10^{-2})$ psnr = 29.26 dB $R_{rcpc} = 0.44$, $R_{rs} = 0.77$ $R_{tot} = 0.34$

2.7 Conclusion

We studied channel coding in a 2D time-frequency resource block of an OFDM system. In particular, we used symmetric n-channel FEC-based multiple descriptions based on the diversity order in the frequency

domain. In the time domain, a concatenation of RCPC codes and CRC codes was employed to protect individual descriptions. We studied the performance of the proposed system in a doubly-selective channel with channel estimation errors. In a slow-fading environment, it was shown as the frequency diversity order increases, the optimal R_{rcpc} increases and the delivered image quality improves accordingly. On the other hand, in a fast-fading environment, the optimal R_{rcpc} is relatively insensitive to the frequency diversity order while the performance is limited by the channel estimation errors and ICI. It was also illustrated that the advantages of UEP protection diminishes as the frequency diversity order increases in both slow and fast fading environment. Thus, since both the optimal R_{rcpc} and R_{rs} vary depending on the channel conditions, a system can be robust only employing a 2D channel coding adaptable to both time and frequency diversity orders. Lastly, we illustrated that the bursty nature of a slow fading environment can lead to a higher application layer throughput and thereby deliver a better image quality while the scattered error pattern in a fast fading environment may lead to poor image quality.

(a) Original Image.

(b) Received Image. $R_{rcpc} = 0.33, R_{rs} = 0.99, \text{PSNR} = 29.0$ dB, $R_{\text{TX}} = 0.08$ bpp, $R_{\text{RX}} = 0.073$ bpp.

(c) Received Image. **Optimal Rate**. $R_{rcpc} = 0.5, R_{rs} = 0.89, \text{PSNR} = 30.5$ dB, $R_{\text{TX}} = 0.15$ bpp, $R_{\text{RX}} = 0.1$ bpp.

(d) Received Image. $R_{rcpc} = 0.66, R_{rs} = 0.18, \text{PSNR} = 25.35$ dB, $R_{\text{TX}} = 0.03$ bpp, $R_{\text{RX}} = 0.02$ bpp.

(e) Received Image. $R_{rcpc} = 0.73, R_{rs} = 0.03, \text{PSNR} = 20.5$ dB, $R_{\text{TX}} = 0.007$ bpp, $R_{\text{RX}} = 0.004$ bpp.

(f) Received Image. $R_{rcpc} = 1, R_{rs} = 0.008, \text{PSNR} = 14.5$ dB, $R_{\text{TX}} = 0.001$ bpp, $R_{\text{RX}} = 10^{-5}$ bpp.

Figure 2.15: Image quality for a system with $f_{nd} = 10^{-1}$, $(N, M) = (32, 4)$, SNR = 16 dB, and imperfect CSI. We denote by R_{TX} the transmitted source rate and by R_{RX} the received source rate.

Chapter 3

Joint source and channel coding for motion-compensated fine granularity scalable video

The previously investigated channel coding optimization is here extended to a joint source and channel coding optimization for video transmissions. Cross-layer motion-compensated multiple descriptions coding for progressive video bitstream is investigated. Based on the diversity order offered by the channel in both time and frequency domain, the optimal compression rate and channel code rates are evaluated.

The remainder of the chapter is organized as follows. In Section 3.1, a description of progressive video bitstreams, together with a brief overview of the multiple description coding, is reported. In Section 3.2, we provide a detailed description of FGS video, considering motion compensation with leaky prediction. In Section 3.3, we describe OFDM systems and the channel model considered in our analysis. In Section 3.4, we provide a framework for the construction of n-channel symmetric motion-compensated MD coding and we formulate the optimization problem, describing the rate-distortion evaluation algorithm adopted. In Section 3.5, we provide simulation results and discussion. Finally, in Section 3.6, we provide a summary and conclusion.

3.1 Motivation and outline of the work

Due to the increasing demand for multimedia services on mobile terminals, and the recent advances in mobile computing, video services are expected to be widely deployed. Moreover, the rising of Internet and wireless communications has widely increased the diffusion of heterogeneity in multiuser systems, and modern studies are focused on meeting each user requirement at the same time. To this aim, network-adaptive scalable video coding and cross-layer optimization have been under intense research [56–60]. Note that, in the past, the aim of video coding was the optimization of the video quality *at a given bit rate*. The encoder should compress the video bitstream to a fixed bit rate, less and hopefully close to the channel capacity, and the decoder should be able to reconstruct the video source from the received bit rate. However, the channel capacity is an information not always available, and unknown is also the bit rate to which optimize the compression. Moreover, due to channel impairments in wireless transmissions, the received data rate is variable, resulting to be a function of the channel conditions. Thus, the decoder has to be able to reconstruct the video from several ranges of received bit rate. For these reasons, the aim of video coding studies is changed to optimizing the video quality over *a given bit rate range* instead of a given bit rate [61–64], meeting the requirements of heterogenous networks.

Moving Pictures Experts Group (MPEG) has provided scalable video coding schemes to accommodate the various levels of picture quality depending on the transmission environments and the performances of the user-level terminals [65], and has also put its considerations in a new advanced video coding standard with ITU-T for broadcasting and internet multimedia services [66]. In scalable coding techniques (SNR, temporal or spatial scalability), adopted in the MPEG-2 for example [67–69], the compressed bitstream is partitioned into a Base Layer (BL) and an Enhanced Layer (EL). The main weakness of this layered scalable coding is that the EL can be either entirely transmitted/received/decoded or it does not provide any enhancement at all. To address this limitation of earlier scalable video coding standards, the Fine Granularity Scalable (FGS) video coding technique was introduced. In addition to the Base

Layer, FGS consists of a single Enhanced Layer encoded in a progressive manner. Although the BL is encoded at a certain rate R_{BL}, such that the minimum received bandwidth is higher than R_{BL} ($R_{\mathrm{BL}} \leq R_{\min}$), the EL can be compressed over any desired bit rate range $[R_{\min}, R_{\max}]$. Thanks to the progressive nature of the enhanced layer, the decoder is able to reconstruct the EL at *any* received bit rate, i.e., the EL can be truncated at any arbitrary location. While in scalable video coding the EL is entirely received or lost, in the FGS, any portion of the EL correctly received improves the quality of the decoded video bitstream. Note that, as deeply described in the previous chapter, a MD coding improves the robustness of the system, and so even of the transmitted EL[1] [27, 70, 71]. However, even considering more reliable transmissions, scalable video standards still preserve their limit.

Most state-of-the-art video codecs incorporate motion-compensated prediction (MCP), leading to a higher compression of the source video [58, 60]. With MCP, a single bit error can cause the so called *drift* problem, that is the quality degradation due to an error propagation as a result of predictor mismatch between the encoder and the decoder. In FGS MPEG-4 coders, the MCP is considered for the BL but not for the EL, avoiding the drift problem when the EL is lost. The encoded bitstream is therefore robust to channel impairments, and the embedded structure support the adoption of prioritized transport protocol or any unequal error protection UEP, as in [24, 72]. However, the robustness of errors propagation is paid by the reduction of compression efficiency. To overcome this issue, motion compensation was introduced within the enhanced layer [64, 73]. In [73], the authors included the EL layer in the MCP loop to exploit the remaining (not coded in the base layer) temporal correlation within this layer. The tradeoff between coding gain and prediction drift is found by varying the portion of the EL included into the MCP loop. However, MC-FGS suffers from error propagation when the portion of the EL employed for the prediction is lost. In [64], the authors proposed a progressive FGS (PFGS) coding scheme by adopting a separate MCP loop in the embedded EL. To address the drift problem

[1]We refer the reader to Section 2.3 and Section 2.5 for further details on MD coding.

in the PFGS coding scheme, a prediction path going from the BL to the highest bitplanes of the EL across several frames is maintained so the coding scheme can gracefully recover from channel errors. To circumvent coding inefficiency and drift issues, leaky prediction layered video coding is considered, and an attenuated version of the enhanced layer is included within the MCP loop. MC-FGS coding with leaky prediction improves the coding efficiency maintaining graceful error resilience performance, thus the tradeoff between coding efficiency and error drift can be achieved. Note that the leaky factor α assumes values between 0 and 1; when $\alpha = 0$ the EL is completely excluded from the MCP loop, avoiding the drift issue and minimizing the coding efficiency. Conversely, when $\alpha = 1$, the whole EL is included in the MCP loop, maximizing the compression efficiency, but having the less error resilience. In [74], the MCP portion of the EL together with the leaky prediction factor was optimized to the channel conditions, i.e., signal-to-noise ratio and order of diversity in both time and frequency domain. The authors proposed an n-channel symmetric motion-compensated multiple description coding and transmission scheme for the delivery of scalable video over OFDM systems. Since the analysis is limited to a slow fading channel case, only a frequency coding is considered.

In this chapter, the delivery of scalable video over OFDM systems is investigated in varying channel conditions. In order to provide a system robust in both time and slow fading as well as in systems with either high and low frequency correlation, a n-channel symmetric motion-compensated MD coding is considered, by adopting a channel coding both in time and frequency domain. The MD mapping scheme, introduced in the previous chapter, is here extended to a video transmission, considering not only the channel coding optimization but also the MCP loop and leaky factor optimization. The best tradeoff between coding efficiency and error resilience is addressed by a joint source and channel coding optimization.

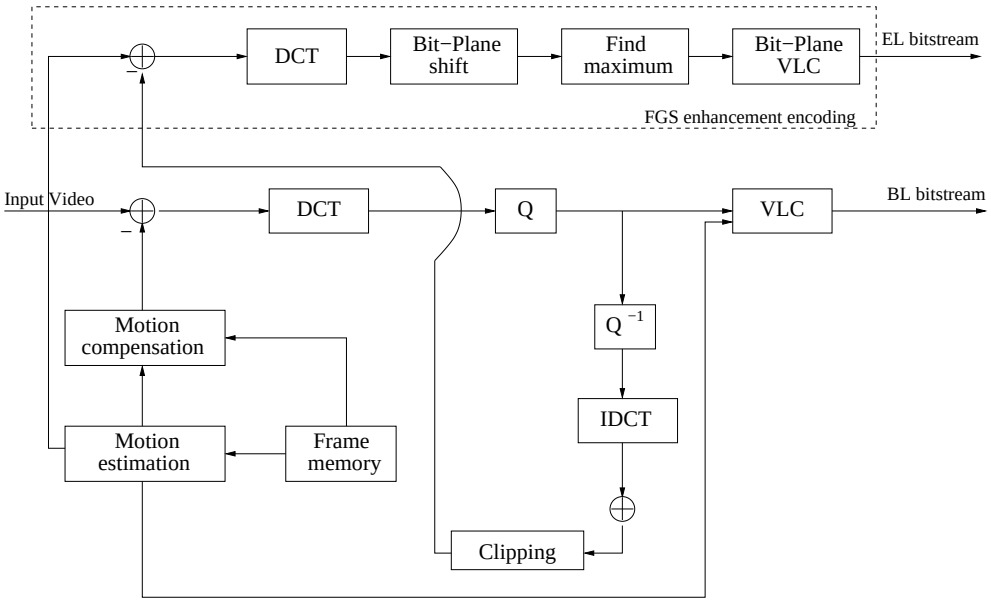

Figure 3.1: Encoder structure of the FGS coding methodology based on MPEG-4.

3.2 Motion-compensated FGS with leaky prediction

As already mentioned, conventional scalable video coding schemes consist of both a base layer and an enhancement layer. The base layer guarantee the basic quality of the encoded video, while an improved quality can be obtained receiving the enhancement layer in addiction to the BL bitstream. Fig. 3.1 shows the encoder structure of the MPEG-4 FGS system. As reported in the figure, the FGS encoder consists of two parts: base layer and enhancement layer. In the base layer, the basic information of the input signal is coded in the same way as the traditional block-based coding method. Note that the encoder structure in the BL is the same of that in MPEG-4 Part 2 coding [65]. In the enhancement layer, the residual signal that is not coded in the base layer is divided into 8×8 blocks and each block is discrete cosine transformed (DCT). After collecting all of the weighted DCT coefficients, the maximum value of the coefficients is found to determine the maximum number of bit-planes.

Finally, the bitplane- based variable length coding (VLC) procedure is then carried out for each bit-plane of each block of the DCT residues. We refer the readers to [64, 75–77] for further details on FGS coding techniques.

When the motion compensated prediction for video coding is considered, high compression is achieved by exploiting similarities between successive frames. Fig. 3.2 illustrates a general framework for MC-FGS coders with leaky prediction [62, 73, 78, 79]. The MCP is considered for both the BL and a portion of the EL, the last opportunely attenuated by a leaky factor α. For sake of simplicity, in this chapter, we assume that the BL, including coding modes and motion vectors (MVs), is correctly received. However, it should be noted that the loss of the BL would cause a substantial degradation of the delivered video quality, rendering sometimes the sequence not decodable [73]. It follows that the BL should be extremely protected, for example, by considering higher FEC level dedicated to the BL rather than the forward error correction (FEC) for the EL in the channel coding process [74].

As already pointed out, the EL is progressively encoded, and the whole block or only a portion of it can be considered for the MCP loop. Note that the portion of the EL included in the MCP loop is denoted by *EL-MCP*, while *EL-extra* is the residual EL, not considered for the MCP loop. Being $R_{\text{el,max}}$ the total bit budget of the EL, the portion of EL included into the MCP loop (MCP point) is denoted by β, which will range between 0 and 1. The MCP point is defined as $\beta = R_{\text{el,mcp}}/R_{\text{el,max}}$, where $R_{\text{el,mcp}}$ is the amount of bits considered for the EL-MCP. When $\beta = 1$ (i.e., $R_{\text{el,mcp}} = R_{\text{el,max}}$), the whole EL is included into the MCP loop, while only the BL is considered when $\beta = 0$. By increasing β, the coding efficiency is improved, at the cost of a less robust system. In fact, the higher the β, the higher is the quality degradation in case of EL-MCP loss. An optimal MCP point can be found regarding the channel conditions and the protection level associated to the EL.

The leak factor $\alpha \in [0, 1]$ is aimed at attenuating the EL-MCP before it is included into the MCP loop [62, 80, 81]. Its purpose is to reduce the drift issue once the EL-MCP is lost. In particular, when $\alpha = 0$,

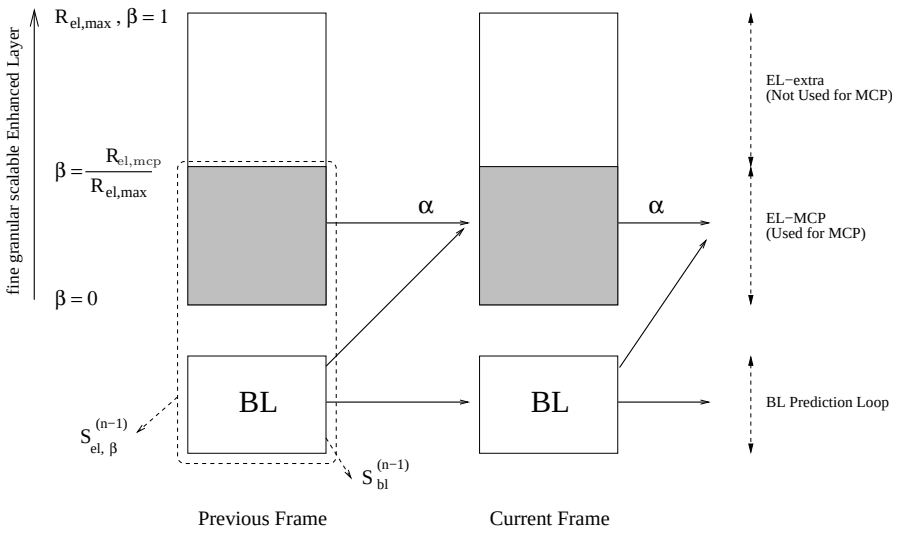

Figure 3.2: Motion-compensated FGS hybrid coder with leaky prediction.

since the EL is not considered in the MCP loop, the drift problem is avoided. By increasing the leak factor, the coding efficiency is improved and the drift effects increase when the EL-MCP is not received. When $\alpha = 1$, the whole EL-MCP is considered within the MCP loop without any attenuation, leading to the best coding efficiency and the least error resilience, and the drift problem can be limited by reducing the portion of the EL considered for the prediction loop only. As a result of the leaky prediction algorithm, the reference $\widehat{S}_{\mathrm{el},\beta}^{(n-1)}$ for the prediction of the current EL is a weighted sum of the BL reference $S_{\mathrm{BL}}^{(n-1)}$ and the partial EL reference $S_{\mathrm{el,mcp}}^{(n-1)}$, i.e.,

$$\widehat{S}_{\mathrm{el},\beta}^{(n-1)} = (1-\alpha) S_{\mathrm{BL}}^{(n-1)} + \alpha S_{\mathrm{el,mcp}}^{(n-1)}. \tag{3.1}$$

In [21], Huang et al. showed that the simultaneous utilization of both parameters α and β on a frame-by-frame basis can greatly improve the delivery of FGS video over wired networks. Similar studies were done by Han and Girod [23], using a multistage embedded quantizer and leaky prediction. In [74], Chan et al. optimized both the parameters for the construction of a n-channel symmetric motion-compensated MD coding, for slow fading channels. Here, the work has been extended to

fast fading channels, providing an optimized scheme robust in several channel conditions.

3.3 System model overview

The system model and the channel coding adopted in this chapter have been already described in the Chapter 2, and they are briefly reported in the following.

3.3.1 Channel model

We assume an OFDM system with an overall bandwidth W_T, in which N independent subchannels can be individuated. Being $(\Delta f)_c$ the coherence bandwith, the number of independent subchannels is evaluated as $N = N_\mathrm{t}/M$, where N_t is the number of total subcarriers (spanning a total bandwidth of W_T) and M is the number of correlated subcarriers (spanning a total bandwidth of $(\Delta f)_c$). Frequency diversity by adding redundancy across the subcarriers can be applied to combat channel errors. Generally, the maximum achievable frequency diversity $\mathcal{D}_f$ is given by the ratio between the overall system bandwidth W_T and the coherence bandwidth $(\Delta f)_c$. In addiction to frequency domain, for time diversity, channel coding plus interleaving can be used in the time domain. However, for the technique to be effective, the time frame has to be greater than the channel coherence time $(\Delta t)_c$. The maximum time-diversity gain $\mathcal{D}_t$ is given by the ratio between the duration of a time frame and $(\Delta t)_c$. In the time domain, a Rayleigh fading is assumed, while in the frequency domain a block fading channel is considered . A modified Jakes' model [39] is considered to simulate different fading rates, resulting in different time diversity orders.

3.3.2 Time-frequency MD coding

In Section 2.3, the proposed scheme for the transmission of an embedded bitstream over a mobile channel characterized by a doubly selective environment was described. In the frequency domain, $N_t = N \times M$ sym-

metric descriptions[2] of approximately equal importance are constructed in which contiguous information from the embedded bitstream is spread across the multiple packets [23, 24]. In the previous chapter the information symbols represented the progressively encoded images, now they represent the progressive EL bits (both the EL-MCP and EL-extra portions). Because of the progressive nature of the encoded bitstream, MD coding based on the priority of the bits in the bitstream is adopted, and the optimization of the FEC allocation in the frequency domain is designed to minimize the expected distortion. In the frequency domain, a (n, k) MDS erasure RS code is adopted, and the code rates are optimized based on the importance of the information symbols. In the time domain, a concatenation of cyclic redundancy check (CRC) codes and rate-compatible punctured convolutional (RCPC) codes, for possible diversity and coding gains, are applied to each description. We recall that it has been demonstrated the importance of the MD coders optimization for multimedia transmissions, [59, 72–74]. In particular, in [72] (for slow channels) and in the previous chapter (for both slow and fast channels), it has been highlighted how the knowledge of the order of diversity offered by the channel greatly improves the system performance for image transmissions. The FEC profile in the MD coding can be optimized based on these diversity orders in both time and frequency domain. When the diversity is available at least in one of the two domains, the system results to be robust in both slow and fast fading channels. Moreover, in flat fading conditions, the UEP in the frequency domain is the optimal FEC allocation, while in highly frequency selective channels, the optimal FEC staircase merges to an EEP. These considerations were extended to video source transmissions in [74], for slow fading channels. The FEC staircase in the frequency domain was optimized together with the α and β parameters for motion-compensated MD coding. In [74], no time conding was considered, leading to a collapse of the performance with the increasing of the Doppler. Here, the CRC/RCPC coding is inserted in the time domain, and both time and frequency coding are optimized in conjunction to the α and β parameters.

[2]Note that each description is a single packet, so we shall use the terms "description" and "packet" interchangeably throughout the paper.

3.4 Problem formulation

In this section, we describe the optimization problem to be solved, and we provide some worthy details on methods and parameters useful for the optimization analysis, as the drift-management and the rate-distortion curve.

3.4.1 Drift management

As already mentioned, the multiple description stream is insensitive to the position of losses in the bitstream, and thus it has the desired feature that the delivery quality is dependent only on the fraction of packets delivered reliably. Most of the initial works in this area has focused on the case of $N_t = 2$ descriptions [82, 83]. Then, the case of $N_t > 2$ was addressed by other authors. In most of these works, one of the main issue is the error propagation that occurs when there is a mismatch between encoder and decoder.

Consider a generic 2-channel nonsymmetric MD system which can be characterized by the quintuple $(R_1, R_2, D_1^{(1)}, D_1^{(2)}, D_2)$, where R_1 and R_2 are the bitrates of the two individual descriptions. $D_1^{(1)}$ is the distortion when description 1 is received, $D_1^{(2)}$ is the distortion when description 2 is received and D_2 is the distortion when both descriptions are received. As a result, there are three possible prediction states at the decoder, corresponding to the successful reception of only description 1, only description 2, or both descriptions (decoded by the central decoder). Each of the three states can form its own prediction loop. Whenever the encoder uses a predictor that depends on a state not available at the decoder, there will be a mismatch between the prediction loops at the encoder and decoder. Similar to single description (SD) MCP coding, this mismatch between encoder and decoder will trigger error propagation, or drift. To avoid such mismatch, one can, for example, construct two independent prediction loops, each based on a single-channel reconstruction. At the expense of decreased compression efficiency, this can completely avoid the mismatches for the side decoders, even when one of the two descriptions is lost [82, 84]. For the symmetric counterpart, since the video quality only

depends on the number of descriptions received, the two independent prediction loops can be reduced to one. Hence, the symmetric property significantly reduces the complexity of encoding and decoding. In general, there are as many as $(2^n - 1)$ possible prediction states, while there are n prediction states for the corresponding symmetric counterpart. However, when n is large, aside from the complexity issue, the probability of simultaneous failure of all but one of them is typically small. Hence, although this approach completely eliminates mismatches, it is not useful in practice. More importantly, as stated above, *mismatch-free* or *drift-free* approaches generally suffer from poorer compression efficiency [85]. Hence, as opposed to the traditional predictive coding paradigm that systems should not be designed to allow drift/mismatch, there is a growing interest in predictive coding schemes (both SD and MD) that attempt to allow some drift/mismatch so as to improve the overall compression efficiency. This is called the drift-managed approach [58, 62, 86–89]. A drift-managed approach does not preclude drift in the prediction strategy. Instead, it allows drift/mismatch to be introduced incrementally, and encompasses drift-free as a special case. In other words, a drift-managed approach optimizes the system performance by trading off the compression efficiency and the amount of mismatch, allowing the drift-free solution to emerge when it is optimal.

The design paradigm can be applied to the construction of n-channel symmetric motion-compensated MD codes. One can, for example, assign $m \in [0, n]$ descriptions as a reference for the temporal prediction, where $m = 0$ corresponds to the drift-free case. Note that if the number of received descriptions $m' < m$, there will be a mismatch. Generally, a higher prediction efficiency can be achieved by using a larger m. However, this comes at a price of greater probability of mismatch. More importantly, although the number of descriptions to be included for the MCP has often been thought as a fine-tuning method for trading off compression and error resilience, and allowing drift to be introduced incrementally (see [87], Section III-G]), the correlation among the subcarriers/channels may make this less effective. For instance, if M out of n descriptions are delivered through M highly correlated channels, i.e., systems with low

diversity order, these M descriptions are likely to be lost or received all together. The encoder should decide whether to include M more or M fewer descriptions in the MCP loop, instead of attempting to fine-tune by including one more or one fewer description in the loop, because the correlated nature of the subcarriers makes it unlikely that only one more or one less of description would be received. The effect becomes more significant when M is large, or, equivalently, when the order of diversity is small. This erratic behavior due to the simultaneous loss of several descriptions transmitted through highly correlated channels may greatly affect the degree of encoder-decoder mismatch, and, hence, the effectiveness of drift control, which may subsequently result in severe unexpected error propagation.

3.4.2 Motion-compensated FEC-MD coding construction

In the following, we describe the problem formulation to be solved, that is the optimal motion compensated FEC-MD coding construction. We extend the cross-layer diversity technique already described in [74], employing time coding in addition to the already considered frequency coding. Based on the channel conditions, a joint source and channel coding optimization is provided. In particular, we demonstrate that taking into consideration the time and frequency diversity in the coding optimization leads to an improvement of the performance, in both fast and slow fading channels as well as in both flat and frequency selective channels. In Fig. 3.3, a MD construction is illustrated. In the FGS enhancement layer bitstream (Fig. 3.3(a)), a portion of the EL is included in the MCP loop (EL-MCP), while the remaining bits are not included into the MCP loop (EL-Extra). Less important EL-Extra can be discarded, based on available bandwidth and channel conditions. In Fig. 3.3(b), the motion compensated MD coding is considered. Similarly to the MD coding of Chapter 2, the embedded bitstream of the EL is mapped into n-channel multiple descriptions. In particular, contiguous symbols of the bitstream are spread across the subcarriers and protected against channel impairments by a (N_t, k) MDS RS coding in the frequency domain,

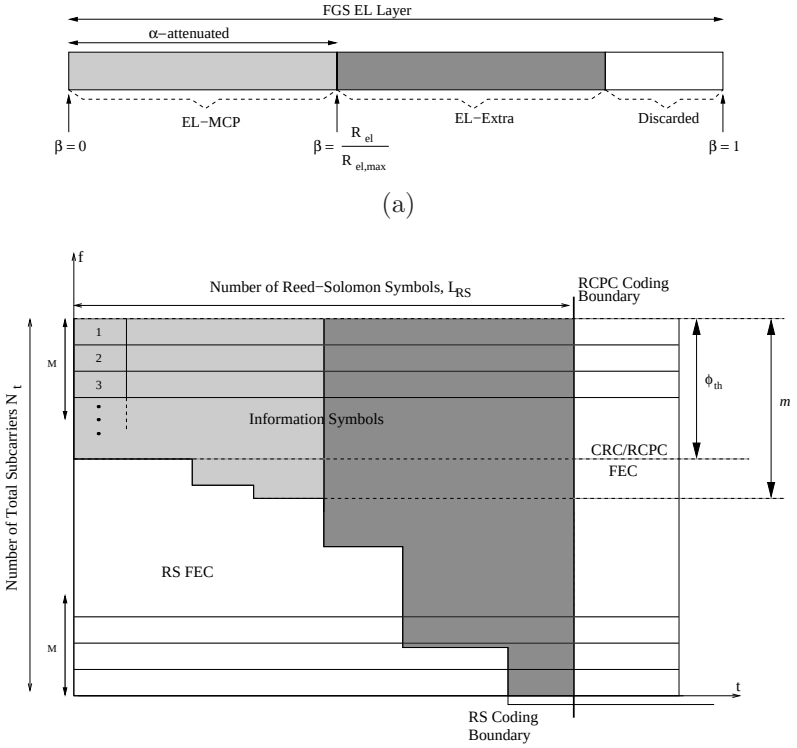

Figure 3.3: Transmission of the embedded bitstream over OFDM mobile wireless networks. (a) FGS embedded bitstream. (b) Motion-compensated MD coding. The white shaded area represents the parity symbols (both in time and frequency domain), the light-grey shaded area represents the EL-MCP symbols, and the dark-grey shaded area represents the EL-Extra symbols. Note that the CRC/RCPC symbols are interleaved with RS symbols in real systems.

where N_t is the number of total subcarriers in the OFDM system. The level of protection on each RS codeword depends on the importance of the symbols in the bitstream and it is actually one of the parameters to be optimized. Then, each description is temporally encoded with a concatenation of CRC codes and RCPC codes. The reception of at least ϕ_{th} descriptions out of N_t allows us to start reconstructing the source. In a (N_t, k) MDS code, in order to reconstruct the k information symbols, up to $N_t - k$ descriptions can be lost. It follows that when more than $N_t - \phi_{\text{th}}$ descriptions are lost, the source can not be reconstructed, and

all the EL of the transmitted frame is discarded. In Fig. 3.3(b), M is the number of highly correlated subcarriers[3], and N is the number of independent subbands in the frequency domain such that $N_t = N \times M$. The white area represents the parity symbols for both CRC/RCPC codes and RS codes. It should be noted that, in actual systems, RS symbols and RCPC parity symbols of each description would be interleaved. However, for illustration, we show the de-interleaved version throughout the chapter so that the relative amounts of RCPC parity symbols and RS symbols can be clearly indicated. Unlike the MD coding with no motion compensation, the information symbols are here classified into EL-MCP (light-grey shaded area), used for the MCP loop at the decoder, and EL-Extra (dark-grey shaded area) carrying information for enhancing the video without being included into the MCP loop. Note that, since the leaky prediction is considered, the EL-MCP symbols are α-attenuated before being included into the MCP loop. Denoting by m the minimum number of descriptions to be received for reconstructing the EL-MCP, the reception of $m' < m$ descriptions leads to an encoder-decoder mismatch. The quality degradation caused by the mismatch depends on the number of EL-MCP descriptions missed, as well as the leaky factor considered in the coding. Intuitively, the mismatch is proportional to $\alpha(\widehat{S}_m - \widehat{S}_{m'})$, where $\widehat{S}_m$ and $\widehat{S}_{m'}$ are the reconstructed frame using m and m' received descriptions.

Mathematically, the optimization for the construction of n-channel symmetric motion-compensated MDs is formulated as follows. Consider N i.i.d. subbands, each with M subcarriers and packet size equal to L_{RS} code symbols before channel coding in the time domain. Since each vertical column corresponds to one RS codeword, before the time coding there are altogether L_{RS} RS codewords. The constraint on the bit budget/packet can then be written as

$$(L_{RS} \times N_{tot} \times B_{RS} + B_{CRC})/R_{rcpc} \leq B_{tot}, \tag{3.2}$$

where B_{CRC} is the bit budget allocated for the CRC codes and R_{rcpc} is the channel code rate of the RCPC codes. B_{RS} is the number of bits-per-

[3]We recall that a block fading model is considered for the channel in the frequency domain.

RS symbol and B_{tot} is the total bit budget of the OFDM resource block (RB).

We assume that for the RS codeword l, where $l \in [1, L_{RS}]$, c_l code symbols are assigned to information data symbols, therefore, $f_l = N_t - c_l$ are the FEC symbols. The reception of $m' > \phi_{\text{th}}$ descriptions leads to a reconstruction of the source with distortion $D(R_{m'})$, where $R_{m'}$ is the allocated bit budget for the information symbols in the first m' descriptions,

$$R_{m'} = \sum_{\{l:c_l \leq m'\}} c_l \times B_{RS}. \tag{3.3}$$

Hence, the overall RS channel code rate equals $R_{rs} = R_{N_t}/(N_t \times L_{RS} \times B_{RS})$. Given the source code rate-distortion curve $D(\bullet)$ and the packet loss probability mass function $P_{\mathcal{J}}(j)$, where $j = N_t - m'$ is the number of lost packets, we can minimize the expected distortion as follows

$$E^*[D] = \min_{\{c_l, R_{rcpc}, \beta, \alpha\}} \left\{ \sum_{j=0}^{N_t - \phi_{th}} P_{\mathcal{J}}(j) D(R_{N_t - j}, \beta, \alpha) + \sum_{j=N_t - \phi_{th}+1}^{N_t} P_{\mathcal{J}}(j) D_{\text{BL}} \right\}, \tag{3.4}$$

subject to the constraint on the overall bit budget

$$\frac{R_{N_t}/R_{rs} + B_{CRC}}{R_{rcpc}} \leq B_{tot} \tag{3.5}$$

where D_{BL} corresponds to the distortion when fewer than ϕ_{th} descriptions are received and only the BL is decoded in the current frame. It is worth noting the tradeoff between reliability and throughput. Given the constraint (3.5), lowering R_{rs} and/or R_{rcpc} will cope with channel impairments, but it will lead to a reduction of R_{N_t}, that is the number of total information symbols transmitted within the resource block (RB). The packet loss probability mass function $P_{\mathcal{J}}(j)$ depends on $(\Delta f)_c$, $(\Delta t)_c$ and R_{rcpc}. Although $P_{\mathcal{J}}(j)$ can be found analytically for uncorrelated fading channels, due to the correlated fading in both time and frequency domains of the mobile environment considered here, we use simulations to find $P_{\mathcal{J}}(j)$. Different algorithms can be considered for solving the optimization problem [90–93], here, we use the iterative procedure described in [24] due to its simplicity. We set the parameter $Q = N_t$ for a full

search. The rate-distortion curves $D(\bullet)$ in (3.4) can be evaluated theoretically [79], or by real video simulations. In both the cases, a careful description of the adopted algorithm is necessary, and it is presented in the following subsection.

3.4.3 Rate-Distortion curve

The overall MC FEC-MD coding construction described in the previous section is based on the rate-distortion (RD) curve of the encoded video sequence. Several works considered theoretical frameworks for studying MCP encoders and RD curve evaluation, [79, 81]. Since we investigate real video sequences, to better estimate the drift issue the simulated RD curve is considered. In theoretical systems as well as in the realistic ones, the algorithm for the RD curve evaluation is a focal point. Two possible methods are compared in the follwing[4]: i) *off-line* method, ii) *on-line* method. It is important to recall that the rate considered in the RD curve is the EL rate, including both EL-MCP and EL-extra. Since we consider the BL always correctly received, the decoded video quality can not be lower than a minimum value, D_{BL}, achieved by receiving only the BL, i.e., $D(R_0) = D_{BL}$[5], where R_0 is the received rate when all the EL is lost. Denoting by $R^{(i)}$ the portion of the EL received for the i-th frame, because of the EL-MCP loop, the RD curve of the $(i+1)$-th frame will be a function not only of $R^{(i+1)}$, but also of the $R^{(i)}$ and $D(R^{(i)})$. In particular, if $R^{(i)} < R_{\text{el,mcp}}$, the EL-MCP for the i-th frame is not correctly received, and a mismatch occurs when the $(i+1)$-th frame is decoded. Moreover, since the (i)-th frame is a reference for the current frame, the quality of the decoded (i)-th frame is another important information for the RD curve of the current frame. This concept is graphically explained in Fig. 3.4(a). Considering the first frame of a given sequence, an I-frame[6], the RD curve is evaluated taking

[4]Note that several works are focused on RD curve and rate control algorithms. Here, we presents the two methods that we elaborated.

[5]Note that, since the rate is the EL rate, a subscript EL should be considered (i.e., R_{EL}), but for sake of simplicity in the notation we omit this subscript. We explicit the subscript only when we refer to the EL-MCP rate, denoted by $R_{\text{el,mcp}}$.

[6]An I-frame is an intra-coded frame, while P and B frames are inter-coded frames. In particular, each P frame is encoded with previous frames as reference, and the B

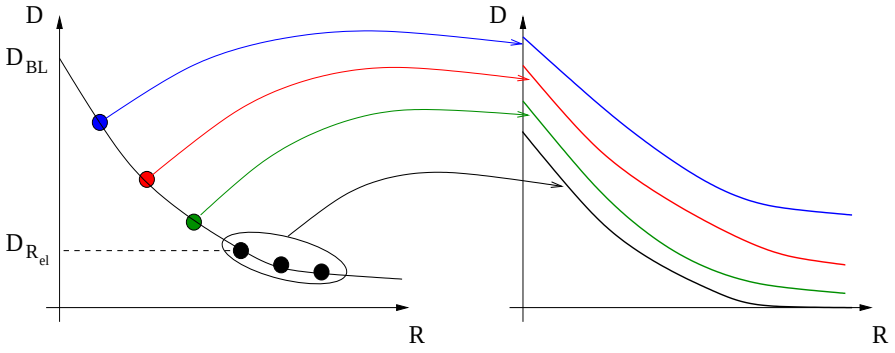

(a) Rate-Distortion curve evaluation for the first and second frame of a given sequence. The RD curve of the second frame highly depends on the rate at which the I frame is decoded.

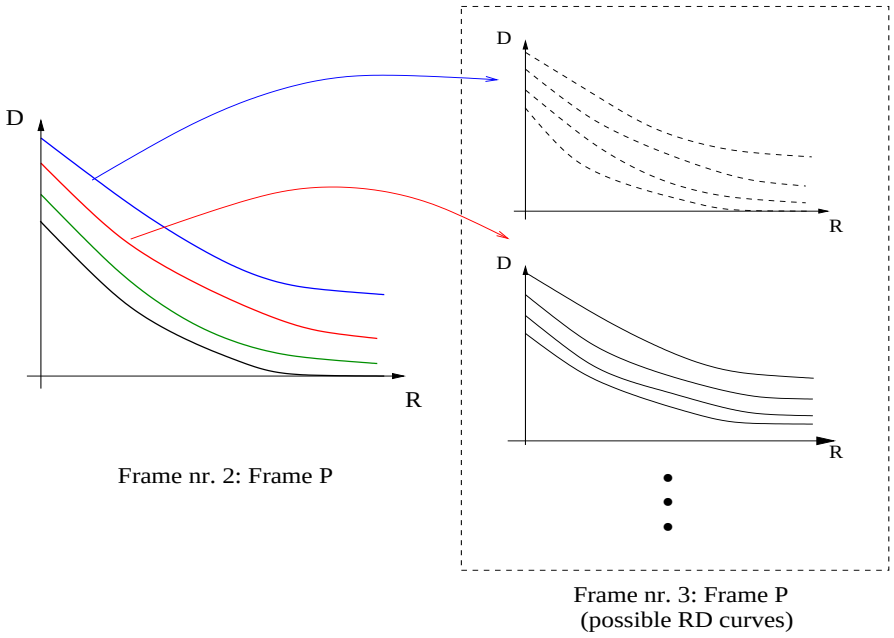

(b) Rate-Distortion curve evaluation for the second and the third frame of a given sequence. Based on the received rate of the first frame, it is known which RD curve (blue, red, green or black) is associated to the second frame, therefore, the RD curve of the third frame can be evaluated.

Figure 3.4: Rate-Distortion curve evaluation.

into account the received rate employed in the decoding. If the received

frames has a bi-directional reference, i.e., either previous and successive frames are references for the B frame.

rate is greater than the EL-MCP rate ($R^{(1)} \geq R_{\text{el,mcp}}$), no mismatch will occur during the decoding of the second frame. In this case, the amount of bits received for the first frame does not influence the evaluation of the RD of the second one (black RD curve). Conversely, when $R^{(1)} < R_{\text{el,mcp}}$, the bit budget received for the first frame is a required information for the evaluation of the RD curve of the second frame. It is important to know how much drift occurs during decoding process (blue, red or orange curve). When the third frame is considered (Fig. 3.4(b)), the RD curve evaluation depends on $R^{(3)}, R^{(2)}$, and $R^{(1)}$, or analogously, on $R^{(3)}, R^{(2)}$, and $D(R^{(2)})$. In fact, it is important to know if the second frame, used as reference for the third one, is drift-free. It follows that, for the evaluation of the $D(R^{(3)})$, it is important to know if a mismatch occurs during the third frame decoding, but also if one was experienced in the past frames. More generally, the rate distortion curve for the $(i+1)$-th frame depends on the rate vector $[R^1, R^2, \ldots, R^{(i+1)}]$, or equivalently, it depends on $(R^{(i+1)}, R^{(i)}, D(R^{(i)}))$, since the distortion of the i-th frame has an implicit dependency on the rates of the previous frames.

Therefore, it is understandable that the RD curve evaluation of an entire sequence is extremely complex and onerous from a computational point of view, and a simplification has to be considered. In [74], the authors based the FEC staircase on an average rate distortion curve, or *off-line* method, graphically described in Fig. 3.5(a). In this algorithm, first the mean RD curve is evaluated for the entire sequence, then the optimal FEC level for the 2D RB is investigated. Since the FEC optimization is based on the same RD curve for each frame, the *off-line* method leads to a single FEC staircase for the whole sequence. To evaluate the average RD curve, the received rate is assumed constant for the entire video, and the distortion values of all the frames are averaged, i.e.,

$$\overline{D} = \frac{1}{\text{GOP}} \sum_{k=1}^{GOP} D\left(R_i^{(k)}\right).$$

Since each frame experiences its own channel noise and fading level, the correctly received rate might me variable from one frame to another. Moreover, the complexity level may vary from one frame to another one, leading to extremely different RD curves within the sequence. Thus,

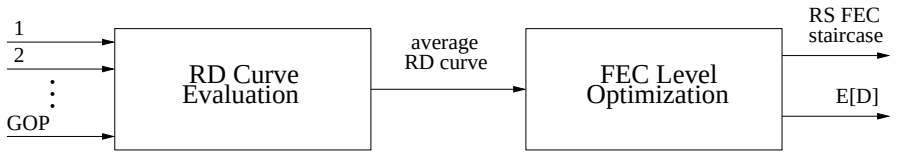

(a) *off-line* method

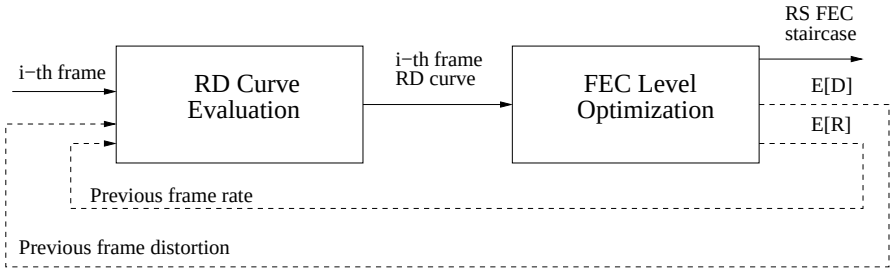

(b) *on-line* method

Figure 3.5: RD curve evaluation methods.

considering the received rate constant for all the frames might be a too rough assumption, most of all when a fast fading channel is considered. However, the approximation error introduced by this method is well-balanced by the gain in simplicity of the *off-line* method, that results to be extremely quick and not expensive from a computational point of view.

The second algorithm for the evaluation of the RD curve, reported in Fig. 3.5(b), is aimed at being a tradeoff between the simplicity of the mean RD curve method and the accuracy of the exact method. Unlike the *off-line* method, the RD curve and the optimized FEC level are evaluated for each frame. In particular, the expected distortion and the expected rate, evaluated during the FEC optimization step of the $(i-1)$-th frame, are assumed to be the received rate and the decoded quality for the previous frame, when the RD curve is evaluated for the i-th frame. As expected, the first frame will be an I-frame, and the feedback from the FEC optimization block will not be considered. It means that, in this algorithm, the RD function evaluation is not run off-line before the channel coding optimization process, but it is one of the two steps jointly considered in the overall optimization process for each frame. Rather

than only one FEC level for the entire sequence, here, each frame has its own optimized FEC level. Note that, in the exact RD evaluation process, the complexity is of the order of $(Nr)^{\mathrm{GOP}}$, where Nr is the number of rate considered in the evaluation. While in this instantaneous RD algorithm, the complexity is downscaled to $Nr \times \mathrm{GOP}$. A comparison between the two algorithms are reported in the following showing that, respect to the *off-line* method, the *on-line* one achieves a substantial improvement of the performance.

3.5 Results and discussion

We carried out simulations of the Foreman sequence. The operational RD curves are obtained based on the H.26L-FGS video codec, comprised of an H.264 TML 9 base layer codec and an EL codec with MPEG-4 FGS syntax. The FGS property is achieved by bitplane coding.We incorporate both partial and leaky predictions into the codec with a coding scheme shown in Fig. 3.3. In the simulations, we apply a uniform quantization parameter (QP) value to all blocks of the BL for both I-frames and P-frames. To facilitate the studies, we set BL $QP = 31$ (the largest quantization step) so as to increase the dynamic range of the EL bitrate. The MV resolution in H.264 is set to be 1/4. The loop filter option is also used. Each sequence is encoded with a frame rate of 30 fps. The serial bitstream was converted into 128 parallel bitstreams using the FEC-based multiple description encoder. The 128 descriptions were mapped to the OFDM system with 128 subcarriers. We used RS codes in the frequency domain and there were 8 bits per RS symbol. The packet size was set equal to 512 bits. We used QPSK modulation and considered perfect CSI. It should be noted that more sophisticated modulation schemes could be used to further improve the system performance, such as the one discussed in [50]. However, for the sake of simplicity and better understanding of the fundamental impact of the time and frequency diversities on the construction of the 2-D OFDM block, a fixed modulation scheme using QPSK was chosen. The RCPC codes of rates $R_{rcpc} = \frac{8}{9}, \frac{8}{10}, \ldots, \frac{8}{24}$, were obtained by puncturing an $R_c = 1/3$ mother

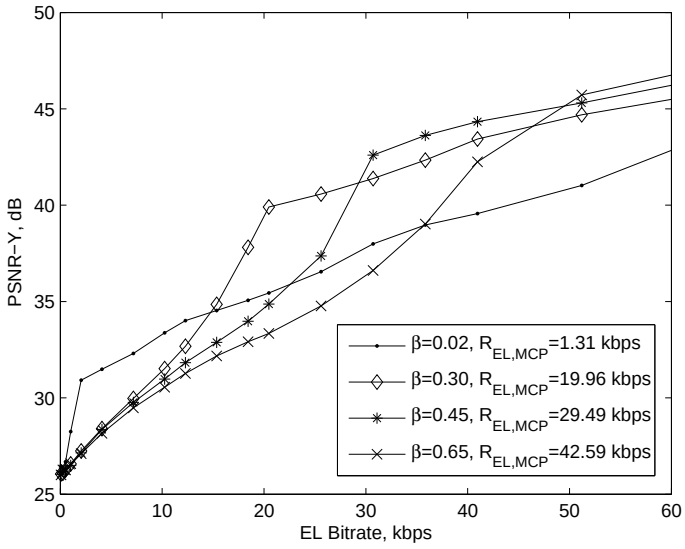

Figure 3.6: Rate-Distortion function for the MC-FGS with various MCP values (β), without leaky prediction ($\alpha = 1$), and with no time coding ($R_{rcpc} = 1$).

code with $K = 7$, $p = 8$ and generator polynomials $(133, 165, 171)_{octal}$ with the puncturing table given in [51]. The decoded quality is reported in terms of PSNR of the luminance, i.e., PSNR-Y $\triangleq 10 \log_{10}(255^2/\text{MSE}^2)$. We begin showing the mean rate-distortion curve, to make the reader understand the importance of receiving the motion compensated loop. Then, a comparison between the two proposed algorithms are reported, showing that the *on-line* method achieves a substantial improvement in the PSNR quality. Finally, we evaluate the luminance PSNR for several levels of mobility (i.e., several orders of diversity in the time domain) and numbers of correlated subcarriers (i.e., several order of diversity in the frequency domain), to make understand the importance of an optimization not only of the α and β parameters, but also of the code rate in the time domain.

In Fig. 3.6, the average RD function vs. the EL-MCP rate is reported for a sequence encoded with several EL-MCP values, and without leaky prediction. No time coding is considered in this first plot. In the figure, the x-axis corresponds to the received (decoding) bit rates of the EL. It

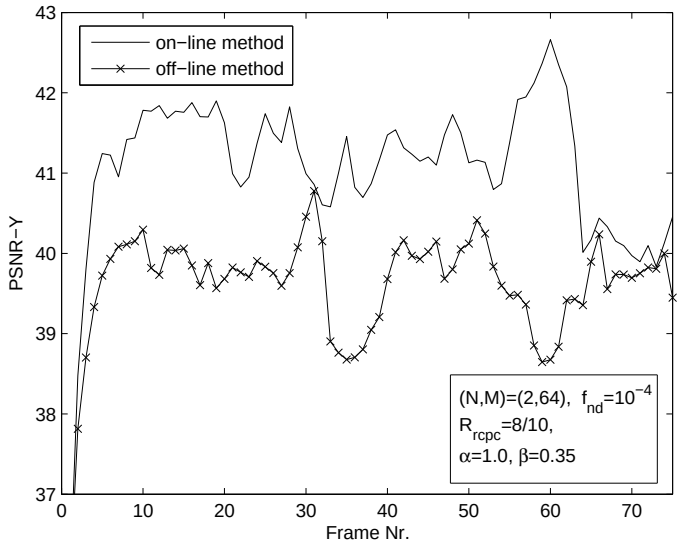

(a) $(N, M) = (2, 64)$, $f_{nd} = 10^{-4}$, $R_{rcpc} = 8/10$, $\alpha = 1.0$ and $\beta = 0.35$

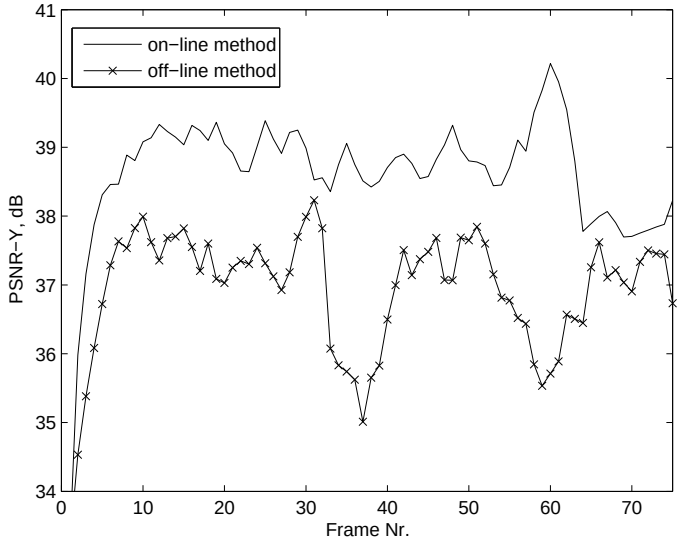

(b) $(N, M) = (4, 32)$, $f_{nd} = 10^{-3}$, $R_{rcpc} = 1$, $\alpha = 1.0$ and $\beta = 0.20$

Figure 3.7: Comparison of the *off-line* and *on-line* method for the FEC level evaluation.

can be noted that sequences encoded with higher β values achieve a good gain in the decoded quality (high PSNR) when the received EL rate is greater than the EL-MCP rate. For example, compare the sequence with $\beta = 0.02$ ($R_{\text{el,mcp}} = 1.30$ kps) with the curve $\beta = 0.65$ ($R_{\text{el,mcp}} = 42.598$ kps). If the bitbudget received in the EL is greater than the EL-MCP, for example equal to 44 kbps, the gain achieved by using $R_{\text{el,mcp}} = 42.598$ kps rather than $R_{\text{el,mcp}} = 1.30$ kps is almost 4 dB. Unfortunately, when the EL-MCP is not received, a mismatch in the predictors of the encoder and decoder occurs, leading to a substantial drop in PSNR performance, as shown in the plots. In the example, considering a received rate of $10 - 20$ kbps, the $R_{\text{el,mcp}} = 1.30$ kps curve outperforms the one with $\beta = 0.65$.

In Fig. 3.7, the *off-line* method for the RD curve evaluation is compared to the *on-line* one. In Fig. 3.7(a), a channel with $(N, M) = (2, 64)$, $f_{nd} = 10^{-4}$ is considered for the transmission of a sequence encoded with $\beta = 0.35$ and $\alpha = 1$, and mapped into a RB with a RCPC code rate equal to 8/10. Conversely, in Fig. 3.7(b), a system with different order of diversity and channel code rates is considered. In particular, $(N, M) = (4, 32)$, $f_{nd} = 10^{-3}$, $\beta = 0.20$, $\alpha = 1$, and $R_{rcpc} = 1$. In both the figures, the PSNR for each decoded frame of the sequence is provided. Even with different system conditions, the *on-line* method achieves a satisfying gain respect to the *off-line* RD curve evaluation. Since the latter method introduces an approximation, an outperforming of the *on-line* method was expected, but, the most interesting observation is that it is achieved a gain of the order of 3 dB or even more. Thus, the drop in terms of PSNR due to the assumption of an *off-line* method rather than the *on-line* one is substantial and it can not be ignored. Therefore, in the following the *on-line* method is considered for the evaluation of the RD curve and the FEC allocation optimization. In Fig. 3.8, the averaged RD curve (Fig. 3.8(a)) and the optimal FEC allocation (Fig. 3.8(b)) are reported for the two methods. Note how the rough approximation in considering a mean RD curve rather than the instantaneous one leads to a different protection level between the two methods.

In Fig. 3.9, we show the optimized construction of RS information

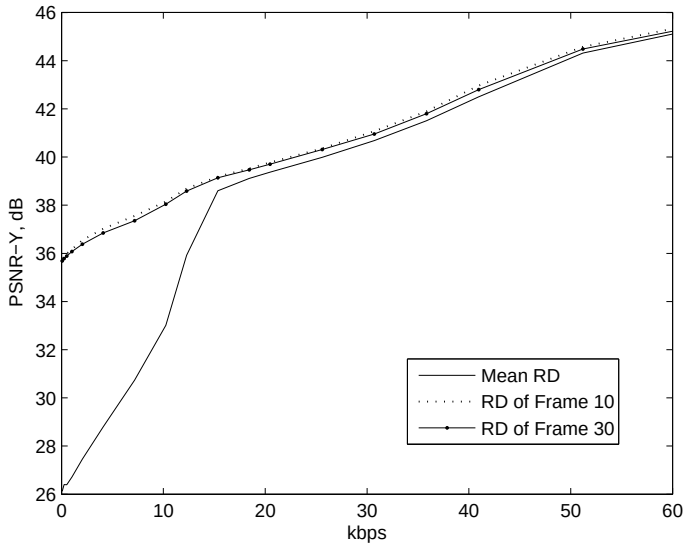

(a) Rate-Distortion function.

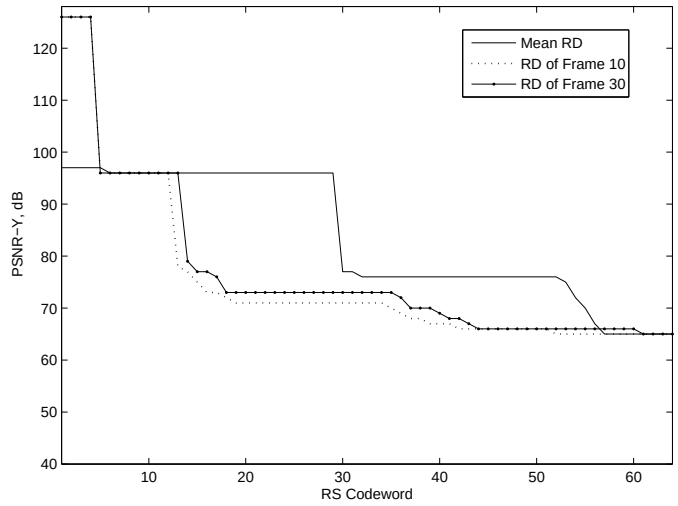

(b) Profile showing the optimal RS-FEC allocation.

Figure 3.8: Rate-distortion function and optimal FEC profiles for both the *off-line* and the *on-line* method for systems with $f_{nd} = 10^{-3}$, $R_{rcpc} = 1$, $(N, M) = (2, 64)$. Note that the frame nr. 10 and nr. 30 are considered in the *on-line* method.

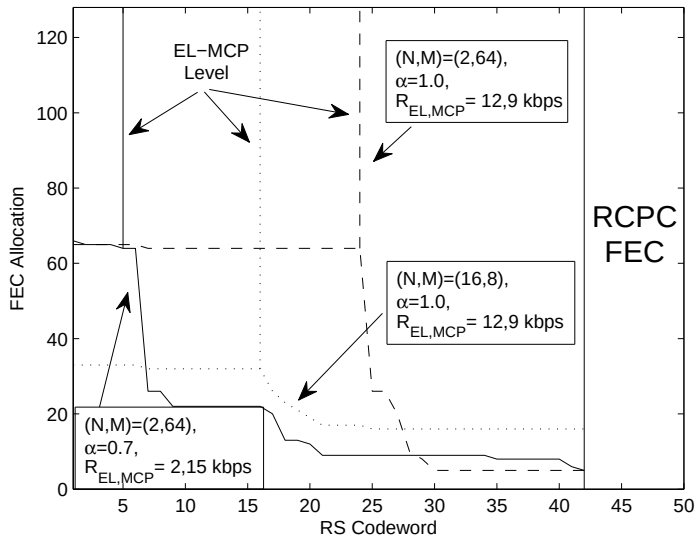

Figure 3.9: Optimal profile of the parity symbols for a system with $f_{nd} = 2.5 \times 10^{-4}$, $R_{rcpc} = 8/12$, and N variable for the transmission of sequences encoded with different α and β parameters. The profile for the 20-th frame is considered.

symbols, RS parity symbols and RCPC parity symbols for normalized Doppler $f_{nd} = 2.5 \times 10^{-3}$, $R_{rcpc} = 8/12$, several order of diversity in the frequency domain, and sequences encoded with different α and β parameters. Note that in the figure, the profile of the 20-th frame is considered[7]. As already observed in [74], due to their importance, the EL-MCP bits are more protected than the EL-extra bits. For example, the $R_{\text{el,mcp}} = 2.15$ kbps curve has few bits highly protected, having a low portion of the EL included into the MCP loop. Conversely, the $R_{\text{el,mcp}} = 12.9$ kbps curve has a high protection level for the first 25 RS symbols. Finally, it should be highlighted that, as already observed in the previous chapter, the higher is the order of diversity available, the lower is the required protection level, as it can be observed comparing the optimal profile of the $R_{\text{el,mcp}} = 2.15$ curve with $N = 2$ to the one with $N = 16$. Because of the more reliable transmission, the $N = 16$

[7]Since the behavior of the staircase, from a qualitative point of view, is similar in each frame, we report the FEC staircase fon only one single frame.

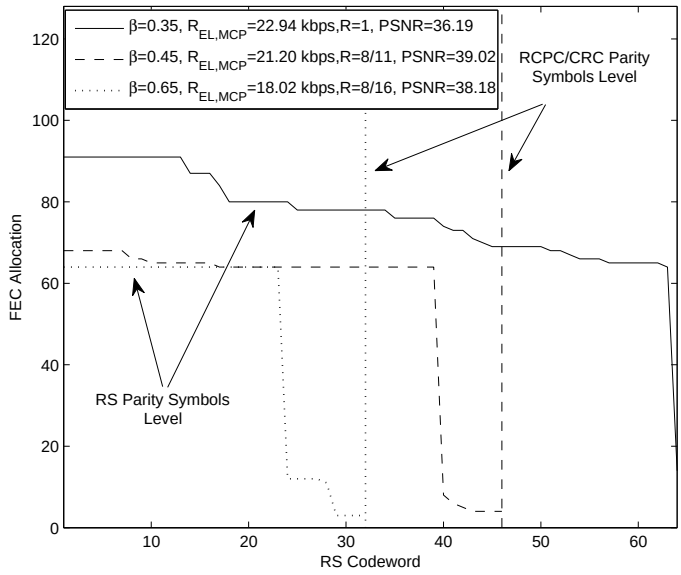

Figure 3.10: Optimal profile of the parity symbols for a system with $f_{nd} = 2 \times 10^{-4}$,$(N, M) = (2, 64)$, and different R_{rcpc} values for the transmission of sequences encoded with $\alpha = 0.9$ and the optimal β parameter. The profile for the 20-th frame is considered, and the PSNR values are expressed in dB.

curve may reduce the FEC level in the frequency domain respect to the $N = 2$ system.

In Fig. 3.10, the behavior of optimal staircase is reported for several coding rates. The optimal profile of the FEC level in both time and frequency domain is provided for the 20-th frame for a system with $f_{nd} = 2 \times 10^{-4}$,$(N, M) = (2, 64)$, and different R_{rcpc} values for the transmission of sequences encoded with $\alpha = 1$ and several β parameters. The maximum order of diversity achieved in the frequency domain is $\mathcal{D}_f = 2$, while the maximum order of diversity in the time domain is $\mathcal{D}_t = 1$. In other words, no diversity can be exploited by using RCPC codes, although coding gain can still be obtained. In general, lower code rates in the time domain improve the packet loss performance, thus reducing the number of RS parity symbols required for minimizing the expected distortion $E[D]$, as can be noticed from the figures. Since the diversity

achieved in the frequency domain is the same in the three systems considered in the figure, the RS code boundaries exhibit similar degree of tilting for both R_{rcpc} rates. As discussed in the previous chapter, although the packet loss performance of an individual subcarrier can be improved by using a lower channel coding rate, the degree of UEP, represented by the tilt of the RS boundaries, mainly depends on the frequency diversity order of the system, and is relatively insensitive to the selection of the channel code rate in the time domain. It is worthwhile noting that by lowering the RCPC code rate, the optimum β value increases, due to a higher protection of the transmitted bitstreams, and due to the reduction of the $R_{\text{el,max}}$. Because of the imposed constraint, (3.5), a reduction of the RCPC code rate leads to a decreasing of the total number of information symbols that can be transmitted. For example, for $R_{rcpc} = 1$, $R_{\text{el,max}} = 66.535$ kbps, while when $R_{rcpc} = 0.5$, the maximum EL rate equals 32.768 kbps. It follows that the same EL-MCP rate represents a different portion of the total EL rate, when two RCPC code rates are employed. Finally, because of the more reliable transmission for low time code rates, by lowering the R_{rcpc} the portion of the EL dedicated to the MCP loops can increase, due to less likely mismatch. Note that, although in the $R_{rcpc} = 1$ curve the optimal EL-MCP rate and the total EL rate are higher than the ones for the $R_{rcpc} = 0.5$ curve, drift issues at the decoder are more likely (because of the less reliable transmission) and therefore, the expected quality is lower than the one achieved by $R_{rcpc} = 0.5$.

In Fig. 3.11, the optimum β value vs. R_{rcpc} is provided for systems with $f_{nd} = 10^{-2}$, $(N, M) = (2, 64)$ and sequences encoded with three different α values. As concluded from the previous figure, by lowering the RCPC code rate, the optimum β value increases. Moreover, since the drift issue can be mitigate with a low α value, for constant packet loss rates (i.e., $\mathcal{D}_t$, $\mathcal{D}_f$, and R_{rcpc} constant), an increasing of the optimum β value is experienced when a reduction of α occurs. For example, for $R_{rcpc} = 0.5$, $f_{nd} = 2 \times 10^{-4}$, and $(N, M) = (2, 64)$, the reliability of each packet can be evaluated. In correspondence to this packet loss rate, the $\alpha = 0.7$ curve achieves an optimum β equal to 0.65, while 0.45 is the optimum β for a source coding with no leaky prediction. Rater than

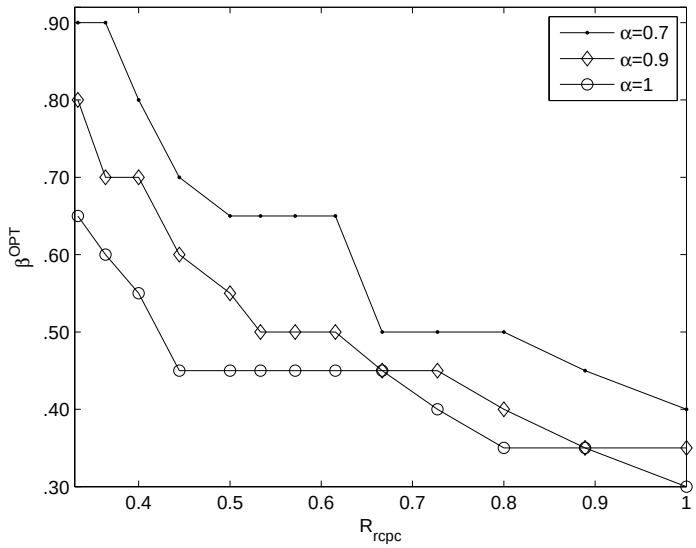

Figure 3.11: Optimum β vs. R_{rcpc} for systems with $f_{nd} = 2 \times 10^{-4}$, $(N, M) = (2, 64)$, and $\alpha = 1, 0.9,$ and 0.7.

varying the source coding parameters (α and β), we now investigate the behavior of the system when the orders of diversity in time and frequency domain are variable.

The importance of code rate optimization when different orders of diversity are available in the frequency domain is shown in Fig. 3.12. The PSNR-Y vs. R_{rcpc} values is provided for systems with several orders of diversity in the frequency domain, and both fast (3.12(a)) and slow (3.12(b)) fading. In the figure, we also mark with a circle (o) the optimal R_{rcpc} value. Note that, from here onwards, the mean PSNR is the average of the expected distortion of each frame, evaluated by means of the *on-line* method. As expected from what observed in the previous chapter, in fast fading systems the $\mathcal{D}_t$ is substantial, and diversity in the frequency domain is not required. Therefore, a minimum protection in the time domain is sufficient to guarantee extremely satisfying video transmissions, even when the number of independent subchannels equals 1. Conversely, as the system experiences low Doppler spread with $\mathcal{D}_t \sim 1$, Fig. 3.12(b), the selection of optimal coding scheme is dominated by the frequency diversity order of the system. As can be observed, generally a better

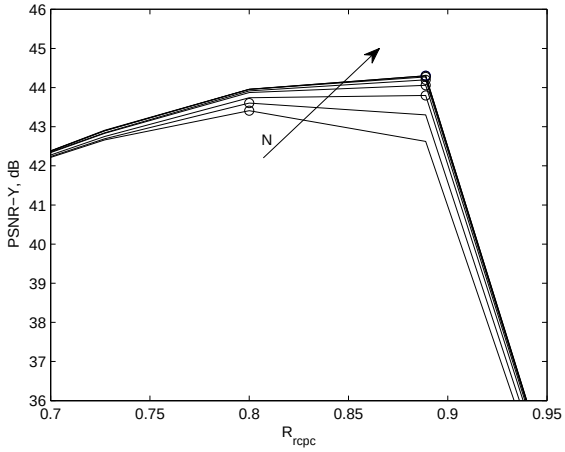

(a) PSNR-Y vs. R_{rcpc} for systems with $f_{nd} = 10^{-1}$, $\beta = 0.20$, $\alpha = 1.0$ and variable order of diversity in the frequency domain

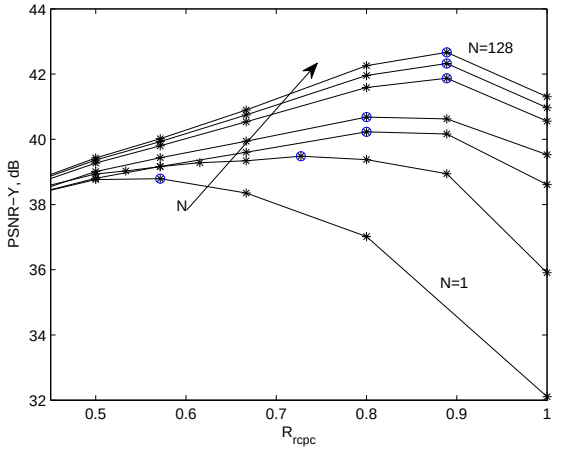

(b) PSNR-Y vs. R_{rcpc} for systems with $f_{nd} = 10^{-3}$, $\beta = 0.20$, $\alpha = 1.0$ and variable order of diversity in the frequency domain

Figure 3.12: PSNR performance for several orders of diversity available in the frequency domain in both slow and fast fading systems.

performance can be achieved with a higher diversity orders. More importantly, as the diversity order N increases, the optimal R_{rcpc} increases and the delivered video quality improves accordingly. The importance of

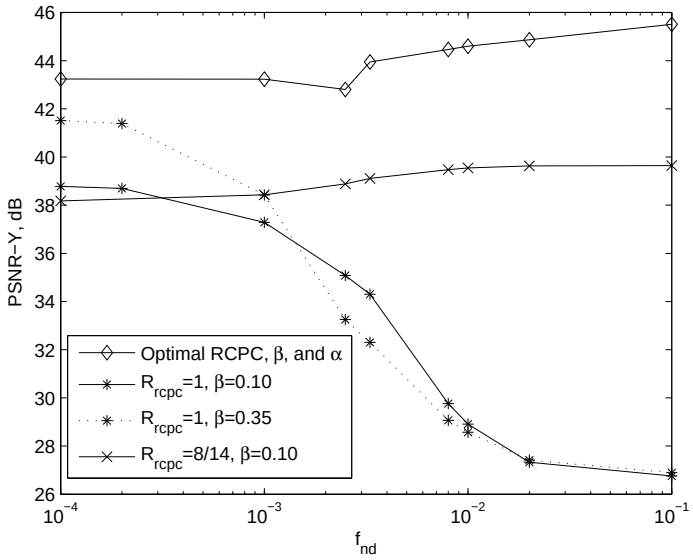

Figure 3.13: Expected PSNR-Y vs. f_{nd} for systems with $(N, M) = (4, 32)$, $\beta = 0.10, \text{and } 0.35$, $\alpha = 1.0$. Both optimal R_{rcpc} values and constant rates ($R_{rcpc} = 1, \text{and } 8/14$) are employed.

having a RCPC code rate optimized to the orders of diversity available can be understood from Fig. 3.12(b). Consider, for instance, a system with $N = 1$ and $R_{rcpc} = 0.57$. This time code rate achieves the best performance for the given system. Then, consider a case of high number of independent subchannels ($N = 128, 64$), and R_{rcpc} always sets to 0.57. Keeping the time code rate constant, rather than employing the optimal one (i.e., $R_{rcpc} = 0.9$), leads to a lost in the PSNR of ~ 3.5 dB.

In Fig. 3.13, the PSNR of a system with optimal R_{rcpc} is compared to other systems with constant source and channel coding parameters. The mean PSNR of the luminance vs. the normalized Doppler is provided for systems with both variable and constant RCPC code rates. In particular, systems with $R_{rcpc} = 1$ and $R_{rcpc} = 8/14$ are considered and compared to a system with the RCPC code rate optimized to each $\mathcal{D}_t$ value. In the figure, the order of diversity in the frequency domain is $\mathcal{D}_f = 4$, and no leaky prediction is supposed in the source coding. The most interesting observation is the monotonic decreasing behavior with an increasing fade rate due to the increasingly scattered error pattern, when no time coding

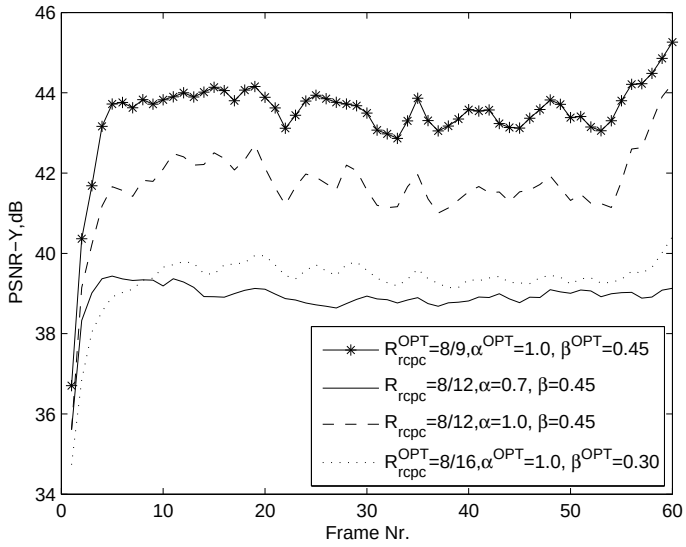

Figure 3.14: PSNR-Y vs. number of frame for systems with $(N, M) = (4, 32)$, $f_{nd} = 10^{-4}$, and several β and α values.

is considered. It is therefore required a temporal coding for fast fading systems. In the Appendix A, to better understand this PSNR drop, we provide some further analysis for the packet error rates due to the effects of error patterns resulting from different fading rates on the application layer throughput. When a time coding is considered, as the $R_{rcpc} = 8/14$ curve in the figure, the system is able to cope with the scattered error pattern in fast fading environments. As expected, in slow fading channel a low RCPC code rate might overprotect the signal, at the cost of a reduction of the maximum EL rate $R_{\mathrm{el,max}}$. Thus, for $f_{nd} = 10^{-4}$ for instance, the $R_{rcpc} = 8/14$ curve is outperformed by the system with no temporal coding. In order to optimize the performance in each channel conditions (i.e., for each diversity order offered by the channel), a variable code rate has to be considered in both time and frequency domain. The RCPC code rate should be such that to exploit the diversity order available in the time domain, improving the reliability of the packets, without wasting information symbols. As observed from the figure, the joint optimization of α, β, and R_{rcpc} outperforms all the other systems, achieving a gain of at least 2 dB.

The worthy performance of the optimized systems compared to other possible suboptimal configurations is reported in Fig. 3.14 in terms of instantaneous PSNR (rather than average). Here the PSNR-Y for each frame of the sequence is provided for systems with fixed coding parameters. Again, a substantial improvement of the decoded quality is experienced by the optimal system, as observed from the figure.

3.6 Conclusion

In this section, we studied the delivery of MC-FGS video employing an OFDM signal format on the physical layer to transmit over a frequency-selective Rayleigh fading, with both low and high level of mobility. We proposed a n-channel symmetric motion-compensated multiple description coding and transmission scheme, employing leaky prediction for mismatch control. We showed that knowing the orders of diversity offered by the channel in both time and frequency domain can improves the overall performance in the construction of symmetric MDs. We proposed an algorithm for the evaluation of the rate-distortion curve for the considered sequence, and, based on this function, the optimal tradeoff between coding efficiency and reliability can be investigated, by varying the EL-MCP rate and the leak factor α, together with the code rates in both time and frequency domain. Moreover, we demonstrated the importance of a time coding in the construction of 2D MDs, and we showed the behavior of the optimal RCPC code rate for different order of diversity in both time and frequency domain.

Chapter 4

Adaptive modulation techniques

In this chapter, adaptive modulation techniques are investigated for systems experiencing channel estimation errors. We evaluate the performance of both slow and fast adaptive modulation techniques when imperfect pilot-assisted channel estimation is considered at both the transmitter and the receiver. Taking into account the number of pilot symbols transmitted, the effective throughput is investigated and the tradeoff between channel estimation quality and throughput is addressed.

The reminder of the chapter is organized as follows. In Section 5.1 an introduction to the work together with a state-of-the-art overview in adaptive modulation techniques is provided. In Section 5.2 we present the system model, describing both adaptive modulation techniques and pilot-assisted channel estimation. Imperfect channel state information at the transmitter is investigated in Section 4.3, and a comparison of the performance between two adaptive modulation techniques is considered. In Section 4.4, we evaluate the effects of estimation errors at the receiver. In particular, slow adaptive modulation systems are investigated for both Rayleigh and Nagakami-m fading channels, and the optimization of the pilot scheme design is addressed in details. In Section 5.6 numerical results are provided, and conclusions are given in Section 5.7.

4.1 Motivation and outline of the work

The diffusion of high-speed digital wireless communications has increased the need of reliable high data rate transmission in variable channel conditions. Since adaptive modulation techniques allow to maximize the transmitted throughput[1] without compromising the performance (in terms of bit error probability or outage probability), they has become very popular in high data rate wireless applications [5–7, 94–96]. By matching system parameters to channel conditions the optimal modulation level can be selected maximizing the transmitted throughput still satisfying the QoS requirement, in terms of bit error probability (BEP) and bit error outage probability (BEO).

Since M-QAM modulation achieves high spectral efficiency, it is widely used in adaptive modulation systems. In [5], for example, power and rate were both adopted to channel conditions for a M-QAM uncoded system. The gain derived from an adaptive rather than a fixed transmitted scheme is reported, together with the negligible channel capacity penalty that the system displays varying only the data-rate rather than both rate and power. In the literature, some authors proposed as adaptive modulation techniques systems that track instantaneous channel variations: the receiver has to estimate the instantaneous signal-to-noise ratio (SNR) and send a feedback to the transmitter with the optimal constellation size and transmitting power to be used, [5–7,94,96,97]. Those parameters are tuned to exploit good channel conditions by increasing the transmitted throughput but, at the same time, to preserve the performance in case of bad channel conditions. It is worth noting that, in perfect channel state information (CSI) systems, tracking the small scale fading, fast adaptive modulation (FAM), leads to best performance, at the cost of a frequent channel estimation and feedback. With respect to FAM, a gain in terms of feedback and complexity can be achieved by slow adaptive modulation (SAM) techniques, that adapt modulation parameters to the average channel variations. In [6], the authors investigated SAM techniques with perfect channel estimation, adapting the system to the shadowing level

[1] Throughout this chapter, we use the terms "throughput" and "spectral efficiency (SE)" interchangeably.

of the channel. Although the throughput achieved with FAM system is slightly better than the one obtained with SAM technique, SAM still achieves improvements in terms of SE and BEO when compared to a fixed modulation scheme, despite the lower complexity and the less frequent feedback.

In fast as well as slow adaptive modulation, a critical role is played by the channel estimation. Imperfect channel estimation poses a serious issue that has been addressed in several ways. The effects of outdated channel estimation are investigated for adaptive coding systems in [7] and for adaptive modulation systems with Rayleigh and Nakagami fading channel in [5] and [97], respectively. In both [5] and [97], authors evaluated the maximum acceptable delay that does not drastically affect the performances. For a BEP target of 10^{-3}, the maximum delay normalized to the Doppler frequency corresponds to 10^{-2} for both Rayleigh and Nakagami fading channels. Rather than delayed channel state information, imperfect channel estimation are quickly investigated in [5]. A general criterium is given to probe the effects of channel estimation errors in the instantaneous SNR in the feedback. More detailed analysis on adaptive modulation system with imperfect CSI are addressed in [98–101] for both single- and multi-carrier systems with or without diversity at the receiver. To the best of our knowledge, the receiver was always assumed to be channel estimation error free and the imperfect CSI was addressed for FAM systems only.

In order to evaluate the effects of channel estimation errors in FAM and SAM systems, in this chapter we investigate both fast and slow adaptive modulation techniques for M-QAM systems with subset diversity (SSD) [102] and with imperfect channel state information. Imperfect CSI will affect diversity, bit reconstruction, and the choice of the optimal modulation size. We recall that, in SAM systems, the large scale fading has to be estimated, while in FAM, the knowledge of the small scale fading is required. Since the coherence time of the small-scale fading is lower than the coherence time of large scale fading, a slower and more accurate estimation can be provided for SAM systems rather than FAM. It follows that, although FAM achieves the best performance in

perfect CSI systems, when errors occur in channel estimation, SAM may even outperform FAM technique, as it will be demonstrated by numerical results, reported in Section 5.6. This explain the importance of investigating FAM and SAM in real systems. In this work, the simplification of assuming the receiver channel estimation error free is not considered. Thus, pilot-based channel estimation errors are assumed to happen at both the transmitter and the receiver. In order to study separately those effects, we address the imperfect CSI at the transmitter first, and then we consider channel estimation errors at the receiver.

4.2 System model

In this section the system model is described and further details on adaptive modulation techniques are provided, following the notation adopted in [6]. We assume a M-QAM modulated symbol transmitted over composite Rayleigh fading and log-normal shadowing channels, employing microdiversity at the receiver, i.e., the shadowing level is the same on each branch. At the receiver, N antennas are considered and a hybrid-selection maximal ratio combiner (H-S/MRC) [19] is adopted for processing the signal. Among N branches, the most powerful L are selected for being processed by the maximal ratio combiner. We define by h_i the fading gain Rayleigh distributed, by E_s the mean (over the fading) symbol energy transmitted and by $N_0/2$ the two-sided spectral density of the AWGN. Since we consider microdiversity, for sake of simplicity, we omit the branch subscript in the averaged SNR notation. The mean signal-to-noise ratio on each branch can be expressed as $\overline{\gamma} = E\{|h|^2\}E_s/N_0$. Since a log-normal shadowing is considered, $\overline{\gamma}_{\mathrm{dB}} = 10\log_{10}(\overline{\gamma})$ is Gaussian distributed with μ_{dB} mean and σ^2_{dB} variance.

4.2.1 Adaptive modulation

As briefly stated before, adaptive modulation techniques achieve the best throughput accordingly with channel conditions, minimizing in the meanwhile the outage probability. When a discrete variable rate is considered, a set of J modulation levels can be adopted in adaptive modula-

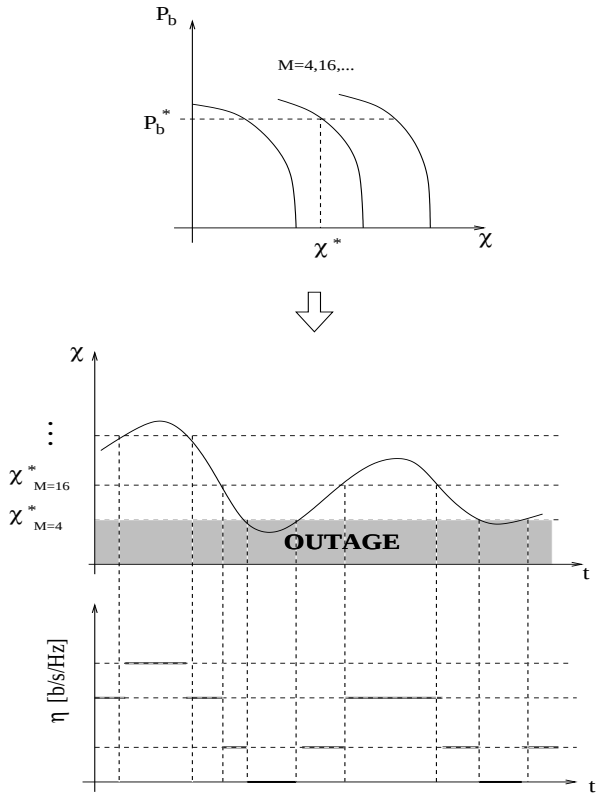

Figure 4.1: Adaptive modulation technique. Starting from the bit error probability expression, the SNR thresholds are evaluated, and then, the optimal modulation level to be adopted is chosen. Note that if FAM (SAM) is considered, the bit error probability, $P_{\rm b}$, considered is the instantaneous (mean) BEP, the SNR parameter, χ, is the instantaneous (mean) SNR, and the observed fluctuations variable with the time are hte small-scale (large-scale) fading.

tion systems, $\{M_0, M_1, \ldots, M_J\}$. The optimal modulation level is chosen depending on the instantaneous SNR or the mean SNR in FAM and SAM, respectively. We denote by χ the SNR parameter based on which the modulation to be adopted is chosen. In particular, $\chi = \gamma_{\rm T}$ in FAM systems and $\chi = \overline{\gamma}_{\rm dB}$ in SAM systems. When χ is not sufficient to guarantee the required target BEP $(P_{\rm b}^{\star})^2$ even with the lowest modulation level M_0, the system is in outage and no bits are transmitted. Other-

[2]The target BEP to be guaranteed is the instantaneous target BEP in FAM systems and the mean target BEP in SAM systems.

wise, the transmitted data rate corresponds to $\log_2 M_j,\ j = 0, \ldots, J$. The optimal data rate is chosen comparing the estimated SNR value in the feedback with the required SNRs per each modulation level, i.e. SNR thresholds, that are set to guarantee the minimum BEP required when the j-th modulation level is adopted, i.e., $P_{\rm b}(\chi_j^\star) = P_{\rm b}^\star$. In particular, when the SNR value falls within the j-th region ($\chi_j^\star < \chi \leq \chi_{j+1}^\star$), the j-th modulation level is adopted for the transmission and $\log_2 M_j$ is the transmitted throughput. If χ up-cross (down-cross) the SNR threshold, the modulation level is switched to a higher (lower) level, leading to an increasing (decreasing) of the throughput. It follows that an important figure of merit is the *mean throughput* [bps/Hz] defined as

$$\begin{aligned}\eta &= \sum_{j=0}^{J-1} \tilde{M}_j\ \mathbb{P}\left\{\chi_j^\star < \chi \leq \chi_{j+1}\right\} + \tilde{M}_J\ \mathbb{P}\left\{\chi_J^\star < \chi\right\} \\ &= \sum_{j=0}^{J-1} \tilde{M}_j\ \left[F_\chi(\chi_{j+1}^\star) - F_\chi(\chi_j)\right] + \tilde{M}_J\ \left[1 - F_\chi(\chi_J^\star)\right] \end{aligned} \tag{4.1}$$

where $\tilde{M}_j = \log_2 M_j$ and $F_\chi(x)$ is the cumulative density function (CDF) of the SNR parameter χ. As far as perfect CSI is concerned, both slow and fast adaptive modulation techniques achieve a mean throughput higher than the one offered by a fixed modulation system, keeping the bit error probability below the BEP target required. Another important measure of the QoS is the *bit error outage probability* (BEO), i.e., the probability that the BEP is greater than the minimum BEP target [103, 104]:

$$P_o(P_{\rm b}^\star) = \mathbb{P}\left\{P_{\rm b}(\chi) > P_{\rm b}^\star\right\} = F_\chi\left(\chi_0^\star\right). \tag{4.2}$$

As already mentioned, when a fast adaptive modulation is considered, $\chi = \gamma_{\rm T}$ and the cumulative density function of the instantaneous SNR is expressed in the canonical expression, derived in [6, eq. (21)], and reported in the Appendix B, (B.1). For SAM systems, $\chi = \overline{\gamma}_{\rm dB}$ and the CDF is expressed as

$$F_{\overline{\gamma}_{\rm dB}}(\xi) = Q\left(\frac{\mu_{\rm dB} - \xi}{\sigma_{\rm dB}}\right) \tag{4.3}$$

where the last equality follows from the Gaussian behavior of the log-normal shadowing and $Q(x) = \int_x^\infty e^{-t^2/2} dt$ is the Gaussian-Q function.

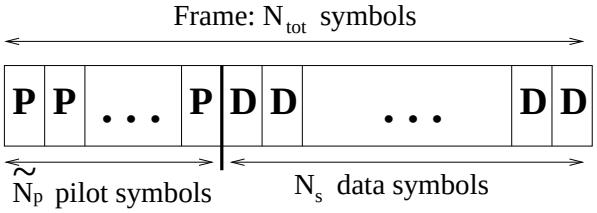

Figure 4.2: Transmitted pilot scheme.

4.2.2 Channel estimation

In order to estimate the complex fading level, a pilot symbols assisted modulation (PSAM) is adopted [44]. By assuming that the transmitted symbols can be grouped together in frames, each of those is equal to the coherence time, $\widetilde{N}_{\rm p}$ symbols are inserted in each frame, and transmitted with $E_{\rm p}$ energy per pilot symbol, as observed in Fig. 4.2. In a generic system with SSD, the number of transmitted pilot symbols, $\widetilde{N}_{\rm p}$, might be different from the number of received pilot symbols, $N_{\rm p}$[3]. We consider a single carrier transmission, and we model the channel as a block fading channel in the time domain. Since a Maximum-Likelihood estimator is considered, the estimated channel coefficient is [102]

$$\widehat{h}_k = h_k + e_k, \tag{4.4}$$

where h_k and e_k are zero-mean Gaussian processes with variance per dimension σ_h^2 and $\sigma_e^2 = \frac{N_0}{2N_{\rm p}E_{\rm p}}$, respectively. It follows that at the output of the MRC with N branches[4], the estimated SNR can be defined as

$$\widehat{\gamma}_{\rm T} = \sum_{k=1}^{N} \widehat{\gamma}_k = \sum_{k=1}^{N} |\widehat{h}_k|^2 \frac{E_s}{N_0}. \tag{4.5}$$

Note that $|\widehat{h}_k|^2 = \mathcal{R}e\{\widehat{h}_k\}^2 + \mathcal{I}m\{\widehat{h}_k\}^2$, and both $\mathcal{R}e\{\widehat{h}_k\}$ and $\mathcal{I}m\{\widehat{h}_k\}$ are zero-mean gaussian distributed with variance $\sigma^2 = \sigma_h^2 + \sigma_e^2$. Therefore, $z = \sum_{k=1}^{N} |\widehat{h}_k|^2$ is chi-square distributed with $2N$ degrees of freedom, and

[3]Although in our system model $\widetilde{N}_p = N_p$, in order to make the study suitable for any SSD system, we denote the number of received or transmitted pilot symbols with two different notations.

[4]We investigate a MRC output first. Then, in Appendix B we extend the framework to H-S/MRC systems.

its PDF is:

$$f_z(\zeta) = \frac{\zeta^{N-1}}{\breve{\gamma}^{\ N}\,\Gamma(N)} \exp\left[-\frac{\zeta}{\breve{\gamma}}\right], \quad \zeta \geq 0 \tag{4.6}$$

where $\breve{\gamma} = 2\sigma^2 E_s/N_0$ is the estimated mean signal-to-noise ratio [5]. It is worthwhile noting that, for M-QAM adaptive modulation systems, imperfect channel state information affects both the transmitter side (in the choice of the optimal modulation) and the receiver side (in the bit reconstruction, for example). It follows that channel estimation errors can doubly affect the system. In order to study separately those effects, we address first imperfect CSI in the feedback, and then at the receiver. Since effects of delayed CSI (outdated channels) have been already deeply investigated in the literature [5, 101], we mainly focus on not delayed feedback.

4.3 Imperfect CSI at the transmitter

In this section, the mean throughput and the BEO for systems with imperfect CSI at the transmitter are investigated. In particular, estimation errors will occur in the estimated fed back SNR value . Recalling that a perfect CSI is assumed at the receiver, we consider the exact BEP expressions, evaluated in [6]. For sake of simplicity, both the instantaneous and mean BEP for systems with SSD are reported in (4.7) and (4.8), respectively.

$$P_b(e|\gamma_T) = \frac{2}{\sqrt{M}\log_2(\sqrt{M})} \sum_{h=1}^{log2(\sqrt{M})} \sum_{i=0}^{(1-2^{-h})\sqrt{M}-1} (-1)^{\lfloor \frac{i2^{h-1}}{\sqrt{M}} \rfloor} \times \left(2^{h-1} - \left\lfloor \frac{i2^{h-1}}{\sqrt{M}} + \frac{1}{2} \right\rfloor\right) Q\left((2i+1)\sqrt{\frac{3\gamma_T}{(M-1)}}\right) \tag{4.7}$$

$$P_{\mathrm{b}}(\overline{\gamma}) = \frac{2}{\sqrt{M}\log_2(\sqrt{M})} \sum_{h=1}^{\log 2(\sqrt{M})} \sum_{i=0}^{(1-2^{-h})\sqrt{M}-1} (-1)^{\lfloor \frac{i2^{h-1}}{\sqrt{M}} \rfloor} \times \left(2^{h-1} - \left\lfloor \frac{i2^{h-1}}{\sqrt{M}} + \frac{1}{2} \right\rfloor\right) I_N\left(\frac{3(2i+1)^2}{2(M-1)}\widetilde{b}_n\right) \tag{4.8}$$

[5] Note that the estimated mean SNR should be noted by $\widehat{\overline{\gamma}}$, but for sake of simplicity, we denote it by $\breve{\gamma}$.

where $I_k(x) = \frac{1}{\pi}\int_0^{\pi/2}\left(\frac{sin^2\theta}{x+sin^2\theta}\right)^k d\theta$. From the bit error probability, exact SNR thresholds are evaluated and compared to the estimated SNR value, i.e., $\chi_i^\star < \widehat{\chi} \leq \chi_{i+1}^\star$. In order to evaluate the mean throughput and the outage probability in systems affected by estimation errors in the feedback, the cumulative density function of $\widehat{\chi}$, $F_{\widehat{\chi}}(\chi)$, has to be evaluated. Considering a fast adaptive modulation system, the PDF of the instantaneous estimated SNR $\widehat{\gamma}_{\mathrm{T}}$, conditioned on a given $\overline{\gamma}$ is

$$f_{\widehat{\gamma}_{\mathrm{T}}|\overline{\gamma}}(\xi) = \begin{cases} \frac{\xi^{N-1}}{\overline{\gamma}^N \sigma_t^{2N}\Gamma(N)}\exp\left[-\frac{\xi}{\overline{\gamma}\sigma_t^2}\right], & \xi \geq 0 \\ 0, & \text{otherwise} \end{cases} \tag{4.9}$$

where $\sigma_t^2 = \frac{\sigma_e^2+\sigma_h^2}{\sigma_h^2}$ and $\overline{\gamma}$ is the averaged signal-to-noise ratio per branch, already defined as

$$\overline{\gamma} = \mathbb{E}\{|h_k|^2\}\frac{E_s}{N_0} = 2\sigma_h^2\frac{E_s}{N_0}.$$

It can be observed that $\sigma_t^2 = 1/\rho^2$, where ρ is the envelope of the complex correlation between h_k and $\widehat{h}_k$ defined as

$$\rho = \frac{\mathbb{E}\{h_k\widehat{h}_k^*\} - \mathbb{E}\{h_k\}\mathbb{E}\{\widehat{h}_k^*\}}{\sqrt{\mathbb{E}\{|h_k - \mathbb{E}\{h_k\}|^2\}\mathbb{E}\{|\widehat{h}_k - \mathbb{E}\{\widehat{h}_k\}|^2\}}} = \frac{\sigma_h^2}{\sqrt{\sigma_h^2(\sigma_h^2+\sigma_e^2)}} = \sqrt{\frac{\sigma_h^2}{\sigma_h^2+\sigma_e^2}}. \tag{4.10}$$

It is worth noting that the correlation depends on the mean SNR per branch and the parameter $N_p\varepsilon$, in particular

$$\sigma_t^2 = \frac{1}{\rho^2} = \frac{\sigma_h^2 + \frac{N_0}{2N_p\varepsilon E_s}}{\sigma_h^2} = \frac{\overline{\gamma} + \frac{1}{N_p\varepsilon}}{\overline{\gamma}}, \tag{4.11}$$

where $\varepsilon = E_{\mathrm{p}}/E_{\mathrm{s}}$ is the ratio between the energy dedicated to pilot symbols and the data symbols energy. Substituting (4.11) in (4.9), the conditioned PDF of the instantaneous estimated SNR $f_{\widehat{\gamma}_{\mathrm{T}}|\overline{\gamma}}$ can be expressed as

$$f_{\widehat{\gamma}_{\mathrm{T}}|\overline{\gamma}}(\xi) = \frac{\xi^{N-1}}{\left(\overline{\gamma} + \frac{1}{N_p\varepsilon}\right)^N \Gamma(N)}\exp\left[-\frac{\xi}{\overline{\gamma} + \frac{1}{N_p\varepsilon}}\right], \quad \xi \geq 0 \tag{4.12}$$

and 0 otherwise ($\xi < 0$). From (4.12), the marginal PDF and CDF of the estimated instantaneous SNR can be derived as

$$f_{\widehat{\gamma}_{\mathrm{T}}}(\xi) = \begin{cases} \int_0^\infty f_{\widehat{\gamma}_T|\overline{\gamma}}(\xi) f_{\overline{\gamma}}(w)dw, & \xi \geq 0, \\ 0, & \text{otherwise} \end{cases} \tag{4.13}$$

and

$$F_{\widehat{\gamma}_{\mathrm{T}}} = \int_0^{\gamma_{\mathrm{T}}^\star} f_{\widehat{\gamma}_{\mathrm{T}}}(\xi)d\xi = \int_0^{\gamma_{\mathrm{T}}^\star} \int_0^{\infty} f_{\widehat{\gamma}_T|\overline{\gamma}}(\xi) f_{\overline{\gamma}}(w)dw\ d\xi \tag{4.14}$$

where the pdf of the average SNR results to be

$$f_{\overline{\gamma}}(w) = \frac{\nu}{\sqrt{2\pi}\sigma_{\mathrm{dB}} w}\exp\left[-\frac{(10\log_{10} w - \mu_{\mathrm{dB}})^2}{2\sigma_{\mathrm{dB}}^2}\right], \quad w \geq 0 \tag{4.15}$$

where $\nu = 10/\ln(10)$.

When a slow adaptive modulation is considered, the system is adapted to the estimated mean SNR, $\breve{\gamma}$. The estimated mean SNR per branch can be expressed as

$$\breve{\gamma} = \mathbb{E}_{h_k}\{\widehat{\gamma}_k\} = 2\sigma^2\frac{E_s}{N_0} = \sigma_t^2\overline{\gamma} = \overline{\gamma} + \frac{1}{N_p\varepsilon}. \tag{4.16}$$

Note that if the variance of the channel estimation error (σ_e^2) is zero, σ_t^2 is equal to 1 and $\breve{\gamma} = \overline{\gamma}$. Knowing the marginal PDF of the log-normal shadowing (4.15), the PDF of the estimated mean SNR is obtained by making a change of variable and it is given by

$$f_{\breve{\gamma}}(\upsilon) = \frac{\nu}{\sqrt{2\pi}\sigma_{\mathrm{dB}}\ (\upsilon - \frac{1}{N_p\varepsilon})}\exp\left[-\frac{\left(10\log_{10}(\upsilon - \frac{1}{N_p\varepsilon}) - \mu_{\mathrm{dB}}\right)^2}{2\sigma_{\mathrm{dB}}^2}\right], \quad \upsilon \geq \frac{1}{N_p\varepsilon} \tag{4.17}$$

From (4.17), the CDF of the averaged estimated SNR can be derived as follows

$$F_{\breve{\gamma}}(x) = \int_{\frac{1}{N_p\varepsilon}}^{x} f_{\widetilde{\breve{\gamma}}}(\upsilon)d\upsilon = \frac{1}{2}\left[\mathrm{erfc}\left(\frac{\mu_{\mathrm{dB}} - 10\log_{10}(x - \frac{1}{N_p\varepsilon})}{\sqrt{2}\sigma_{\mathrm{dB}}}\right)\right] \tag{4.18}$$

The presented analysis is limited to systems employing MRC at the receiver, but it can be easily extended to a SSD system, as explained in the Appendix B.

4.3.1 Mean throughput

In adaptive modulation systems with imperfect CSI, the mean throughput strictly depends on the adopted pilot scheme. Since in each frame, $\widetilde{N}_{\mathrm{p}}$

symbols are inserted (Fig.4.2), only a fraction n_{s} of N_{tot} symbols within a frame is dedicated to data transmission. Assuming the following notation

$$\begin{cases} \widetilde{N}_{\mathrm{p}} = n_{\mathrm{p}}\ N_{\mathrm{tot}} \\ \\ N_{\mathrm{s}} = n_{\mathrm{s}}\ N_{\mathrm{tot}} \end{cases} \Rightarrow n_{\mathrm{p}} + n_{\mathrm{s}} = 1 \tag{4.19}$$

it can be observed the tradeoff between n_{s} and n_{p}, that is the tradeoff between performance and the determined throughput: the more pilot symbols are adopted, the better is the channel estimation quality, but the less is the transmitted throughput. In addition to n_{p} and n_{s}, another important parameter in the pilot scheme design is the ratio between the energy dedicated to pilot symbols and the one dedicated to data symbols, that has been already defined as $\varepsilon = E_{\mathrm{p}}/E_{\mathrm{s}}$. In a system with no constraint on the maximum transmitted energy, a high E_{p} would provide an improvement in the channel quality, without affecting the BEP performance. Unfortunately, in real systems, a maximum transmitted energy is imposed and the following constraint has to be considered

$$\widetilde{N}_{\mathrm{p}} E_{\mathrm{p}} + N_{\mathrm{s}} E_{\mathrm{s}} \leq E_{\mathrm{tot}}. \tag{4.20}$$

Imposing the constraint (4.20), an increasing of the energy dedicated to the pilot symbols has to be balanced by a reduction of the number of pilot symbols $\widetilde{N}_{\mathrm{p}}$, or by a reduction of the energy E_{s}. Note that, when $\varepsilon = 1$, the constraint (4.20) merges to the constraint (4.19), i.e., $\widetilde{N}_{\mathrm{p}} + N_{\mathrm{s}} = N_{\mathrm{tot}}$. The optimization of the energy distribution between data and pilot symbols has been already investigated in [105]. In this section we assume $\varepsilon = 1$. Note that the aim of this section is the comparison of FAM and SAM techniques in the presence of estimation errors in the feedback. In the next section, we will investigate the effects of imperfect CSI at the receiver for the SAM case only, and the $\widetilde{N}_{\mathrm{p}}\varepsilon$ optimization issue will be addressed in more details.

Considering the mean throughput evaluation, it is worth noting that, knowing the CDF for both SAM and FAM systems, (4.18) and (4.14), the mean throughput η can be evaluated from (4.1). For both the techniques, η is the mean throughput for each symbol among the N_{s} data symbols transmitted. To obtain the effective mean throughput per frame, the

number of pilot symbols has to be considered. In particular, the effective mean throughput per symbol per frame is:

$$\eta^{(\text{eff})} = \eta\ n_{\text{s}} = \eta\ (1 - n_{\text{p}}) = \eta\ \left(1 - \frac{\widetilde{N}_{\text{p}}}{N_{\text{tot}}}\right). \tag{4.21}$$

Since we are interested in a comparison between FAM and SAM, the effective mean throughput per symbol per frame has to be considered. We recall that in SAM systems, the coherence time as well as the frame size are greater than the ones in FAM. Therefore, keeping constant the channel estimation quality, (i.e., N_{p}), the symbols dedicated to information symbols in SAM systems are greater than the ones in FAM systems, that is $n_{\text{s}}^{\text{FAM}} \leq n_{\text{s}}^{\text{SAM}}$. Conversely, when the n_{p} value is constant, in SAM systems the number of symbols dedicated to pilot insertion is greater than the one in FAM, it follows that n_{s} is constant between SAM and FAM, but the former has a better channel estimation. This is obvious if we consider that $\widetilde{N}_{\text{p}}^{\text{FAM}} \leq \widetilde{N}_{\text{p}}^{\text{SAM}}$, and we assume E_{p} constant.

4.3.2 Outage probability

In systems with imperfect CSI at the transmitter, the estimated SNR $\widehat{\chi}$ can be either underestimated or overestimated. The former case leads to a reduction of the throughput, while the latter leads to an increase of either the mean throughput and outage probability. In particular, when $\widehat{\chi} > \chi$, although the real SNR falls within the j-th modulation range, the $(j+1)$-th modulation might be adopted. In this case, the effective bit error probability is greater than the target BEP and the system is in outage. It means that the system is in outage when $\chi < \chi_0^\star$, and also when the following condition is verified

$$\begin{cases} \widehat{\chi} > \chi_i^\star \\ \chi \leq \chi_i^\star \end{cases} \quad \forall i. \tag{4.22}$$

Assuming that $\widehat{\chi} = \chi + \Delta\chi$, the previous condition can be expressed as

$$\chi_i^\star - \Delta\chi < \chi \leq \chi_i^\star. \tag{4.23}$$

It follows that the outage probability of an adaptive modulation system with imperfect CSI at the transmitter can be expressed as

$$P_o = F_\chi(\chi_0^\star) + \sum_{j=1}^{J} \left[F_\chi(\chi_j^\star) - F_\chi(\chi_j^\star - \Delta\chi) \right]. \tag{4.24}$$

For a slow adaptive modulation, considering the CDF of the average SNR in (4.16), $\Delta\chi = 1/N_\mathrm{p}\varepsilon$ and the outage probability conditioned on the adopted pilot scheme is

$$\begin{aligned} P_o &= Q\left(\frac{\mu_\mathrm{dB} - \overline{\gamma}^*_{0,\mathrm{dB}}}{\sigma_\mathrm{dB}}\right) + \\ &+ \sum_{j=1}^{J} \left[Q\left(\underbrace{\frac{\mu_\mathrm{dB} - \overline{\gamma}^*_{j,\mathrm{dB}}}{\sigma_\mathrm{dB}}}_{a_j} \right) - Q\left(\underbrace{\frac{\mu_\mathrm{dB} - 10\log_{10}\left(\overline{\gamma}^*_j - \frac{1}{N_\mathrm{p}\varepsilon}\right)}{\sigma_\mathrm{dB}}}_{b_j} \right) \right] = \\ &= Q\left(\frac{\mu_\mathrm{dB} - \overline{\gamma}^*_{0,\mathrm{dB}}}{\sigma_\mathrm{dB}}\right) + \sum_{j=1}^{J} \int_{a_j}^{b_j} e^{-\frac{y^2}{2}} dy. \end{aligned} \tag{4.25}$$

As expected, increasing $N_\mathrm{p}\varepsilon$, the estimation accuracy increases and the outage probability converges to the BEO of systems with perfect CSI.

4.4 Imperfect CSI at the receiver

In this section, the bit error probability (BEP) and bit error outage (BEO) expressions for SSD are evaluated in slow adaptive modulation systems with imperfect CSI at the receiver and Rayleigh or Nakagami-m fading channels. We recall that, to estimate the channel, a pilot symbols assisted modulation (PSAM) is adopted and a Maximum-Likelihood estimator is employed. We denote by $\widetilde{N}_\mathrm{p}$ the pilot symbols inserted in each frame equal to the coherence time and transmitted with E_p energy per pilot symbol. The estimated channel coefficients are given by (4.4), where e_k is a zero-mean Gaussian process with variance per dimension $\sigma_e^2 = \frac{N_0}{2N_\mathrm{p}E_\mathrm{p}}$.

4.4.1 Bit error probability

The performance of N-branch diversity combining in the presence of imperfect CSI was studied in [102] and [106] for MRC and SSD, respectively. In [106], the symbols error probability (SEP) was obtained for i.i.d. Nakagami-m fading channels for arbitrary two-dimensional signaling constellations. When M-QAM modulation is considered, the SEP as a function of the SNR averaged over the small scale fading and the $\{s_i\}$ symbols is expressed by

$$\begin{aligned} P_e(\overline{\gamma}, N_p\varepsilon) =& \frac{1}{M}\sum_i \omega_i^{(a)} I_N\left(\zeta^{(i)}, \Phi_2, \frac{\pi}{4}\right) + \\ & \frac{1}{M}\sum_i \omega_i^{(b)} I_N\left(\zeta^{(i)}, \Phi_4, 0\right), \end{aligned} \tag{4.26}$$

$$I_N(\zeta, \phi, \psi) = \frac{1}{2\pi}\int_0^{\phi}\prod_{n=1}^{N}\left(\frac{sin^2(\theta+\psi)m}{sin^2(\theta+\psi)m + b_n\zeta}\right)^m, \tag{4.27}$$

where $\Phi_M = \pi(M-1)/M$, and $N_{\rm p}$ is the number of received pilot symbols. The set of $\{\zeta^{(i)}\}$ is a function of the averaged SNR:

$$\begin{aligned} \zeta^{(i)}(\overline{\gamma}, N_{\rm p}\varepsilon) \triangleq& \frac{E_s\rho^2}{\sigma_h^2\left(\frac{N_0}{2} + |s_i|^2\sigma_e^2\rho^2\right)} \\ =& \frac{\overline{\gamma}N_p\varepsilon\ c_{\rm MQAM}}{\frac{1}{\overline{\gamma}} + N_{\rm p}\varepsilon + \xi_i}, \end{aligned} \tag{4.28}$$

where $c_{\rm MQAM} = 3/(2(M-1))$, and $\rho = \sigma_h^2/(\sigma_h^2+\sigma_e^2)$. The parameters $\omega_i^{(a)}$, $\omega_i^{(b)}$ and $\xi_i \triangleq E_i/E_S$ depend on the modulation format, and are given in [106]. Note that the summation in (4.26) is performed over the non zero values $\omega_i^{(a)}$, $\omega_i^{(b)}$ and ξ. Moreover, the BEP for Rayleigh fading channels can be obtained by setting $m = 1, \forall n$ in (4.26). In the case of ideal channel estimation ($N_p\varepsilon \longrightarrow \infty$), (4.28) results given by $\zeta^{(i)} = \overline{\gamma}\ c_{\rm MQAM}$. The set $\{b_n\}$ depends on the SSD technique. When a hybrid-selection maximal ratio combiner (H-S/MRC) [19] is adopted at the receiver, among N branches the strongest L are selected for being processed by the maximal ratio combiner. For such systems, the b_n's are expressed as

$$b_n = \begin{cases} 1 & n \le L \\ L/n & \text{otherwise.} \end{cases}$$

When a MRC is considered at the receiver, $L = N$ and $b_n = 1, \forall n$.

In a perfect CSI system, as well as in an imperfect one, the modulation regions are bounded by SNR thresholds evaluated from the BEP. Starting from the SEP, and assuming Gray coding between bits and symbols, the bit error probability, P_{b}, can be expressed by a lower bound:

$$P_{\mathrm{b}}(\overline{\gamma}, N_{\mathrm{p}}\varepsilon) \geq \frac{P_{\mathrm{e}}(\overline{\gamma}, N_{\mathrm{p}}\varepsilon)}{\log_2(M)}. \tag{4.29}$$

By numerical root evaluations, the SNR estimated thresholds $\breve{\gamma}^{\star}$ are obtained from (4.29) as the values that satisfy the target BEP, i.e. $P_{\mathrm{b}}(\breve{\gamma}^{\star}, N_{\mathrm{p}}\varepsilon) = P_{\mathrm{b}}^{\star}$. Note that, in an imperfect CSI system, the thresholds are a function of the modulation level as well as the channel estimation quality.

Together with the bit error probability, the BEO depends on the quality of the channel estimation. Since the estimated thresholds $\breve{\gamma}^{\star}$ are greater than the ideal ones ($\Delta\overline{\gamma}_{\mathrm{dB}}$ is always greater or equal to zero), the condition (4.22) is not verified and the BEO can be expressed as

$$P_o = F_{\chi}(\widehat{\chi}_0). \tag{4.30}$$

4.4.2 Mean throughput

As already observed, the throughput in adaptive modulation systems with imperfect CSI strictly depends on the adopted pilot scheme. For systems with SSD, the portion of the frame dedicated to pilot insertion is defined as $n_{\mathrm{p}} = \widetilde{N}_{\mathrm{p}}/N_{\mathrm{tot}}$, and the following constraints are imposed

$$\begin{cases} \widetilde{N}_{\mathrm{p}} + N_{\mathrm{s}} = N_{\mathrm{tot}} \\ \\ \widetilde{N}_{\mathrm{p}} E_{\mathrm{p}} + N_{\mathrm{s}} E_{\mathrm{s}} = E_{\mathrm{tot}}. \end{cases} \tag{4.31}$$

As already observed, when $\varepsilon \neq 1$, the increasing of E_{p} has to be balanced by the reduction of $\widetilde{N}_{\mathrm{p}}$ or E_{s}. It follows that the energy dedicated to the information symbols strictly depends on the adopted pilot scheme. In particular, from (4.31), it can be derived the following expression

$$E_{\mathrm{s}} = \frac{E}{\frac{\widetilde{N}_{\mathrm{p}}}{N_{\mathrm{tot}}}(\varepsilon - 1) + 1}, \tag{4.32}$$

where $E \triangleq E_{\text{tot}}/N_{\text{tot}}$. It can be better understood that the increasing of $\widetilde{N}_{\text{p}}\varepsilon$ leads to an improvement of the performance due to a better quality of the channel estimation on one hand, and to a reduction of the performance due to a lowering of E_{s} on the other hand. It follows that even the exact mean SNR in (4.26) is a function of the pilot scheme, i.e., $\overline{\gamma} = \overline{\gamma}(\widetilde{N}_{\text{p}}\varepsilon)$, as expressed in the following

$$\overline{\gamma} = \mathbb{E}\{|h|^2\}\frac{E_{\text{s}}}{N_0} = \frac{\mathbb{E}\{|h|^2\}}{N_0}\frac{E}{\frac{\widetilde{N}_{\text{p}}}{N_{\text{tot}}}(\varepsilon-1)+1} = \frac{1}{\frac{\widetilde{N}_{\text{p}}}{N_{\text{tot}}}(\varepsilon-1)+1}\Upsilon, \quad (4.33)$$

where $\Upsilon = \mathbb{E}\{|h|^2\}E/N_0$. Substituting (4.33) in (4.26), the bit error probability can be expressed as a function of two parameters: $N_{\text{p}}\varepsilon$ characterizing the pilot scheme design, and Υ representing the mean SNR per frame.

$$P_{\text{b}} = P_{\text{b}}\left(\overline{\gamma}(\widetilde{N}_{\text{p}}\varepsilon), N_{\text{p}}\varepsilon\right) = P_{\text{b}}\left(\Upsilon\frac{1}{\frac{\widetilde{N}_{\text{p}}}{N_{\text{tot}}}(\varepsilon-1)+1}, N_{\text{p}}\varepsilon\right) \Longrightarrow P_{\text{b}} = P_{\text{b}}(\Upsilon, \widetilde{N}_{\text{p}}\varepsilon) \quad (4.34)$$

Note that, unlikely the mean SNR $\overline{\gamma}$, Υ does not depend on the pilot scheme, but only on the mean energy over the frame, N_0 and $\mathbb{E}\{|h|^2\}$. This independent variable might be employed to compare systems with different pilot schemes. Thus, from here onwards, the SNR averaged over the frame, Υ, will be the SNR variable in the BEP expression, and thus the SNR thresholds will be denoted by $\Upsilon^\star$. We assume that the SNR averaged over the frame is a log-normal distributed[6], i.e., $\Upsilon_{\text{dB}} \sim N(\mu_{\text{dB}}, \sigma^2_{\text{dB}})$. Thus, the cumulative density function of Υ_{dB} is

$$F_{\Upsilon_{\text{dB}}}(\xi) = Q\left(\frac{\mu_{\text{dB}} - \xi}{\sigma_{\text{dB}}}\right) \quad (4.35)$$

and the mean throughput of each information symbols of the frame is

$$\eta = \sum_{j=1}^{J-1} \tilde{M}_j \left[F_{\Upsilon_{\text{dB}}}(\Upsilon^\star_{\text{dB},j+1}) - F_{\Upsilon}(\Upsilon^\star_{\text{dB},j})\right] + \tilde{M}_J \left[1 - F_{\Upsilon}(\Upsilon^\star_{\text{dB},J})\right]. \quad (4.36)$$

[6]Note that, in the previous section, $\overline{\gamma}$ was log-normal distributed. Since here we do not have any comparison with performance of the previous case, or with any FAM systems (i.e., we do not have any comparison with systems employing $\overline{\gamma}$ as variable rather than Υ), we make the simplification that Υ is log normal with mean μ_{dB} and variance σ^2_{dB}. Note that, eventually, knowing the PDF of $\overline{\gamma}$, the PDF of Υ can be easily derived.

Recalling that in SSD systems, the number of transmitted pilot symbols is not necessarily equal to the received pilot symbols, the effective mean throughput per symbol per frame is

$$\eta^{(\mathrm{eff})} = \eta \; n_{\mathrm{s}} = \eta \; \frac{N_{\mathrm{tot}} - \widetilde{N}_{\mathrm{p}}}{N_{\mathrm{tot}}}. \tag{4.37}$$

From (4.21), the tradeoff between estimation quality and transmitted data can be observed. The more pilot symbols are transmitted, the better is the channel quality at the cost of a lower effective throughput.

4.5 Numerical results

In this section, numerical results are presented in terms of effective throughput $\left(\eta^{(\mathrm{eff})}\right)$ and BEO for both slow and fast adaptive modulation systems. Coherent detection of M-QAM with H-S/MRC and Gray code mapping in composite Rayleigh or Nakagmai-m fading and log-normal shadowing channels with both perfect and imperfect CSI was considered. In the subsection 4.5.1, we provide numerical results when channel estimation errors occur at the transmitter side, while in the subsection 4.5.2, results for systems with imperfect CSI at the receiver are considered. In both the cases, pilot symbol assisted modulation with $\widetilde{N}_{\mathrm{p}} = N_{\mathrm{p}}$ is considered.

4.5.1 Imperfect CSI at the transmitter

For systems with imperfect CSI at the transmitter, the effective throughput is evaluated by (4.21) and (4.1), by imposing a target BEP of 10^{-2}, and a maximum outage probability of 5%. The exact BEP expressions are reported (4.8) and (4.7), while the CDFs are given by (4.18) and (4.14) for SAM and FAM systems, respectively. In the effective throughput evaluation, the constraint (4.19) is assumed for the energy repartition ($\varepsilon = 1$).

In Fig. 4.3, the outage probability as a function of μ_{dB} is reported for SAM systems, with MRC with 4 branches and $M_{\max} = 256$. Several channel estimation quality levels are considered and compared to

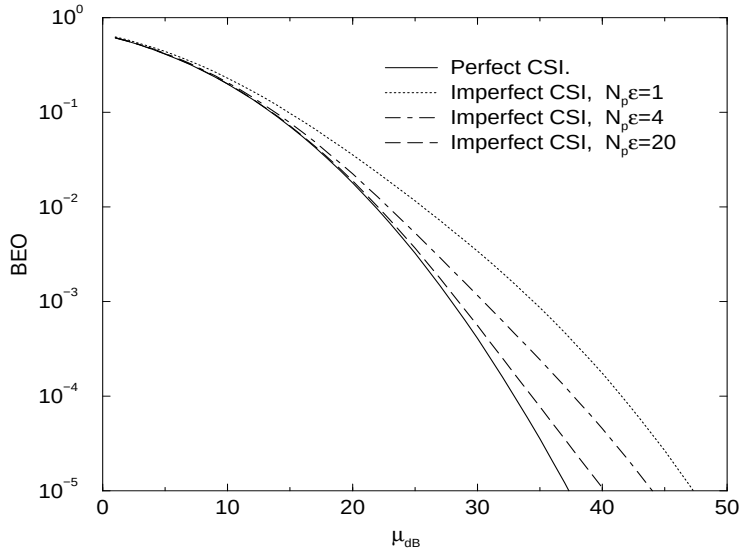

Figure 4.3: BEO vs. μ_{dB} for SAM system with maximum modulation size 256, $N = 4$, $P_{\mathrm{b}}^{\star} = 10^{-2}$, and $\sigma_{\mathrm{dB}} = 8$. A comparison between perfect and imperfect CSI is reported.

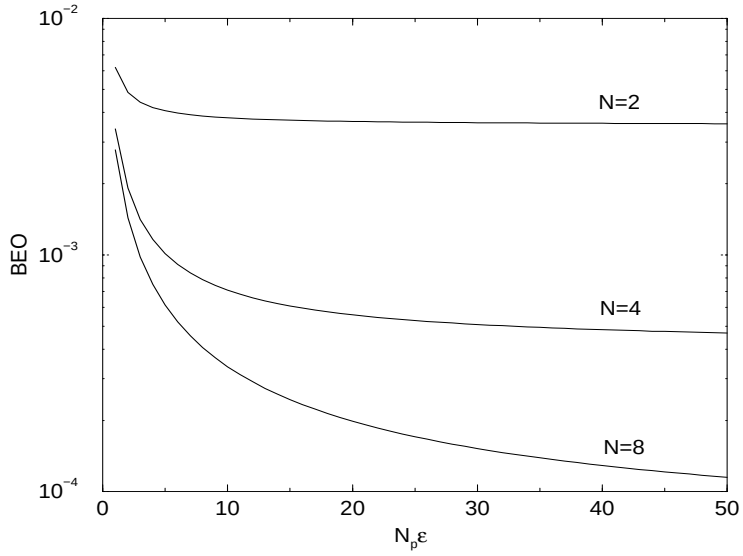

Figure 4.4: BEO vs. $N_{\mathrm{p}}\varepsilon$ for SAM systems with imperfect CSI, maximum modulation size 256, $N = 2, 4$, and 8, $P_{\mathrm{b}}^{\star} = 10^{-2}$, $\mu_{\mathrm{dB}} = 35$ and $\sigma_{\mathrm{dB}} = 8$.

the outage probability of the perfect CSI system. As expected, a low channel estimation quality deeply affects the system in terms of outage

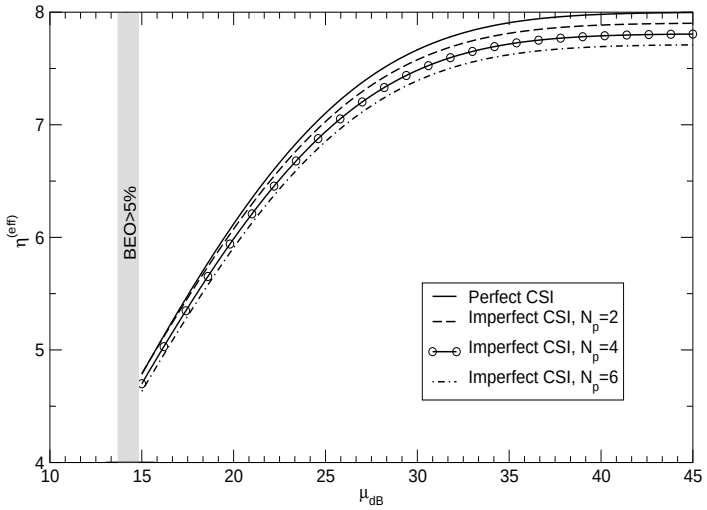

Figure 4.5: Effective throughput vs. μ_{dB} for SAM systems with MRC ($N = 4$), maximum constellation size 256, maximum outage 5%, $P_{\mathrm{b}}^{\star} = 10^{-2}$, and $\sigma_{\mathrm{dB}} = 8$. Results are evaluated for both perfect and imperfect CSI, considering several channel estimation quality levels.

probability (see, for example, $N_{\mathrm{p}}\varepsilon = 1$). By increasing the channel estimation quality (increasing $N_{\mathrm{p}}\varepsilon$), the outage probability curve merges to the BEO of a perfect CSI system. This behavior can also be observed in Fig. 4.4, where the outage probability as a function of $N_p\varepsilon$ is reported for systems with $N = 2, 4$, and 8 branches at the receiver. For all the diversity orders, the outage probability experiences an asymptotic behavior. Increasing $N_{\mathrm{p}}\varepsilon$ the BEO tends to the outage probability of a perfect CSI system. In Fig. 4.5, the effective throughput vs. μ_{dB} is reported for system with slow adaptive modulation, MRC ($N = 4$) and imperfect CSI at the transmitter. As already preannounced from the theory, the increasing of pilot symbols improves the channel estimation quality, but it reduces at the same time the transmitted data symbols. The tradeoff between estimation quality and throughput can be observed in the figure, where for the considered system, $N_{\mathrm{p}} = 2$ provides a sufficient quality estimation, without affecting the mean throughput.

A comparison between SAM and FAM in terms of effective throughput is reported in Fig. 4.6. It is worth noting that, since SAM and FAM have different coherence times, the comparison can be done keeping con-

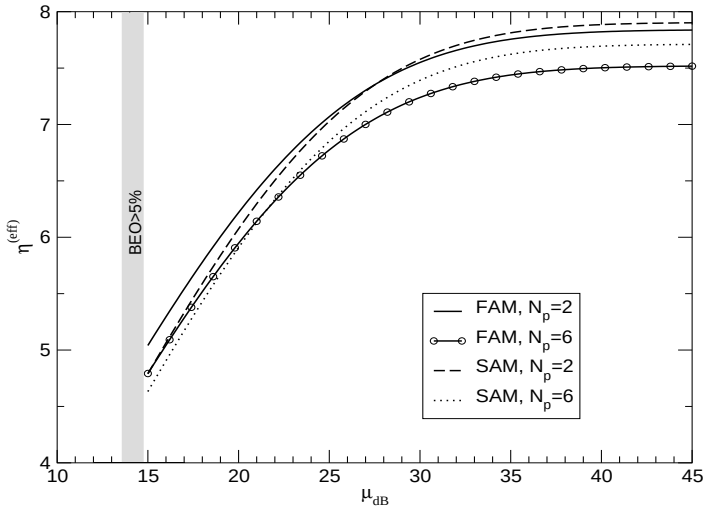

Figure 4.6: Comparison between effective throughout in SAM and in FAM systems with imperfect CSI, maximum modulation level 256, maximum outage 5%, $P_{\rm b}^{\star} = 10^{-2}$, and $\sigma_{\rm dB} = 8$.

stant the number of pilot symbols ($N_{\rm p}$) or the portion of coherence time dedicated to pilot symbols ($n_{\rm p}$). In our simulation, we kept constant $N_{\rm p}$, thus, in SAM systems, the number of data symbols in a coherence time will be greater than the $N_{\rm s}$ in FAM systems. It follows that, when an imperfect channel estimation is considered, SAM can outperform fast adaptive modulation technique, as observed in Fig. 4.6. For both $N_{\rm p}$ values considered in the figure, it can be noticed a crossing point (in terms of $\mu_{\rm dB}$) where the SAM system outperforms the FAM one, and it decreases with the number of pilot symbols. This means that, by increasing the number of pilot symbols inserted within the frame (i.e., by increasing the estimation quality), the crossing point beyond which SAM outperforms FAM is reduced. This very important result allow to demonstrate the sentence already mentioned in the introductory section, that is "Although FAM achieves the best performance in perfect CSI systems, when errors occur in channel estimation, SAM may even outperform FAM technique". It follows that, in real systems, in addiction to the fact that SAM are less expensive than FAM because of the less frequent feedback, SAM takes advantage from the lower coherence time, leading to an effective SE close

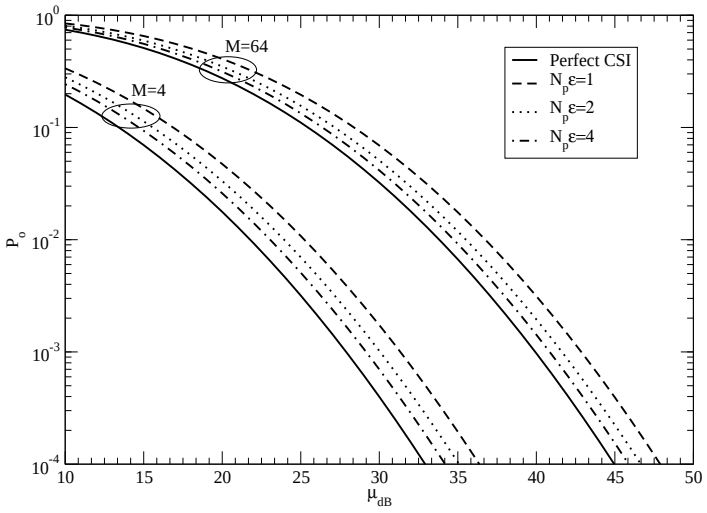

Figure 4.7: BEO vs. μ_{dB} for a non adaptive scheme with $P_{\mathrm{b}}^{\star}$, $\sigma_{\mathrm{dB}} = 8$, $N = 4$ (MRC), different constellation sizes M ($M = 4$, $M = 64$) and both perfect and imperfect CSI systems.

(and sometimes even higher) than the one achieved by FAM.

4.5.2 Imperfect CSI at the receiver

We now present the numerical results in terms of effective throughput $\left(\eta^{(\mathrm{eff})}\right)$ and outage probability for slow adaptive modulation systems with imperfect CSI at the receiver. The effective throughput is evaluated by (4.37) and (4.1), by adopting a target BEP of 10^{-2} and an maximum outage probability of 5%. For the imperfect channel estimation case, the BEP is obtained from (4.29) and (4.26). The SEP for perfect CSI systems is easily derived substituting in (4.37) $\zeta^{(i)} = \overline{\gamma}\ c_{\mathrm{MQAM}}$. In the effective throughput evaluation, the constraint (4.31) is assumed for the energy repartition. In the following, first we show the results for the case $\varepsilon = 1$, then we provide results for a more general case $\varepsilon \neq 1$.

In Fig. 4.7, the outage probability as a function of the median value μ_{dB} for non adaptive modulation systems with eight-branches MRC is shown for both perfect and imperfect CSI ($N_{\mathrm{p}}\varepsilon = 1, 2$, and 4) unconstrained systems. As expected, increasing the $N_{\mathrm{p}}\varepsilon$ parameter, the estimation quality improves, leading to a reduction of the BEO. In Fig. 4.8,

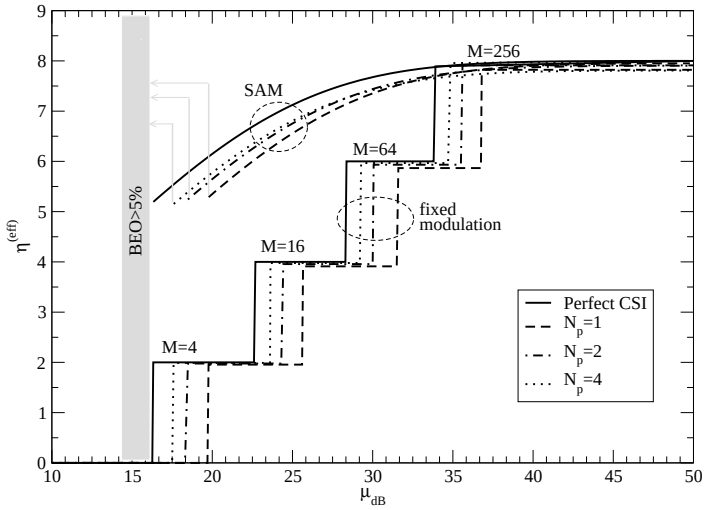

Figure 4.8: Effective throughput vs. μ_{dB} for adaptive and non-adaptive scheme with $P_{\mathrm{b}}^{\star}$, $\sigma_{\mathrm{dB}} = 8$, $N = 4$ (MRC), $\varepsilon = 1$, maximum modulation $M_{\max} = 256$, and $N_{\mathrm{tot}} = 180$.

we compare the fixed modulation scheme with SAM in terms of effective throughput for various N_{p} values and modulation levels ranging from $M = 4$ to $M = 256$. A four-branches MRC is considered at the receiver, and $\varepsilon = 1$. Even for systems with imperfect CSI, it can be observed the gain achieved by adopting the SAM technique rather than the non-adaptive one. Note that if an outage level of 5% is considered, the minimum μ_{dB} value that guarantee that minimum outage depends on the channel estimation quality, as a consequence of the fact that the BEO is affected by estimation errors. Note that the channel estimation errors affect not only the minimum μ_{dB}, but also the effective spectral efficiency.

Increasing the channel estimation quality, and thus N_{p}, the number of transmitted data $(N_{\mathrm{tot}} - N_{\mathrm{p}})$ decreases, leading to a reduction of the effective throughput. It follows that the number of pilot symbols has to be the optimal tradeoff between the effective throughput penalty and the gain achieved by having an improved channel estimation. It is worth noting that, increasing μ_{dB}, the system with low N_{p} may outperform system with better channel estimation quality. This crossing behavior

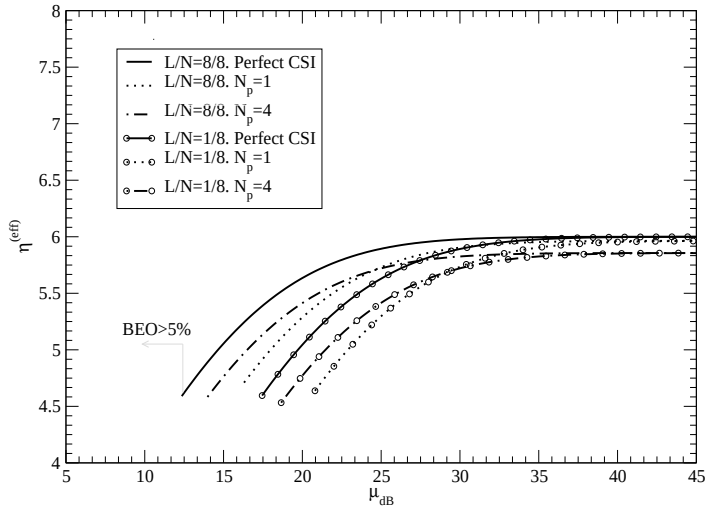

Figure 4.9: Effective throughput vs. μ_{dB} for SAM systems with $P_{\mathrm{b}}^{\star}$, $\sigma_{\mathrm{dB}} = 8$, H-S/MRC (L/N=2/8) and MRC (L/N=8/8), $\varepsilon = 1$, maximum modulation $M_{\max} = 64$, and $N_{\mathrm{tot}} = 180$.

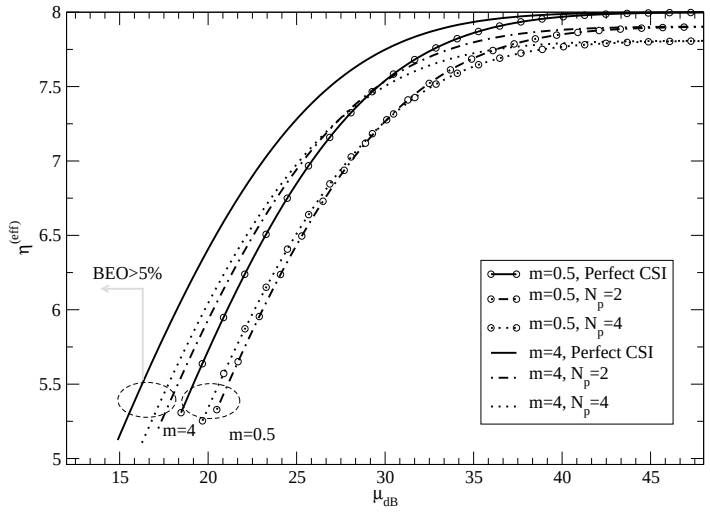

Figure 4.10: Effective throughput vs. μ_{dB} for SAM systems with $P_{\mathrm{b}}^{\star} = 10^{-2}$, Nakagami$-m$ channels with $m = 0.5$ and $m = 4$, $\sigma_{\mathrm{dB}} = 8$, MRC (N=8), $\varepsilon = 1$, maximum modulation $M_{\max} = 64$, and $N_{\mathrm{tot}} = 180$.

can be better observed in Fig. 4.9 and in Fig. 4.10. In the former, the effective throughput is shown as a function of μ_{dB} for both H-S/MRC

($L/N = 2/8$) and MRC ($L/N = 8/8$) systems with $M_{\max} = 64$, and $\varepsilon = 1$. As expected, the more complex MRC system achieves higher diversity than the H-S/MRC with $L/N = 2/8$, leading to a higher mean throughput and a lower outage probability. In Fig. 4.10, the effective throughput is shown as a function of μ_{dB} for a four-branches MRC and Nakagami-m channel with m=0.5 and m=4, $M_{\max} = 64$, and $\varepsilon = 1$. As expected from the Nakagami channels properties, even with channel estimation errors, higher m values achieves better effective throughput. More important, in both the figures, channel estimation errors affect the system and the tradeoff between estimation quality and transmitted data can be evaluated. The more pilot symbols are inserted, the better is the estimation quality but the lower is the number of transmitted data. It follows that, only for low performance system, it is worthy having a high number of pilot symbols. The throughput penalty paid for inserting pilot symbols can be observed from the asymptotic behavior of the throughput. For high μ_{dB} values, for example $\mu_{\text{dB}} = 40$, the system with good channel estimation quality ($N_{\text{p}} = 4$) is outperformed by the system with a lower estimation quality ($N_{\text{p}} = 1$ and $N_{\text{p}} = 2$). On the contrary, for low μ_{dB} values, for example $\mu_{\text{dB}} = 20, 25$, the system with $N_{\text{p}} = 4$ achieves the best performance.

In Fig. 4.11 the effective throughput as a function of N_{p} is shown for different median values μ_{dB} and an eight-branches MRC receiver. Here, the optimal pilot scheme design issue is addressed for a system with $\varepsilon = 1$. Increasing of the number of pilot symbols, the effective throughput does not have a monotonically behavior, as it can be observed in the figure, where the N_{p} value that achieves the best throughput is highlighted with a circle. The pilot scheme that adopts the best N_{p} value is able to compensate the throughput penalty with the improvement of the performance, given by the channel estimation improvement. Considering the curve of $\mu_{\text{dB}} = 25$, for example, the best effective throughput is achieved by $N_{\text{p}} = 4$. For N_{p} higher than this value ($N_{\text{p}} = 4$ for the system with $\mu_{\text{dB}} = 25$), the lost of effective throughput is not rewarded by the channel estimation, and a reduction of the effective throughput is experienced. By increasing the median value μ_{dB}, a worthy channel

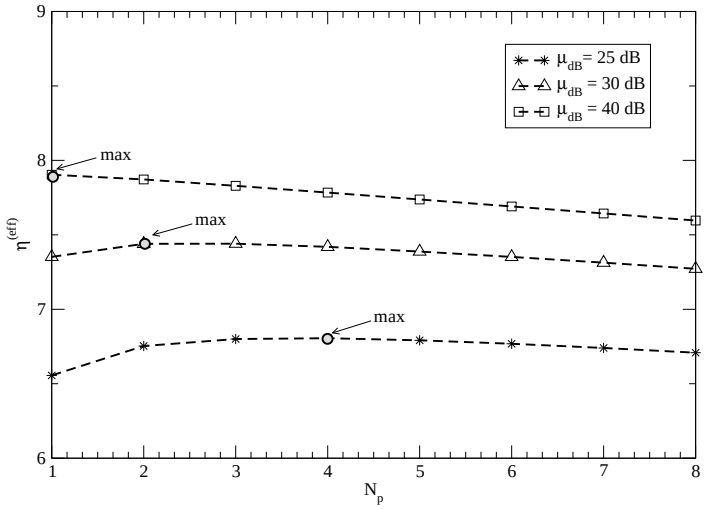

Figure 4.11: Effective throughput vs. $N_{\rm p}$ for SAM systems with $P_b^\star$, $\sigma_{\rm dB} = 8$, MRC ($N = 8$), $\varepsilon = 1$, and maximum modulation $M_{\rm max} = 256$. Several median values $\mu_{\rm dB}$ are considered, $\mu_{\rm dB} = 25, 30, 40$. $N_{\rm tot} = 180$.

estimation quality can be achieved by a low number of received pilot symbols. Thus, the optimal the optimal number of pilot symbols per frame decreases by increasing the $\mu_{\rm dB}$ value, as observed in the figure.

A more general system ($\varepsilon \neq 1$) is considered in Fig. 4.12 and Fig. 4.13, where the constraint (4.31) is considered. In Fig. 4.12, the effective throughput vs. $N_{\rm p}$ is provided for SAM systems with $M_{\rm max} = 256$, and MRC receiver with order of diversity 4. Several $\mu_{\rm dB}$ and ε values are considered. The first important observation to be done is that, by keeping the $N_{\rm p}\varepsilon$ product constant, but varying both the values $N_{\rm p}$ and ε values, different results can be achieved. For example, for the curve of $\mu_{\rm dB} = 20$, considering $N_{\rm p}\varepsilon = 9$, the systems with $N_{\rm p} = 3$ and $\varepsilon = 3$ outperforms the one with $N_{\rm p} = 9$ and $\varepsilon = 1$. This is due to the fact, for a constant frame size, that the latter has a lower number of data symbols. Note also that $E_{\rm s}$ decreases at the increasing of $N_{\rm p}$. Thus, for high $N_{\rm p}$ values, a low ε parameter might outperform systems with high ε values. Considering $\mu_{\rm dB} = 20$, and $N_{\rm p} = 12$ in Fig. 4.12, for example, the system with $\varepsilon = 0.5$ achieves a higher $\eta^{(\rm eff)}$ than the other systems. The pilot scheme design issue, and therefore the tradeoff between channel estimation quality and throughput, can also be observed in the Fig. 4.13, where

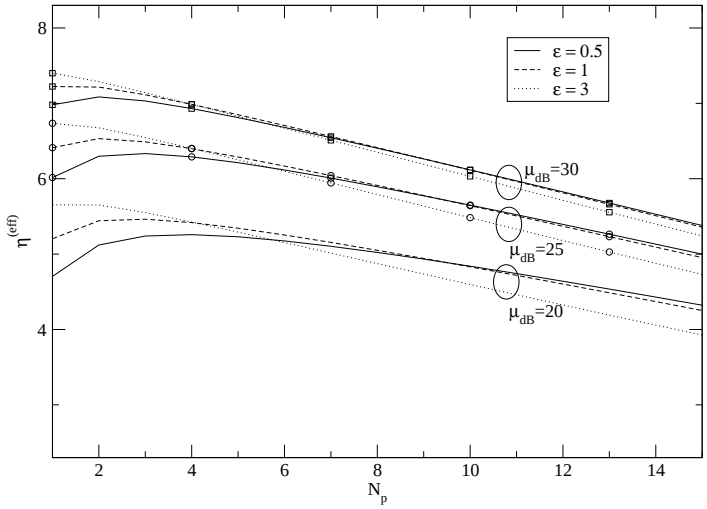

Figure 4.12: Effective throughput vs. $N_{\rm p}$ for SAM systems with $P_b^\star = 10^{-2}$, $\sigma_{\rm dB} = 8$, MRC (N=4), maximum modulation $M_{\rm max} = 256$. Several median values $\mu_{\rm dB}$ ($\mu_{\rm dB} = 25, 30, 40$) and ε values ($\varepsilon = 0.5, 1, 3$) are considered. $N_{\rm tot} = 100$.

the SNR outage penalty and the throughput penalty vs. ε are reported for SAM systems with $M_{\rm max} = 256$, 8-branch MRC receivers, amd several $N_{\rm p}$ values. The SNR outage penalty, reported in Fig. 4.13 (a), is the difference between the $\mu_{\rm dB}^{\rm BEO}$ value that reaches the minimum BEO for a perfect CSI system and the $\mu_{\rm dB}^{\rm BEO}$ of imperfect CSI system. Again, although the $N_{\rm p}\varepsilon$ product is constant, varying $N_{\rm p}$ or ε does not provide the same effective throughput. In particular, the minimum SNR BEO penalty is achieved by $N_{\rm p} = 6$ and $\varepsilon \sim 1$. Analogously, the mean throughput penalty (Fig. 4.13 (b)) represents the difference (in dB) between the mean throughput achieved by the perfect and imperfect CSI systems. Note that, in this case, $N_{\rm p} = 6$ does not provide the minimum penalty, that is reached by $N_{\rm p} = 1$ and $\varepsilon \sim 9$. It means that, in order to reduce the throughput penalty, low $N_{\rm p}$ values are preferred, due to the fact the the higher the pilot symbol number, the lower the data symbol number within each frame. In conclusion, based on the requirement of the user (minimization of the BEO or $\eta^{(\rm eff)}$) the best performance might be achieved employing the most suitable pilot scheme design.

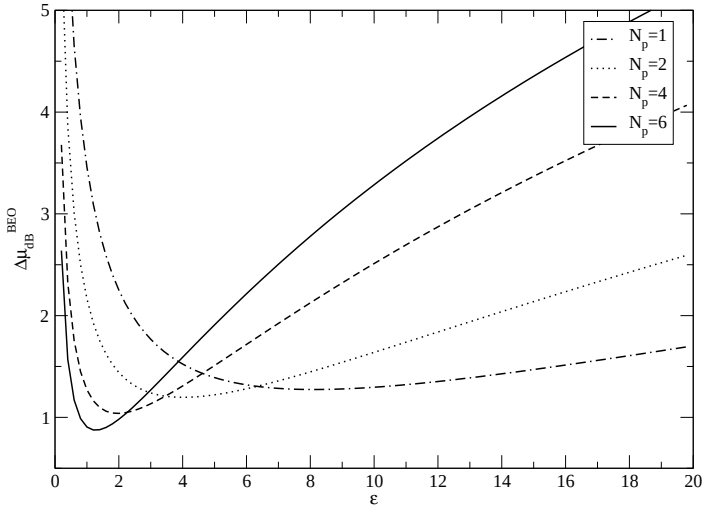

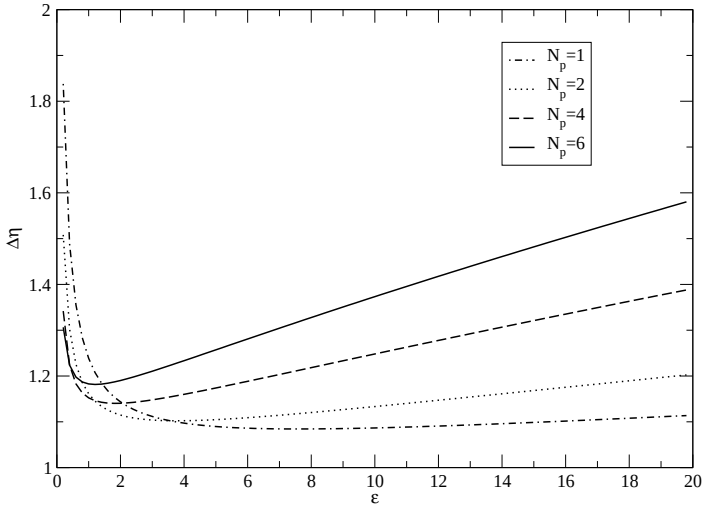

(b) Mean throughput penalty

Figure 4.13: SNR outage penalty and Mean throughput penalty vs. ϵ for SAM systems with $P_b^\star$, $\sigma_{\mathrm{dB}} = 8$, MRC (N=4), and several values of pilot symbols ($N_{\mathrm{p}} = 1, 2, 4$,and 6). In the throughput penalty plot(b), $\mu_{\mathrm{dB}} = 15$.

4.6 Conclusion

In this chapter, we investigated both fast and slow adaptive modulation techniques when channel estimation errors are assumed. We addressed the effects imperfect CSI both at the transmitter and the receiver on adaptive modulation. In the former case, a comparison between FAM and SAM was provided for systems with MRC, showing that, for some system configurations, the slow adaptive modulation technique can outperform the FAM. Then, channel estimation at the receiver was investigated for SAM systems with H-S/MRC for Rayleigh and Nakagami-m channels. We compared SAM with fixed-modulation schemes in terms of outage probability and effective spectral efficiency. Even for imperfect CSI systems, SAM technique achieves substantial improvement over non adaptive schemes. Moreover, the optimal pilot scheme design was investigated for systems employing subset diversity. A high number of pilot symbols achieves a good estimation quality at the cost of a spectral efficiency reduction. Thus, the tradeoff between estimation quality and throughput was addressed. In particular, the higher is the median value μ_{dB}, the lower is the number of pilot symbols required.

Chapter 5

Adaptive modulation in the presence of interference and imperfect thresholds

In this chapter, we address the effects of signal-to-noise ratio thresholds shifting in adaptive M-ary quadrature amplitude modulation systems with diversity at the receiver. As already mentioned in the previous chapter, in adaptive modulation systems the optimal modulation to be employed in the transmission is evaluated by comparing the estimated signal-to-noise ratio (SNR) to some thresholds levels. Co-channel interference signals or approximated bit error probability expressions employed in the system may lead to a variation of the thresholds. Here, we investigate the effects of this thresholds variation on the system performance, evaluated in terms of bit error outage and mean throughput.

The remainder of this chapter is organized as follows. In Section 5.1, the motivations of the work together with a brief description of adaptive modulation techniques are provided. In Section 5.2, the system model description is provided for both slow and fast adaptive modulation techniques. Then, the analysis of the effects of SNR thresholds shifting is reported in Section 5.3 and two applicative examples are considered in Section 5.4 and Section 5.5. In Section 5.6 numerical results are provided, and conclusions are given in Section 5.7.

5.1 Motivation and outline of the work

The diffusion of high speed digital wireless communications has increased the need of reliable high data rate transmission in variable channel conditions. As already observed in the previous chapter, adaptive modulation techniques allow to maximize the transmitted throughput [1] without compromising the performance in terms of bit error probability (BEP) and bit error outage (BEO). Adaptive modulation techniques can be classified into slow or fast adaptive modulation, SAM and FAM respectively. The former adapts modulation parameters to the large-scale fading, while FAM tracks the small-scale fading. In both FAM and SAM, the overall performance might be affected by imperfect channel estimations (as investigated in Chapter 4) or by approximations in the SNR thresholds that reach the target BEP for possible system configurations. When the system experiences any non-idealities that affect the BEP performance compared to in ideal system, a SNR thresholds shift occurs, compromising therefore the overall performance. In particular, the modulation level switch can appear later (before) than the ideal case, leading to a reduction (increasing) of the mean throughput (outage probability). A possible cause of this thresholds shifting can be represented by any approximation introduced in the system, leading to a computational simplification, as the employment of approximation BEP expressions. Being the exponential BEP expression [5] invertible, for example, it is extremely appealing and widely used in the literature, but, on the other hand, the SNR thresholds achieved by the approximated BEP expression may diverge from the original ones [107]. To the best of our knowledge, there is no evaluation of the effects of SNR thresholds shifting in terms of mean throughput and outage probability. Moreover, another possible issue that affects the system performance is the presence of interfering signals. Thus, in interfered systems, SNR thresholds shifting might occurs, and the rising question is "How much an adaptive system is robust to interferers?". In the literature, some works addressed this question, as in [108] and in [109]. In the former, the performance are quantified

[1] Throughout this chapter, we shall use the terms "throughput" and "spectral efficiency (SE)" interchangeably.

in terms of BER for OFDM systems, while in the latter, the authors evaluated the mean throughput of an interfered system. Both the works were limited to FAM systems and did not provide performance in terms of BEO.

In this chapter, we probe the effects of SNR thresholds shifting, due to co-channel interference or approximated BEP, investigating both slow and fast adaptive modulation techniques for M-QAM systems with optimum combiner at the receiver. First, the thresholds shifting issue is investigated in the most general way, including all the possible causes, i.e., imperfect channel estimation, presence of interference, employment of approximated BEP expressions, or any other issue that affects the system performance. Then, we address two applicative examples of thresholds shifting: approximated bit error probability expressions and presence of co-channel interference signals [110, 111]. The performance in terms of mean throughput and bit error outage probability are then quantified in the result section.

Notation: throughout the chapter, vectors and matrices are indicated by bold $\mathbf{m}$ and $\mathbf{M}$, respectively; det[$\mathbf{M}$] denotes the determinant of the matrix $\mathbf{M}$; the superscript H indicates the conjugation and transposition, and $\mathbf{I}_N$ is the $N \times N$ identity matrix.

5.2 System model

We assume M-QAM modulated symbols transmitted over Rayleigh fading and log-normal shadowing channels employing microdiversity at the receiver, i.e., the shadowing level is the same on each branch. At the receiver, N antennas are considered and the optimum combiner is employed for processing the signal. Maximum ratio combining (MRC) and minimum mean square error (MMSE) are adopted for uninterfered and interfered systems, respectively. We denote by E_{S} the mean (over the fading) symbol energy transmitted, by $\mathbf{h} = \{h_i\}_{i=1,\ldots,N}$ the channel vector, whose elements h_i represent the Rayleigh distributed fading gain, and by $\mathbf{n}(k)$ the additive Gaussian noise with zero mean and $\mathbb{E}\{\mathbf{n}(k)\mathbf{n}(k)^H\} = N_0\mathbf{I}_N$, where $N_0/2$ is the two-sided thermal noise power spectral den-

sity. For sake of simplicity, we omit the branch subscript in the mean SNR notation. The average signal-to-noise ratio on each branch can be expressed as $\overline{\gamma} = E\{|h|^2\}E_\mathrm{s}/N_0 = E_\mathrm{s}/N_0$, where $E\{|h|^2\} = 2\sigma_h^2 = 1$. Since we consider a log-normal shadowing, $\overline{\gamma}_\mathrm{dB} = 10\log_{10}(\overline{\gamma})$ is Gaussian distributed with mean μ_dB mean and σ^2_dB variance.

As briefly stated before, adaptive modulation techniques allow to achieve the best throughput accordingly with channel conditions, minimizing in the meanwhile the outage probability, [6]. In particular, when a discrete variable rate is considered, a set of J modulation levels can be adopted, $\{M_0, M_1, \ldots, M_J\}$. As observed in the previous chapter, the optimal modulation level is chosen depending on the instantaneous or mean SNR in FAM or SAM, respectively. We denote by χ the SNR parameter, in particular, in SAM systems $\chi = \overline{\gamma}$, while in FAM systems $\chi = \gamma_\mathrm{T}$, where γ_T is the instantaneous SNR at the combiner output[2]. When, even with the lowest modulation level M_0, χ is not sufficient to guarantee the target BEP $P_\mathrm{b}^\star$, the system is in outage. Otherwise, the transmitted data rate corresponds to $\log_2 M_j,\ j = 0, \ldots, J$. The optimal data rate is chosen comparing the χ value with modulation level thresholds, that are set to guarantee the minimum BEP required when the j-th modulation level is adopted, that is $P_\mathrm{b}(\chi_j^\star) = P_\mathrm{b}^\star$. In particular, when the SNR value falls within the j-th region ($\chi_j^\star < \chi \leq \chi_{j+1}^\star$), the j-th modulation level is adopted for the transmission. It follows that an important figure of merit is the *mean throughput* [bps/Hz] defined as

$$\begin{aligned}
\eta &= \sum_{j=0}^{J-1} \tilde{M}_j\ \mathbb{P}\left\{\chi_j^\star < \chi \leq \chi_{j+1}^\star\right\} + \tilde{M}_J\ \mathbb{P}\left\{\chi_J^\star < \chi\right\} \\
&= \sum_{j=0}^{J-1} \tilde{M}_j\ \left[F_\chi(\chi_{j+1}^\star) - F_\chi(\chi_j^\star)\right] + \tilde{M}_J\ \left[1 - F_\chi(\chi_J^\star)\right] \\
&= \sum_{j=0}^{J-1} \tilde{M}_j\ \left[F_{\chi_\mathrm{dB}}(\chi_{\mathrm{dB},j+1}^\star) - F_{\chi_\mathrm{dB}}(\chi_{\mathrm{dB},j}^\star)\right] + \tilde{M}_J\ \left[1 - F_{\chi_\mathrm{dB}}(\chi_{\mathrm{dB},J}^\star)\right]
\end{aligned} \tag{5.1}$$

where $\tilde{M}_j = \log_2 M_j$ and $F_{\chi_\mathrm{dB}}(x)$ is the CDF of the SNR value in dB,

[2]Note that, unlike the notation in the Chapter 4, here χ represents the SNR parameter in linear scale in both FAM and SAM.

i.e., $\chi_{\mathrm{dB}} = 10\log_{10}(\chi)$. Another important measure of the QoS is the *bit error outage probability* (BEO), i.e., the probability that the bit error probability is greater than the target BEP:

$$P_o(P_{\mathrm{b}}^{\star}) = \mathbb{P}\left\{P_{\mathrm{b}}(\chi) > P_{\mathrm{b}}^{\star}\right\} = F_{\chi}\left(\chi_0^{\star}\right). \tag{5.2}$$

For SAM systems, in log-normal shadowing, the CDF of the averaged SNR is expressed as

$$F_{\overline{\gamma}_{\mathrm{dB}}}(\xi) = Q\left(\frac{\mu_{\mathrm{dB}} - \xi}{\sigma_{\mathrm{dB}}}\right) \tag{5.3}$$

where $Q(\cdot)$ is the Gaussian-Q function.

5.3 Imperfect thresholds

In this section, the effects of imperfect thresholds in terms of throughput and outage probability are investigated for a general system, i.e., without explicating the causes of threshold shifting. When the system experiences a decreasing of the performance, the BEP expression diverges from the ideal one, and a shift of the SNR thresholds occurs. This approximation can be expressed as $\breve{\chi}_{j,\mathrm{dB}}^{\star} = \chi_{j,\mathrm{dB}}^{\star} + \Delta_{j,\mathrm{dB}}$. Note that $\Delta_{j,\mathrm{dB}}$ might be either a deterministic or a random variable that might assume positive and negative values.

To evaluate the mean throughput in realistic systems, (5.1) can still be considered by replacing the ideal thresholds $\chi_{j,\mathrm{dB}}^{\star}$ with $\breve{\chi}_{j,\mathrm{dB}}^{\star}$. Conversely, the outage probability is not always given by (5.2). In particular, when $\breve{\chi}_{j,\mathrm{dB}}^{\star} < \overline{\chi}_{j,\mathrm{dB}}^{\star}$, although the real SNR falls within the j-th modulation range, the $(j+1)$-th modulation might be adopted. In this case, the effective bit error probability is greater than the target BEP and the system is in outage. It means that the system is in outage when $\chi_{\mathrm{dB}} < \chi_{0,\mathrm{dB}}^{\star}$, and also when the SNR value falls within the range $(\chi_{j,\mathrm{dB}}^{\star} - |\Delta_{j,\mathrm{dB}}|, \chi_{j,\mathrm{dB}}^{\star}]$ for $j = 1, \ldots, J$. Thus, when approximated thresholds are obtained, the

BEO is given by[3]

$$P_o = F_{\chi_{\mathrm{dB}}}(\chi^{\star}_{\mathrm{dB},0}) + \sum_{j=1}^{J} \left[F_{\chi_{\mathrm{dB}}}(\chi^{\star}_{j,\mathrm{dB}}) - F_{\chi_{\mathrm{dB}}}(\chi^{\star}_{\mathrm{dB,j}} - |\Delta j|) \right] \tag{5.4}$$

For a slow adaptive modulation, considering the CDF of the averaged SNR in (5.3), the outage probability is given by

$$\begin{aligned} P_o &= Q\left(\frac{\mu_{\mathrm{dB}} - \overline{\gamma}^{*}_{0,\mathrm{dB}}}{\sigma_{\mathrm{dB}}}\right) + \sum_{j=1}^{J} \left[Q\left(\underbrace{\frac{\mu_{\mathrm{dB}} - \overline{\gamma}^{*}_{j,\mathrm{dB}}}{\sigma_{\mathrm{dB}}}}_{a_j} \right) - Q\left(\underbrace{\frac{\mu_{\mathrm{dB}} - \overline{\gamma}^{\star}_{j,\mathrm{dB}} - |\Delta j|}{\sigma_{\mathrm{dB}}}}_{b_j} \right) \right] \\ &= Q\left(\frac{\mu_{\mathrm{dB}} - \overline{\gamma}^{*}_{0,\mathrm{dB}}}{\sigma_{dB}}\right) + \sum_{j=1}^{J} \int_{a_j}^{b_j} e^{-\frac{y^2}{2}} dy \end{aligned} \tag{5.5}$$

It is worth noting that the greater is the mean value μ_{dB}, the more P_o tends to the outage probability of a system with fixed modulation equals to the maximum modulation level M_J.

We now consider approximated BEP expressions or co-channel interference as possible causes of the SNR threshold shifting. In both the cases, the average BEP expression is deduced and the thresholds shifting is quantified.

5.4 Approximated BEP expressions

Although M-QAM has been studied for several years, only recently an exact BEP expression was carried out [107, 112], and the averaged exact BEP was derived in [6] for a system with diversity. For sake of simplicity, the instantaneous and average BEP expressions for M-QAM with SSD, derived in [6], have been reported in the Appendix C in (C.1) and (C.5), respectively.

In the literature, several invertible approximations are considered. Starting from the exponential expression for the instantaneous BEP [96], reported in (C.2), and considering the characteristic function $\psi_{\gamma_{\mathrm{T}}}(j\nu) =$

[3]Note that, when random thresholds are considered, both the mean throughput and the outage probability evaluated in this section are conditioned to the error $\Delta_{j,\mathrm{dB}}$.

Table 5.1: $\Delta_{j,\mathrm{dB}}$ for SAM and FAM techniques for different modulation levels when no diversity is considered ($N = 1$).

SAM					
	$M = 4$	$M = 16$	$M = 64$	$M = 256$	$M = 1024$
A1	-1.34	-0.32	0.68	1.62	2.46
A2	$\sim 10^{-10}$	0.21	0.34	0.40	0.43
A3	-0.44	-0.96	-1.24	-1.40	-1.51
FAM					
	$M = 4$	$M = 16$	$M = 64$	$M = 256$	$M = 1024$
A1	0.16	0.58	0.98	1.35	1.71
A2	$\sim 10^{-10}$	$\sim 10^{-10}$	$\sim 10^{-9}$	$\sim 10^{-9}$	$\sim 10^{-9}$
A3	-0.007	-0.15	-0.025	-0.03	-0.05

$\mathbb{E}_{\gamma_\mathrm{T}}\{e^{j\nu\gamma_\mathrm{T}}\} = \prod_{n=1}^{\tilde{N}} \left[\frac{1}{1-\overline{\gamma}j\nu}\right]$, as explained in the Appendix C, the averaged BEP expression (**A1**) can be derived as

$$P_\mathrm{b}^{(\mathrm{A1})}(\overline{\gamma}) \simeq \int_0^\infty P_\mathrm{b}^{(\mathrm{A1})}(e|\gamma_\mathrm{T}) f_{\gamma_\mathrm{T}|\overline{\gamma}}(\xi) d\xi = 0.2 \left[\frac{1}{1+\frac{1.6}{M-1}\overline{\gamma}}\right]^N. \tag{5.7}$$

Starting from another approximation introduced in [113], (C.3), averaging the instantaneous BEP over the fading, the averaged BEP expression (**A2**) can be expressed as

$$P_\mathrm{b}^{(\mathrm{A2})}(\overline{\gamma}) \simeq \frac{2A_M}{\log_2 M} \sum_{i=1}^{\sqrt{M}/2} I_k\left[(2i-1)^2 B_M \overline{\gamma}\right], \tag{5.8}$$

where $I_k(x) = \frac{1}{\pi}\int_0^{\pi/2} \left(\frac{sin^2\theta}{x+\sin^2\theta}\right)^N d\theta$, $A_M = 2[1-(1/\sqrt{M})]$ and $B_M = [3/2(M-1)]$. Starting from the third instantaneous approximation [107], (C.4), the approximated averaged BEP (**A3**), as derived in the Appendix C, can be expressed as

$$P_\mathrm{b}^{(\mathrm{A3})}(\overline{\gamma}) \simeq \frac{2A_M}{\log_2 M} I_k\left(B_M\overline{\gamma}\right) - \frac{A_M^2}{\log_2 M}\frac{1}{\pi}\int_0^{\pi/4} \left(\frac{\sin^2\theta}{B_M\overline{\gamma}+\sin^2\theta}\right)^N d\theta. \tag{5.9}$$

Although MRC receivers are considered in this chapter, for sake of completeness, in the Appendix C, the approximated BEP expressions for

Table 5.2: $\Delta_{j,\mathrm{dB}}$ for SAM technique for different modulation levels and orders of diversity when the approximation (A1) is considered.

SAM					
	$M=4$	$M=16$	$M=64$	$M=256$	$M=1024$
N=1	-1.34	-0.32	0.68	1.62	2.46
N=2	-0.33	0.42	1.11	1.74	2.31
N=8	0.09	0.58	1.04	1.48	1.87

a more general system employing H-S/MRC are reported. In Table 5.1, the thresholds shifting values, $\Delta_{j,\mathrm{dB}}$, are reported for different modulation levels, for both SAM and FAM techniques, when no diversity is considered ($N = 1$), while several orders of diversity are considered in Table 5.2, where the $\Delta_{j,\mathrm{dB}}$ values are reported for SAM systems employing the exponential approximation. Note that the gap between the perfect and imperfect thresholds increases accordingly with the modulation level. Moreover, it is worth noting that $|\Delta_{j,\mathrm{dB}}{}^{(\mathrm{A1})}|$ results to be higher than the other delta values, leading to a rough BEP approximation when the exponential expression is employed. Finally, from Table 5.1, it can be observed that, for the approximation (A3), $\Delta_{j,\mathrm{dB}} < 0$. It follows that, compared to the exact system, (A3) will achieve a higher mean throughput at the cost of a higher outage probability, given by (5.4).

5.5 Co-channel interference

We now consider the case in which the SNR thresholds shifting, $\Delta_{j,\mathrm{dB}}$, is given by the presence of co-channel interference. We denote the received signal on each branch after the matched filtering and the sampling at the symbol rate by $z_i(k) = z_i^{(\mathrm{P})}(k) + jz_i^{(\mathrm{Q})}(k)$, where k represents the time index. The vector output $\mathbf{z}(k) = [z_1(k), \ldots, z_N(k)]$ can be written

as[4] [114]

$$\begin{aligned}\mathbf{z}(k) &= \mathbf{z}^{(\mathrm{P})}(k) + j\mathbf{z}^{(\mathrm{Q})}(k) \\ &= \sqrt{E_{\mathrm{S}}}\mathbf{h}\; b_0(k) + \sqrt{E_{\mathrm{I}}}\sum_{n=1}^{N_{\mathrm{I}}} \mathbf{h}_{\mathrm{I},n} b_{\mathrm{I},n}(k) + \mathbf{n}(k), \end{aligned} \tag{5.10}$$

where E_{I} is the mean symbol energy transmitted of each interfering signals; $b_0(k) = b_0^{(\mathrm{P})}(k) + jb_0^{(\mathrm{Q})}(k)$ is the desired signal sample and $b_{\mathrm{I},n}(k) = b_{\mathrm{I},n}^{(\mathrm{P})}(k) + jb_{\mathrm{I},n}^{(\mathrm{Q})}(k)$ is the interfering signal sample of the n-th interferer. Since we assume a slow frequency flat Rayleigh distributed fading, the vectors $\mathbf{h}$ and $\mathbf{h}_{\mathrm{I},n}, n = 1, \ldots, N_{\mathrm{I}}$ have distribution $\mathcal{CN}(0, \mathbf{I}_N)$, and we denote by $\mathbf{H}_{\mathrm{I}} = \{\mathbf{h}_{\mathrm{I,j}}\}_{j=1,\ldots,N_{\mathrm{I}}}$ the interference channel matrix. Being the desired signal affected by fading, the Gaussian approximation for the interferers is justified [115]. Thus, $b_1(k), \ldots, b_{N_{\mathrm{I}}}(k)$ are independent zero-mean complex Gaussian random variables, each with variance one because of the normalization.

Following the steps in [114], we derive the bit error probability as a function of the averaged signal-to-interference-plus-noise ratio (SINR) for a M-QAM system with optimum combining at the receiver. The optimum weight vector that maximizes the SINR is $\mathbf{w} = \alpha\mathbf{R}^{-1}\mathbf{c}_D$, where α is an arbitrary constant and $\mathbf{R}$ the covariance matrix, expressed as

$$\begin{aligned}\mathbf{R} &= \mathbb{E}_{\mathbf{n}(k),b_j(k)}\left\{\left[\sqrt{E_{\mathrm{I}}}\sum_{n=1}^{N_{\mathrm{I}}}\mathbf{h}_{\mathrm{I},n}b_{\mathrm{I},n}(k) + \mathbf{n}(k)\right]\left[\sqrt{E_{\mathrm{I}}}\sum_{n=1}^{N_{\mathrm{I}}}\mathbf{h}_{\mathrm{I},n}b_{\mathrm{I},n}(k) + \mathbf{n}(k)\right]^H\right\} \\ &= E_{\mathrm{I}}\underbrace{\sum_{j=1}^{N_{\mathrm{I}}}\mathbf{h}_{\mathrm{I},j}\mathbf{h}_{\mathrm{I},j}^H}_{\mathbf{R}_I} + N_0\mathbf{I}_N, \end{aligned} \tag{5.11}$$

where the last equality holds because the desired signal, the interference and the noise are assumed independent from each other. Considering an overloaded system (i.e., $N_I \geq N$)[5] the SINR of the output at the combiner can be written as

$$\gamma = \sum_{i=1}^{N}\frac{E_S\left|\mathbf{h}_S^H\mathbf{u}_i\right|^2}{E_I\lambda_i + N_0},$$

[4]Note that the superscripts (P) and (Q) stand for the in-phase and quadrature symbols, respectively.

[5]The extension to the underloaded case is reported in the Appendix D.

where $\mathbf{u}_1, \dots \mathbf{u}_N$ are the orthonormal eigenvectors of the interference correlation matrix $\mathbf{R}_I$, corresponding to the eigenvalues $\lambda_1, \dots, \lambda_N$. The instantaneous exact bit error probability for M-QAM systems is expressed in (C.1) and the averaged BEP can be determined by averaging over the SINR,

$$\begin{aligned} P_{\mathrm{b}} &= \int P(e|\gamma_{\mathrm{T}}) f_{\gamma_{\mathrm{T}}}(\xi) d\xi \\ &= \frac{2}{\sqrt{M}\log_2(\sqrt{M})} \sum_{h=1}^{\log 2(\sqrt{M})} \sum_{n=0}^{(1-2^{-h})\sqrt{M}-1} (-1)^{\lfloor \frac{n2^{h-1}}{\sqrt{M}} \rfloor} \\ &\times \left(2^{h-1} - \left\lfloor \frac{n2^{h-1}}{\sqrt{M}} + \frac{1}{2} \right\rfloor \right) \frac{1}{\pi} \underbrace{\int_0^{\pi/2} \Psi_{\gamma_{\mathrm{T}}} \left\{ -\frac{c_{M,n}}{\sin^2\theta} \right\} d\theta}_{\zeta_n(\gamma_{\mathrm{T}})}, \end{aligned} \tag{5.12}$$

where $c_{M,n} = \frac{3(2n+1)^2}{2(M-1)}$ and the last equality is due to the use of the Craig's formula of the Gaussian Q function [9]. Using the chain rule of conditional expectation, we obtain

$$\zeta_n(\gamma_{\mathrm{T}}) = \int_0^{\pi/2} \int_0^{\infty} \dots \int_0^{\infty} \Psi_{\gamma_{\mathrm{T}}|\boldsymbol{\lambda}} \left\{ -\frac{c_{M,n}}{\sin^2\theta} \right\} f_{\boldsymbol{\lambda}}(\mathbf{x}) d\theta d\mathbf{x}.$$

Since the elements of the $(N \times N_{\mathrm{I}})$ matrix $\mathbf{H}_{\mathrm{I}}$, $\mathbf{h}_{\mathrm{I},j,i}$, are complex random variable belonging to a normal distribution $\mathcal{CN}(0,1)$, the Hermitian matrix $\mathcal{W} = \mathbf{H}_{\mathrm{I}}\mathbf{H}_{\mathrm{I}}^H$ is the central Wishart matrix. A useful property of $\mathcal{W}$ is the joint pdf of the unordered real eigenvalues, $f_{\boldsymbol{\lambda}}(\mathbf{x})$, that can be expressed as [116]. Knowing $f_{\lambda}(\mathbf{x})$, and considering the Lemma 1 in [114], after some mathematical steps, reported in the Appendix D, the mean BEP expression can be expressed as

$$\begin{aligned} P_{\mathrm{b}} &= \frac{2}{\sqrt{M}\log_2(\sqrt{M})} \sum_{h=1}^{\log 2(\sqrt{M})} \sum_{n=0}^{(1-2^{-h})\sqrt{M}-1} (-1)^{\lfloor \frac{n2^{h-1}}{\sqrt{M}} \rfloor} \\ &\times \left(2^{h-1} - \left\lfloor \frac{s2^{h-1}}{\sqrt{M}} + \frac{1}{2} \right\rfloor \right) \left[\pi \prod_{i=1}^{N} (N-i)!(N_I-i)! \right]^{-1} \int_0^{\pi/2} \det \mathcal{G}(\theta) d\theta, \end{aligned} \tag{5.13}$$

where $\mathcal{G} = \{G_{i+j+N_{\mathrm{I}}-N}\}_{i,j=0,\dots,N-1}$ is the Hankel matrix, with elements

given by

$$G_k(\theta) = \left(\frac{c_{M,n}N_{\mathrm{I}}\overline{\gamma}}{\sin^2\theta\ \overline{\gamma}_{\mathrm{I}}} + \frac{N_{\mathrm{I}}}{\overline{\gamma}_{\mathrm{I}}}\right)^k \exp\left(\frac{c_{M,n}N_{\mathrm{I}}\overline{\gamma}}{\sin^2\theta\ \overline{\gamma}_{\mathrm{I}}} + \frac{N_{\mathrm{I}}}{\overline{\gamma}_{\mathrm{I}}}\right) k! \times \left[\left(\frac{c_{M,n}N_{\mathrm{I}}\overline{\gamma}}{\sin^2\theta\ \overline{\gamma}_{\mathrm{I}}} + \frac{N_{\mathrm{I}}}{\overline{\gamma}_{\mathrm{I}}}\right)(1+k)\Gamma\left(-1-k, \frac{c_{M,n}N_{\mathrm{I}}\overline{\gamma}}{\sin^2\theta\ \overline{\gamma}_{\mathrm{I}}} + \frac{N_{\mathrm{I}}}{\overline{\gamma}_{\mathrm{I}}}\right) + \frac{N_{\mathrm{I}}}{\overline{\gamma}_{\mathrm{I}}}\Gamma\left(-k, \frac{c_{M,n}N_{\mathrm{I}}}{\sin^2\theta\ \overline{\gamma}_{\mathrm{I}}} + \frac{N_{\mathrm{I}}}{\overline{\gamma}_{\mathrm{I}}}\right)\right], \tag{5.14}$$

where $\overline{\gamma}_I = (N_I E_I)/N_0$ denotes the interference-to-noise ratio (INR). Note that, when no interference signals are considered, the optimum combiner merges to the MRC, thus the mean BEP expression is given by (4.8).

It is worthwhile noting that, since also the interference signal is affected by the shadowing, the $\overline{\gamma}_{\mathrm{I}}$ is a RV, modeled as a log-normal RV, i.e. $\overline{\gamma}_{\mathrm{I}} \sim \mathcal{N}(\mu_{\mathrm{I,dB}}, \sigma_{\mathrm{dB}})$. A simplified analysis of the effects of co-channel interference is considered first. In particular, as starting point, we consider the overall performance conditioned to the signal-to-interference ratio, $\mathrm{SIR} = E_{\mathrm{D}}/(N_{\mathrm{I}}E_{\mathrm{I}}) = \overline{\gamma}/\overline{\gamma}_{\mathrm{I}}$[6]. In this conditioned model, (5.13) is considered for the SNR thresholds evaluation, that is, we evaluate that SNR value such that $P_{\mathrm{b|SIR}}(\overline{\gamma}) = P_{\mathrm{b}}^{\star}$. Once evaluated these thresholds, the mean throughput and the BEO can be evaluated by (5.1) and (5.4), respectively. Then, a more general case is investigated assuming that the interference shadowing level does not equal the useful signal shadowing level. It follows the the evaluation of the performance is not limited to conditioned cases. In particular, the BEP expression is a function of two random variables, SNR and INR, and therefore the couple $(\overline{\gamma}_{\mathrm{I}}, \overline{\gamma})$ has to be evaluated as the SINR threshold that reaches the target BEP for given system configurations. As far as an interfered system is concerned, the SINR thresholds are represented by a threshold line rather than a single point, as it can be observed in Fig. 5.1. Here, the SINR threshold lines are reported for a system with $N_{\mathrm{d}} = 1$, $N_{\mathrm{I}} = 2$, and M ranging from 4 to 256. Note that a floor is observed for low INR values, due

[6]Conditioning the system to the SIR value implies that, for further evaluation analysis (i.e., BEO or SE evaluation), the interference shadowing level follows the useful signal shadowing level.

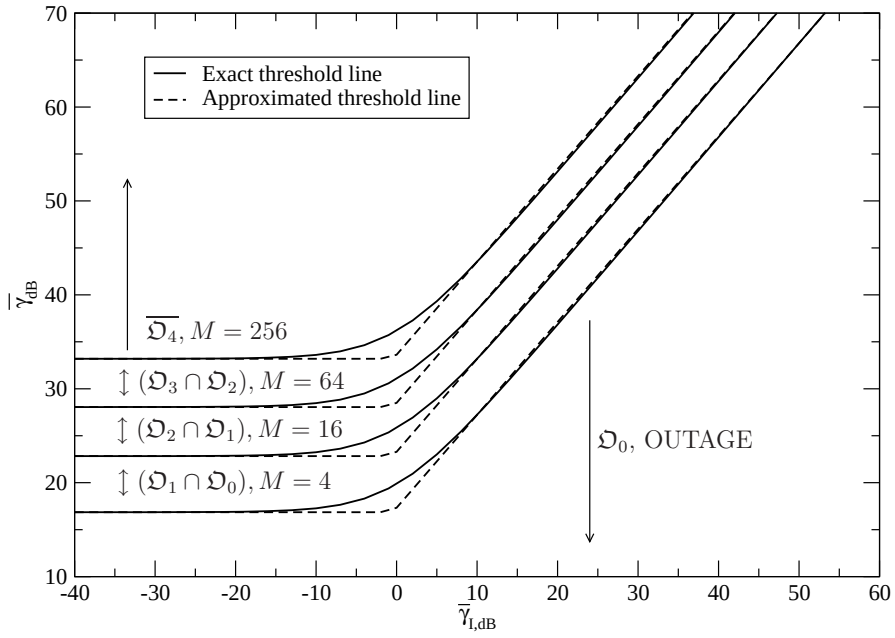

Figure 5.1: Approximated and Exact threshold lines for a system with $N_d = 1$, $N_{\mathrm{I}} = 2$, and M ranging from 4 to 256.

to the lowering of the interference signal power. In particular, the lines merges to the SNR threshold value ($\overline{\gamma}^{\star}$) of the uninterfered system. It is worthwhile noting the almost linear behavior of the threshold line for high INR values. This can be explained from (5.13), where by increasing the INR value, the value $N_{\mathrm{I}}/\overline{\gamma}_{\mathrm{I}}$ become negligible, and only the linear relation between SNR and INR is present in the BEP expression. Thus, the thresholds lines might be approximated with some straight line limited by the floor value. These approximated threshold lines are represented in the Fig. 5.1 by the dashed lines.

In the considered system, when the couple $(\overline{\gamma}_{\mathrm{I,dB}}, \overline{\gamma}_{\mathrm{dB}})$ falls within the region $(\mathfrak{O}_{j+1} \cap \mathfrak{O}_j)$, the j-th modulation is adopted, where $\cap$ stands for the intersection operator. We denote by $\mathfrak{O}_j$ the region limited by the threshold line of the M_j modulation, and by $\overline{\mathfrak{O}_j} = \mathbb{R}_2 - \mathfrak{O}_j$ the complementary region of $\mathfrak{O}_j$. When $(\overline{\gamma}_{\mathrm{I,dB}}, \overline{\gamma}_{\mathrm{dB}}) \in \mathfrak{O}_0$, the target BEP can not be reached and the system is in outage. The bit error outage

probability can be defined as

$$\begin{aligned} P_o &= F_{(\overline{\gamma}_{\mathrm{I,dB}},\overline{\gamma}_{\mathrm{dB}})}(\mathfrak{O}_0) = \mathbb{P}\left\{(\overline{\gamma}_{\mathrm{I,dB}},\overline{\gamma}_{\mathrm{dB}}) \in \mathfrak{O}_0\right\} \\ &= \int_{-\infty}^{\infty}\int_{-\infty}^{\overline{\gamma}^{\star}_{0,\mathrm{dB}}(\overline{\gamma}_{\mathrm{I,dB}})} f_{\overline{\gamma}_{\mathrm{dB}}}(\xi) f_{\overline{\gamma}_{\mathrm{I,dB}}}(\xi_{\mathrm{I}}) d\xi d\xi_{\mathrm{I}} \\ &= \int_{-\infty}^{\infty} Q\left(\frac{\mu_{\mathrm{dB}} - \overline{\gamma}^{\star}_{0,\mathrm{dB}}}{\sigma_{\mathrm{dB}}}\right) f_{\overline{\gamma}_{\mathrm{I,dB}}}(\xi_{\mathrm{I}}) d\xi_{\mathrm{I}}, \end{aligned} \tag{5.15}$$

where $f_{\overline{\gamma}_{\mathrm{I,dB}}}(\cdot)$ and $f_{\overline{\gamma}_{\mathrm{dB}}}(\cdot)$ are the PDF of the SNR and INR, respectively, and $\overline{\gamma}^{\star}_{0,\mathrm{dB}}(\overline{\gamma}_{\mathrm{I,dB}})$ is the SNR value that reaches the target BEP when INR$=\overline{\gamma}_{\mathrm{I,dB}}$. Analogously, the mean throughput is given by

$$\begin{aligned} \eta &= \sum_{j=0}^{J-1} \tilde{M}_j \ \mathbb{P}\left\{(\overline{\gamma}_{\mathrm{I,dB}},\overline{\gamma}_{\mathrm{dB}}) \in (\mathfrak{O}_{j+1} \cap \mathfrak{O}_j)\right\} + \tilde{M}_J \ \mathbb{P}\left\{(\overline{\gamma}_{\mathrm{I,dB}},\overline{\gamma}_{\mathrm{dB}}) \in \overline{\mathfrak{O}}_J\right\} \\ &= \sum_{j=0}^{J-1} \tilde{M}_j \ \left[F_{(\overline{\gamma}_{\mathrm{I,dB}},\overline{\gamma}_{\mathrm{dB}})}(\mathfrak{O}_{j+1}) - F_{(\overline{\gamma}_{\mathrm{I,dB}},\overline{\gamma}_{\mathrm{dB}})}(\mathfrak{O}_j)\right] + \tilde{M}_J \ \left[1 - F_{(\overline{\gamma}_{\mathrm{I,dB}},\overline{\gamma}_{\mathrm{dB}})}(\mathfrak{O}_J)\right] \end{aligned} \tag{5.16}$$

where, as already observed from (5.15), since the SNR and INR are log-normal RVs, the joint CDF can be expressed as

$$\begin{aligned} F_{(\overline{\gamma}_{\mathrm{I,dB}},\overline{\gamma}_{\mathrm{dB}})}(\mathfrak{O}_j) &= \mathbb{P}\left\{(\overline{\gamma}_{\mathrm{I,dB}},\overline{\gamma}_{\mathrm{dB}}) \in \mathfrak{O}_j\right\} \\ &= \int_{-\infty}^{\infty}\int_{-\infty}^{\overline{\gamma}^{\star}_{j,\mathrm{dB}}(\overline{\gamma}_{\mathrm{I,dB}})} f_{\overline{\gamma}_{\mathrm{dB}}}(\xi) f_{\overline{\gamma}_{\mathrm{I,dB}}}(\xi_{\mathrm{I}}) d\xi d\xi_{\mathrm{I}} \\ &= \int_{-\infty}^{\infty} Q\left(\frac{\mu_{\mathrm{dB}} - \overline{\gamma}^{\star}_{j,\mathrm{dB}}}{\sigma_{\mathrm{dB}}}\right) f_{\overline{\gamma}_{\mathrm{I,dB}}}(\xi_{\mathrm{I}}) d\xi_{\mathrm{I}}, \end{aligned} \tag{5.17}$$

5.6 Numerical results

In this section, numerical results are presented in terms of mean throughput and BEO for both fast and slow adaptive modulation. Coherent detection of M-QAM with optimum combiner and Gray code mapping in composite Rayleigh fading and log-normal shadowing channels with perfect CSI was considered. The mean throughput is evaluated by (5.1), where the thresholds are evaluated as the SNR values that achieve a target BEP of 10^{-2} for different modulation sizes and a maximum outage probability of 5% is considered. For the approximated BEP case,

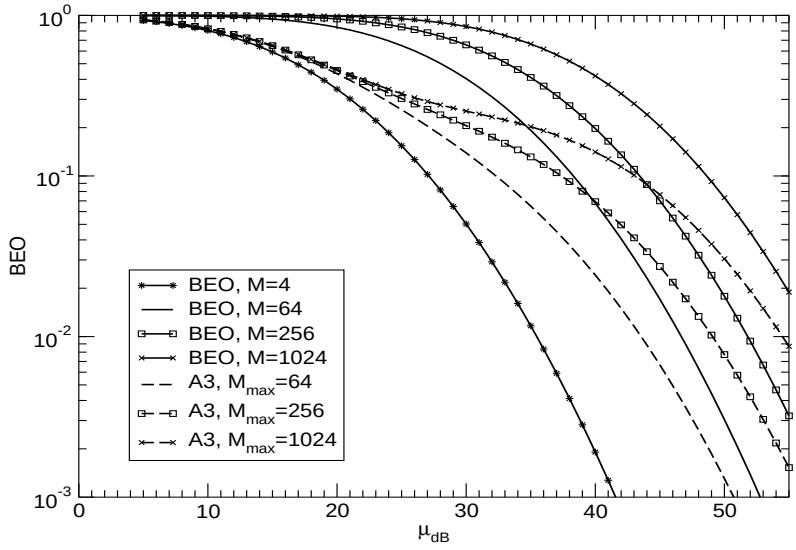

Figure 5.2: Outage probability vs. μ_{dB} for SAM systems with maximum modulation size $64, 256, 1024$, no diversity at the receiver, $P_{\mathrm{b}}^{\star} = 10^{-2}$, $\sigma_{\mathrm{dB}} = 8$. To evaluate SNR thresholds, the BEP approximation A3 is adopted.

the BEP expressions are obtained from (C.1)-(C.4) and (C.7)-(C.11) for FAM and SAM, respectively, and the exact BEP expressions have been reported in (C.5). In the case of interfered system, the BEP evaluated in (5.13) is considered.

In Fig. 5.2, the outage probability as a function of the median value μ_{dB} is considered for both fixed modulation systems, with the modulation level ranging from $M = 4$ to $M = 1024$, and adaptive modulation systems with the approximation (A3) employed, that is the approximation that provides $\Delta_{j,\mathrm{dB}} < 0$. As already mentioned, the outage probability obtained with a modulation level equals to 4, is also the outage probability of an adaptive modulation system when the exact BEP expression is considered. Conversely, when the approximation (A3) in employed, $\Delta_{j,\mathrm{dB}} < 0$ and the outage probability will increase, as observed in the figure. It is worth noting that the higher the maximum modulation adopted in the system, the higher is the outage probability. Moreover, it can be confirmed what mentioned before, i.e., asymptotically ($\mu_{\mathrm{dB}} \to \infty$) the outage probability of an adaptive modulation system, with maximum

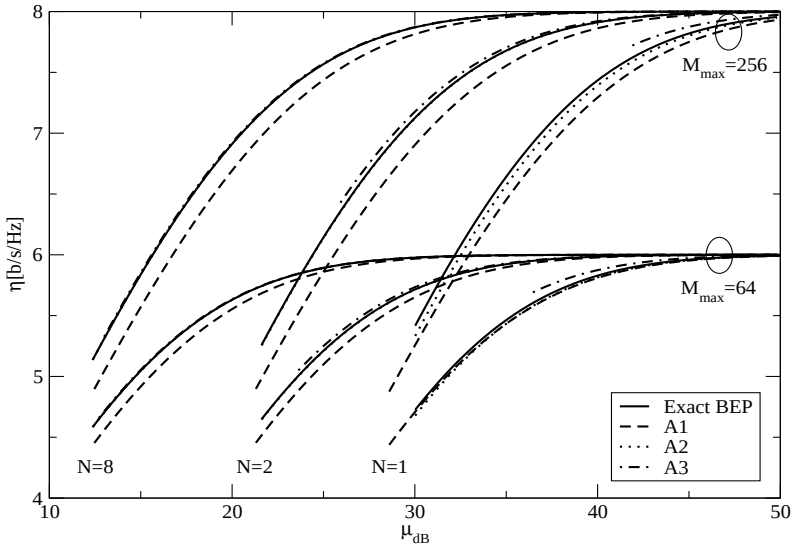

Figure 5.3: Mean SE vs. μ_{dB} for SAM systems with maximum modulation size $64, 256, 1024$, MRC with $N = 1, 2, 8$, maximum outage 5%, $P_{\mathrm{b}}^{\star} = 10^{-2}$, and $\sigma_{\mathrm{dB}} = 8$. The mean SE is evaluated with both perfect and imperfect BEP expressions.

modulation $M_{\max}$ and approximation (A3) employed, merges to the outage probability of a system with fixed modulation equals to $M_{\max}$. This outage penalty can be observed also in Fig. 5.3, where the mean throughput as a function of the median value μ_{dB} is shown for SAM systems employing exact BEP or the approximated BEP expressions (A1), (A2), and (A3) with maximum modulation size equal to 64 and 256. As expected, when no diversity is considered, the approximation (A3) results in a higher mean throughput at the cost of a higher outage probability. Observe that, when $M_{\max} = 256$ and $N = 1$, for example, the median SNR value that achieves an outage probability lower than 5% is around 42dB, while in the case of perfect BEP expression, it is around 29 dB. Considering the other approximations, it can be observed that the exponential BEP approximation (A1) achieves a lower SE than the exact BEP expression for all the diversity orders. It means that the simplification of system obtained by (A1) has to be payed in terms of mean throughput. For example, considering $N = 2$, and $\mu_{\mathrm{dB}} = 25$, the system employing

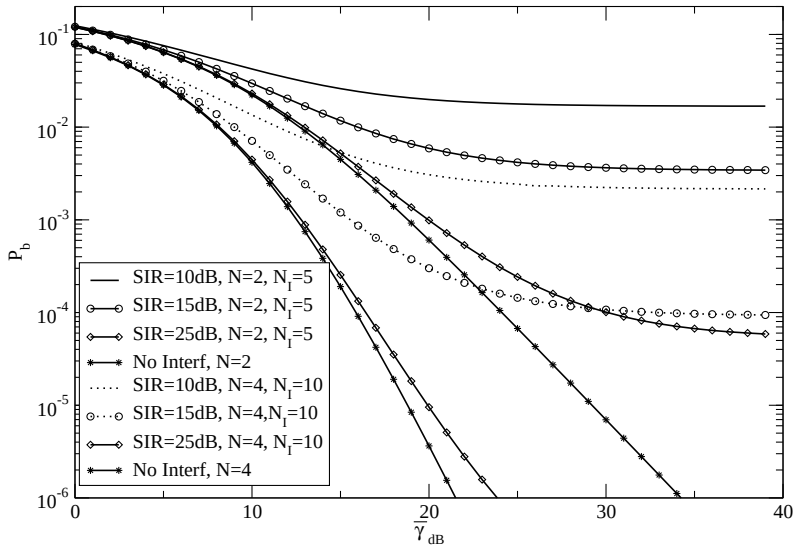

Figure 5.4: BEP vs. $\overline{\gamma}_{\rm dB}$ for M-QAM systems with modulation size $M = 16$, maximum outage 5%, $P_{\rm b}^{\star} = 10^{-2}$, and $\sigma_{\rm dB} = 8$. The bit error probability, conditioned to SIR, is evaluated for several N and $N_{\rm I}$ values.

the exact BEP expression achieves a mean throughput $\eta \sim 6.1$ bps/Hz, while by employing the approximation (A1) only a mean throughput of 5.6 bps/Hz can be reached. Conversely, (A2) is a tight approximation and it turns into a transmitted throughput extremely close to one provided by the exact BEP expression.

We now provide results for systems with co-channel interference. First, results conditioned to the SIR value are provided. Then, a more general case is studied, showing the modulation regions and the performance for SAM systems with MRC receivers. As far as the conditioned case is concerned, the SNR thresholds are evaluated from the bit error probability in (5.13), while the BEO and mean SE are given by (5.1) and (5.2), respectively. The bit error probability as a function of the mean SNR is reported in Fig. 5.4 for SAM systems with different number of antennas at the receiver, different numbers of interference signals, and several SIR values. As expected, the curves show a floor at the increasing of the mean SNR, and the lower is the SIR, the higher is the BEP floor value. Moreover, some system configurations (i.e., M or N) might not

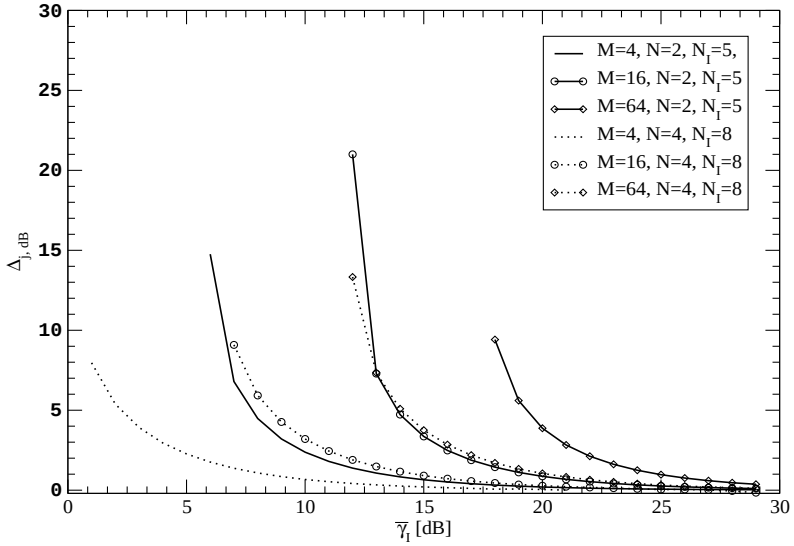

Figure 5.5: $\Delta_{j,\mathrm{dB}}$ vs. $\overline{\gamma}_{\mathrm{I,dB}}$ for SAM systems with $M_{\max} = 256$, maximum outage 5%, $P_{\mathrm{b}}^{\star} = 10^{-2}$, $\sigma_{\mathrm{dB}} = 8$, and several N and N_{I} values. The analysis is conditioned to the SIR value.

overcome the presence of interference, and the system experiences such low performance that the target BEP can not be reached for any μ_{dB}. It follows that the system might not switch to the maximum modulation level, even with asymptotically high SNR. This can be observed also in Fig. 5.5, where the $\Delta_{j,\mathrm{dB}} = \breve{\gamma}_{j,\mathrm{dB}}^{\star} - \overline{\gamma}_{j,\mathrm{dB}}^{\star}$ is reported for $j = 1, \ldots, 4$, for SAM systems with different N_{I} and N values. It is worth noting that, by increasing of the modulation size, the system is less robust to the interference, and it follows that the system might not reach the target BEP. This explain why, for some low SIR values (for example 7 dB), the $\Delta_{j,\mathrm{dB}}$ can be evaluated only for the modulation size $M = 4$. Moreover, it can be observed that, since at the increasing of the SIR value, the interfered system tends to the uninterfered one, the higher the SIR, the lower the SNR delta thresholds.

This behavior, together with the fact that in some system configurations the target BEP can not be reached, can be translated in terms of mean throughput, and observed in Fig. 5.6. Here, the mean SE as a function of the median value μ_{dB} is provided for SAM systems with $N_{\mathrm{I}} = 6$, different diversity orders N, and different signal-to-interference ratios. It

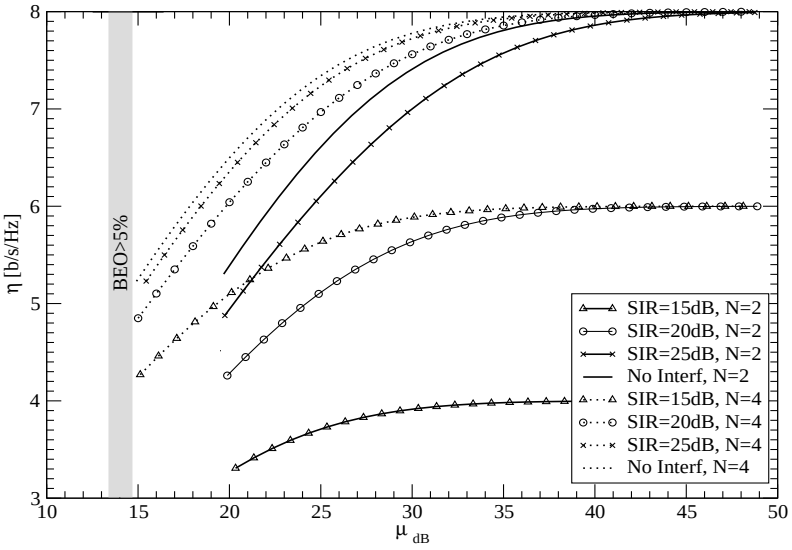

Figure 5.6: Mean throughput (conditioned to SIR) vs. μ_{dB} for SAM systems with $M_{\max} = 256$, maximum outage 5%, $P_{\mathrm{b}}^{\star} = 10^{-2}$, $\sigma_{\mathrm{dB}} = 8$, $N_{\mathrm{I}} = 6$, and number of antennas equals to 2 and 4.

is worthwhile noting the extremely low performance of the system when $N = 2$ and SIR = 15dB. The system can switch the modulation level between $M = 4$ and $M = 16$, which are actually the only values that satisfy the target BEP of 10^{-2}. Increasing the SIR value or the diversity of the system, the mean throughput increases reaching values close to the exact system throughput.

We now provided results for an unconditioned system affected by co-channel interference. In particular, the bit error probability is given in (5.13), the BEO and mean throughput are expressed in (5.15) and (5.16), respectively. In Fig. 5.7, the bit error probability vs. $\overline{\gamma}_{\mathrm{dB}}$ is reported for systems with $M = 4$, MRC receiver with $N = 1$, and 2 as order of diversity. Un overloaded case is considered, i.e, $N_{\mathrm{I}} = 4 > N$. As expected, the interfered systems preserve the diversity order, but they experience a decreasing of the performance respect to the uninterfered system. In particular, the higher the INR value, the more dominant are the inference signals, and thus the worse is the performance. Considering a system with

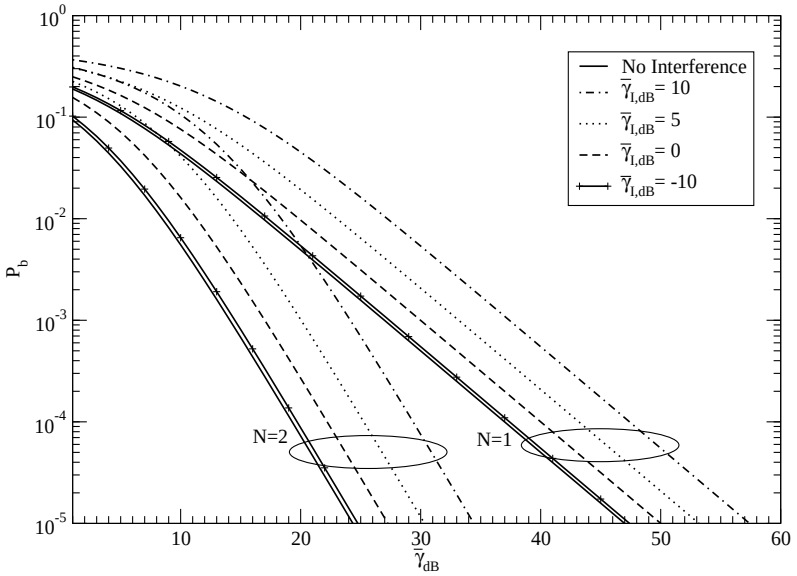

Figure 5.7: BEP vs. $\overline{\gamma}_{\mathrm{dB}}$ for M-QAM systems with $M = 4$, $N = 1$, $N_{\mathrm{I}} = 4$.

$\overline{\gamma}_{\mathrm{I,dB}} = 10$ and $N = 1$, for example, a SNR value of almost 28 dB is required to reach the target BEP ($P_{\mathrm{b}} = 10^{-2}$), despite the 17 dB needed in the uninterfered system. By decreasing the INR value, the performance get closer to the BEP value of the exact system, as it can be observed in the figure. As already mentioned in the previous section, a couple $(\overline{\gamma}_{\mathrm{dB}}, \overline{\gamma}_{\mathrm{I,dB}})$ has to be evaluated as that thresholds SINR values reaching the target BEP. It follows that a threshold line can be individuated has the set of points such that $P_{\mathrm{b}}(\overline{\gamma}_{\mathrm{dB}}, \overline{\gamma}_{\mathrm{I,dB}}) = P_{\mathrm{b}}^{\star}$. These threshold lines are reported in Fig. 5.8 for a SAM systems with $M_{\max} = 256$, $N = 1$, and 2 interfering signals. Note the almost linear behavior for high INR values, and the floor behavior for low INR value. In particular, by decreasing the $\overline{\gamma}_{\mathrm{I,dB}}$, the SNR thresholds tend to the $\overline{\gamma}_{\mathrm{dB}}^{\star}$ thresholds of uninterfered systems.

Finally, the mean throughput vs. μ_{dB} can be observed in Fig. 5.9 for SAM systems with $M_{\max} = 64$, $N = 1$, $N_{\mathrm{I}} = 2$, and several $\mu_{\mathrm{I,dB}}$ values, $\mu_{\mathrm{I,dB}} = -10, -5, 0$. Note that, even with low $\mu_{\mathrm{I,dB}}$ values, i.e., $\mu_{\mathrm{I,dB}} = -5$, a substantial reduction of the throughput is experienced

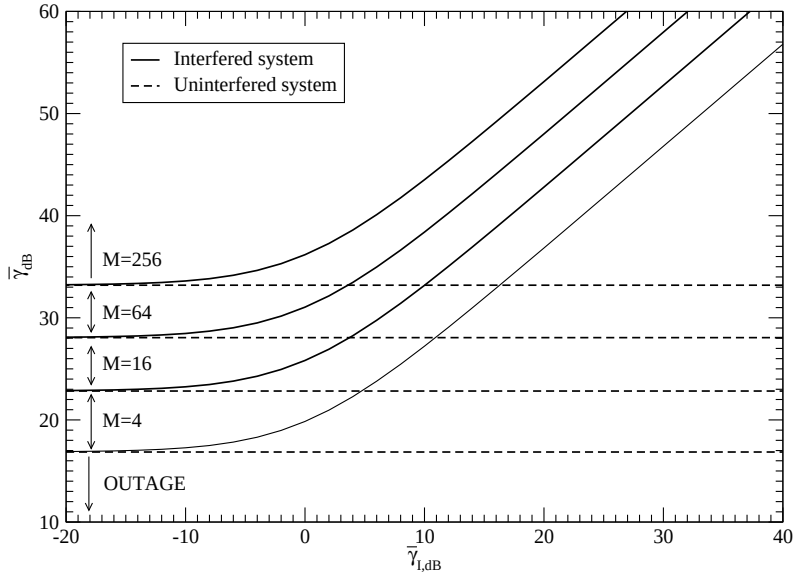

Figure 5.8: SNR thresholds vs. INR thresholds for SAM systems with $M_{\max} = 256$, $N = 1$, $N_{\mathrm{I}} = 2$.

together with an increase of the bit error outage probability. Note, for example, that the system with $\mu_{\mathrm{I,dB}} = -5$ has a minimum μ_{dB} value that reaches the minimum BEO equal to 34 dB, while the uniterfered system is in outage only for $\mu_{\mathrm{dB}} < 31$ dB. Moreover, for a constant value of μ_{dB}, i.e., $\mu_{\mathrm{dB}} = 35$ the interfered system provides a mean throughput of 4.9 bps/Hz, depside the 5.3 bps/Hz achieved by the uniterfered system. As expected, increasing $\mu_{\mathrm{I,dB}}$ the performance is even more affected by the interfering signals, as showed by the $\mu_{\mathrm{I,dB}} = 0$ system.

5.7 Conclusion

In this chapter, we investigated adaptive modulation techniques when a signal-to-noise ratio threshold occurs. We investigated the effects of this shifting in terms of bit error outage and mean throughput. We considered two applicative examples, showing how the employing of appealing approximation BEP expressions may lead to a substantial increasing of the bit error outage or of average throughput, compared to the case with exact BEP expression. Then, we considered the effects of interfering signals

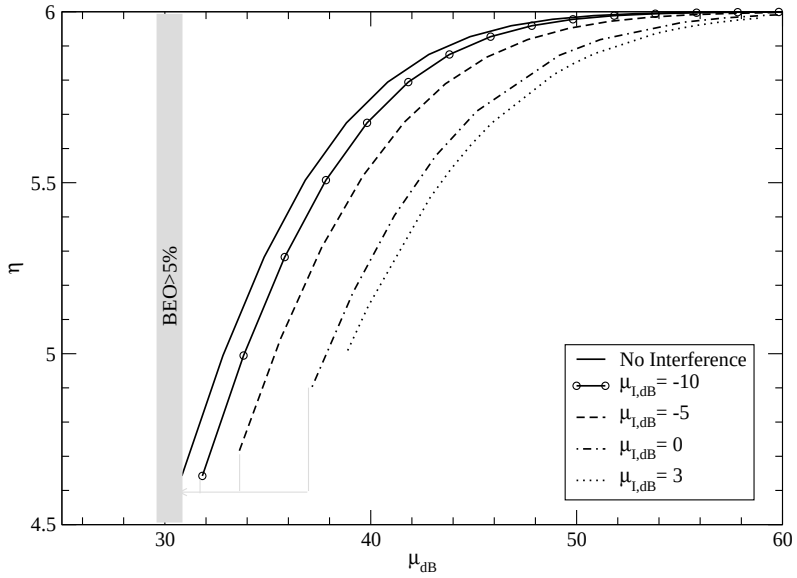

Figure 5.9: Mean throughput vs. μ_{dB} SAM systems with $M_{\max} = 64$, $N = 1$, and $N_{\mathrm{I}} = 2$.

in slow adaptive modulation systems, by carrying out QoS measurements for several signal-to-interference ratio, showing the system configurations able to overcome the interfering issue.

Chapter 6

Conclusion

This final chapter summarizes the contributions of this dissertation and highlights numerous areas for further research. We developed a framework for optimizing multimedia applications over wireless channels. We showed how to take advantage from channel conditions, by adopting to them transmitting parameters at the physical layer, such as source and channel coding rates, as well as modulation levels. Specifically, as far as the joint source and channel coding was concerned, we investigated the optimal design of joint source and channel coding (JSSC) in a 2D time-frequency resource block for multimedia transmissions over OFDM systems. We used symmetric n-channel FEC-based multiple descriptions with time coding based on the diversity order in the frequency and time domains. Results showed that, even with only one of the two diversities available, extremely worthy performance can be achieved. As far as video bitstreams are concerned, important considerations on the methods to evaluate the rate distortion (RD) curve were provided. We showed that great simplification can be considered in the algorithm for the RD function and the optimal staircase design, without jeopardizing the overall performance system. Beyond JSSC, as another method to improve the reliable data rate to be decoded, adaptive modulation techniques was investigated. We investigated adaptive modulation techniques in real systems, affected by channel estimation errors, co-channel interference or any possible issue compromising the bit error probability (BEP) performance. First, we compared slow adaptive modulation techniques to the fast ones in the presence of imperfect channel estimations. Results

showed that tracking the large-scale fading achieves an enormous improvement in the performance compared to a fixed modulation systems, and it can also outperform fast adaptive modulation techniques, that follows the small scale fading. Then, we provide a general analysis for the evaluation of system performance when imperfect signal-to-noise thresholds are experienced. We also studied two applicative examples, showing the effects of co-channel interference, and demonstrating that employing approximated BEP expression might reduce the system performance.

A large number of areas exists for future research on wireless multimedia transmissions and related topics. The proposed model can be applied to some existing standards, as WiMax for example, investigating an optimization suitable for the given system. The channel and model conditions of the standard might drive us to different considerations in the transmission scheme design. Due to the high decorrelation in the frequency domain, and due to the high number of subcarriers in WiMax systems, more than one frame might be transmitted in all the available subcarriers, for example, introducing a new parameter in the optimization problem. Moreover, a multicast scenario can be investigated, aimed at satisfying all the user requirements, providing at least a target quality to each user, or maximizing the sumrate capacity of the system. Adaptive modulation techniques can be applied to OFDM systems, for transmission of both images and video bitstreams. The optimal modulation level might be chosen for each independent subchannel, or suboptimal bit-loading algorithms can be employed. Finally, a cross-layer (physical-scheduling-application level) optimization in the multimedia transmission can be considered, introducing therefore the scheduling level in the optimization problem.

Appendix A

Packet loss rate

For a Rayleigh fading process $r(t)$, consider a simple two-state threshold model [52] with R_{th} being the threshold for the Rayleigh fading signal. If the signal level is above R_{th} (strong fade), the channel is considered to be in the good state, in which the probability of receiving the information is equal to 1, while if the signal level is below R_{th} (deep fade), the probably of receiving the particular information bit is equal to 0. Let us further assume that τ_f, τ_{nf} and τ_s are the deep fade duration, the strong fade duration and the deep fade inter-arrival intervals, so that

$$\tau_s = \tau_f + \tau_{nf}. \tag{A.1}$$

The average deep fade inter-arrival interval is the inverse of the level crossing rate (the expected rate at which the signal crosses the R_{th}), defined as [14]

$$\overline{\tau_s} = \frac{1}{\sqrt{2\pi} f_D \rho e^{-\rho^2}}, \tag{A.2}$$

where f_D is the maximum Doppler frequency, $\rho^2 = (R_{th}/R_{rms})^2$ is the inverse of the fade margin and R_{rms} is the root mean square of the fading signal. Denoting by N_r the level crossing rate, the average deep fade duration is defined as [14]

$$\overline{\tau_f} = \frac{P(r(t) \leq R_{th})}{N_r} = \frac{e^{\rho^2} - 1}{\sqrt{2\pi} f_D \rho}, \tag{A.3}$$

so that the average strong fade duration can be expressed as

$$\overline{\tau_{nf}} = \overline{\tau_s} - \overline{\tau_f} = \frac{1}{\sqrt{2\pi} \rho f_D}. \tag{A.4}$$

Note that the ratio between the average strong fade duration and the average deep fade duration is not a function of the Doppler spread. Thus, increasing f_D causes a reduction of the average deep fade inter-arrival interval ($\overline{\tau_s}$), but also a shorter deep fade duration, as can be observed from (A.2) and (A.3), respectively. Hence, faster fading produces deep fade events that are shorter in duration but occur more frequently.

Since $r(t)$ is a Rayleigh random process, $r^2(t)$ is a χ^2 process and thus its asymptotic[1] level down-crossing rate forms a Poisson process [117]. From the properties of Poisson random variables [118], it follows that

$$P_{\tau_s}(\tau) = \text{Prob}(\tau_s \leq \tau) = 1 - \exp\left(-\frac{\tau}{\overline{\tau_s}}\right), \tag{A.5}$$

and we can define the probability of having k deep fade arrivals within an interval of T_{PL} seconds as

$$\text{Prob}\left\{\mathcal{K}(T_{PL}) = k\right\} = \frac{(T_{PL}/\overline{\tau_s})^k e^{-T_{PL}/\overline{\tau_s}}}{k!} \tag{A.6}$$

where T_{PL} corresponds to the duration of a packet, and $\mathcal{K}(T_{PL})$ is a random variable representing the number of deep fade arrivals in T_{PL} seconds.

Thus, in an uncoded system, the probability of having a packet correctly received (P_{succ}) is

$$P_{succ} = P_{good} \cdot \text{Prob}\left(\mathcal{K}(T_{PL}) = 0\right) = \exp\left(-\rho^2 - \frac{T_{PL}}{\overline{\tau_s}}\right) \tag{A.7}$$

where:

$$P_{good} = \text{Prob}\left(\text{packet starts in good fade}\right) = P(r(t) > R_{th}) = \exp(-\rho^2) \tag{A.8}$$

is the probability that a packet starts in the good state. From (A.7), it can be seen that the packet success rate probability decreases with decreasing inter-arrival time of the deep fades due to the fact that deep fading arrival are shorter but occur more frequently. In Fig. A.1, we show both the simulation results and analytical results with different fade rates. As

[1] We use "asymptotic level down-crossing" to mean the level crossing of a very low threshold ($R_{th} \to 0$) [117].

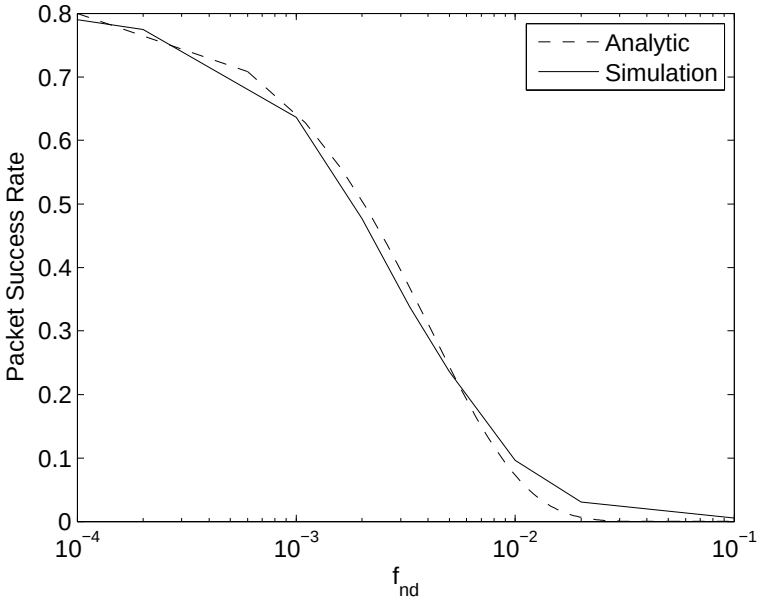

Figure A.1: Simulation and analytic results for the packet success rate for an uncoded system with different f_{nd} with $\mathrm{SNR}(R_{th}) = 9$ dB.

can be seen from the figure, the simulation and analytical results closely track one another. In particular, the packet success rate decreases with increasing fade rate. This explains the performance of Fig. 2.10, in which the PSNR of systems with either perfect CSI or imperfect CSI decreases monotonically with increasing fade rates.

Appendix B

Canonical expression

Antenna sub-set diversity (ASD) systems uses only a subset of the branches available at the receiver. When the most powerful branches are selected, H-S/MRC is adopted. For ASD techniques, the PDF of the signal-to-noise ratio at the combiner output is [6]

$$f_{\gamma_{\mathrm{T}}|\overline{\gamma}}(\xi) = \sum_{n=1}^{\tilde{N}} \sum_{k=1}^{\mu_n} A_{n,k}\ g_{n,k}(\xi)\,, \tag{B.1}$$

where $\tilde{N} = N - L + 1$, $\tilde{b}_n$ and $A_{n,k}$ are given in (B.3) and (B.4), respectively, and

$$g_{n,k}(\xi) = \begin{cases} \frac{\xi^{k-1}}{\tilde{b}_n^k\ \Gamma(k)}\ e^{-\xi/\tilde{b}_n} & \xi \geq 0, \\ 0 & \text{otherwise}, \end{cases} \tag{B.2}$$

$$\tilde{b}_n = \begin{cases} \overline{\gamma} & n = 1, \\ \overline{\gamma}\ L/(L+n-1) & n = 2, .., \tilde{N}\,. \end{cases} \tag{B.3}$$

$$A_{n,k} = \frac{\varphi_{n,k}}{c_n^k(\mu_n - k)!}\,, \tag{B.4}$$

with $n = 1, .., \tilde{N}$ and $k = 1, .., \mu_n$. In (B.4), $\varphi_{n,k}$ denotes the $(\mu_n - k)^{\underline{\text{th}}}$ derivative of $\varphi_n(x) \triangleq x^{\mu_n}\psi_{\gamma_{\mathrm{T}}}(x - c_n)$ evaluated at $x = 0$, where $\psi_{\gamma_{\mathrm{T}}}(x)$ represent the characteristic function of γ_{T}. Finally, the parameter μ_n is defined as

$$\mu_n = \begin{cases} L & n = 1, \\ 1 & n = 2, .., \tilde{N}\,, \end{cases}$$

When an imperfect CSI in considered in the feedback, the instantaneous SNR at the output of a N branches MRC is expressed in (4.5). When ASD and imperfect CSI at the transmitter are considered, steps similar to [19] can be adopted. The instantaneous output signal-to-noise ratio is given by

$$\widehat{\gamma}_{\mathrm{T}} = \langle \boldsymbol{a}, \widehat{\boldsymbol{\gamma}}_{[N]} \rangle \,, \tag{B.5}$$

where $\boldsymbol{a}$ is a $N \times 1$ vector that allow to select the branches to combine. For a H-S/MRC $a_n = 1\,,$for $1 \leq n \leq L\,, 0$ otherwise. $\widehat{\boldsymbol{\gamma}}_{[N]}$ is the $N \times 1$ vector of the ordered SNR, i.e., $\widehat{\boldsymbol{\gamma}}_{[N]} = [\widehat{\gamma}_{[1]}\ \widehat{\gamma}_{[2]} \dots\ \widehat{\gamma}_{[N]}]^T$ where $\widehat{\gamma}_{[1]} > \widehat{\gamma}_{[2]} > \ldots > \widehat{\gamma}_{[N]}$ and $(.)^T$ denotes transpose. The joint pdf of the no longer independent $\widehat{\gamma}_{[i]}$ is

$$f_{\widehat{\boldsymbol{\gamma}}_{[N]}}\left(\left\{\xi_{[i]}\right\}_{i=1}^{N}\right) = \begin{cases} \frac{N!}{\breve{\gamma}^N} e^{-\langle \boldsymbol{a}, \boldsymbol{\xi}_{[N]} \rangle / \breve{\gamma}} & \gamma_{[1]} > \gamma_{[2]} > \ldots > \gamma_{[N]}, \\ 0 & \text{otherwise.} \end{cases} \tag{B.6}$$

where $\breve{\gamma} = \mathbb{E}_{h_k}\{\widehat{\gamma}_k\} = \overline{\gamma} + 1/N_p\varepsilon$, as derived in (4.16). We recall that N_p is teh number of pilot symbols received within each frame, and $\varepsilon = E_{\mathrm{p}}/E_{\mathrm{s}}$. By adopting the virtual branch technique of [19], and considering the transformation matrix $\boldsymbol{\mathcal{T}}_{\mathrm{VB}} : \mathbb{R}^N \to \mathbb{R}^N$ given by

$$\boldsymbol{\mathcal{T}}_{\mathrm{VB}} = \begin{pmatrix} \breve{\gamma}/1 & \breve{\gamma}/2 & \cdots & \breve{\gamma}/N \\ & \breve{\gamma}/2 & \cdots & \breve{\gamma}/N \\ & & \ddots & \vdots \\ & & & \breve{\gamma}/N \end{pmatrix} \tag{B.7}$$

the pdf of the SNR at the combiner output is still given by (B.1), with $g_{n,k}(\xi)$ given by (B.2) and $\tilde{b}_n$ expressed as

$$\tilde{b}_n = \begin{cases} \breve{\gamma} & n = 1, \\ \breve{\gamma}\ L/(L+n-1) & n = 2, .., \tilde{N}\,. \end{cases} \tag{B.8}$$

Substituting (4.16) in (B.8), we obtain

$$\tilde{b}_n = \begin{cases} \overline{\gamma} + \frac{1}{N_p\varepsilon} & n = 1, \\ (\overline{\gamma} + \frac{1}{N_p\varepsilon})\ L/(L+n-1) & n = 2, .., \tilde{N}\,. \end{cases} \tag{B.9}$$

Therefore, the PDF and the CDF for a FAM system employing H-S/MRC at the receiver is given by (4.13) and (4.14), respectively, where the $\tilde{b}_n$

values are given by (B.9). The SNR thresholds are evaluated from the BEP expression in (C.1). For SAM systems, the PDF and CDF are represented by (4.17) and (4.18). The SNR thresholds are evaluated from the BEP expression in (C.6).

Appendix C

Approximation on BEP expressions

In the following, the derivation of the exact and the approximated BEP expressions is reported for both the instantaneous and mean case, for systems with H-S/MRC receiver.

C.1 Instantaneous BEP

The exact BEP expression for a M-QAM system was carried out in [112]. In particular, for a given modulation level M, the instantaneous exact bit error proability can be expressed as

$$P_{\mathrm{b}}(e|\gamma_T) = \frac{2}{\sqrt{M}\log_2(\sqrt{M})} \sum_{h=1}^{\log_2(\sqrt{M})} \sum_{i=0}^{(1-2^{-h})\sqrt{M}-1} (-1)^{\left\lfloor \frac{i2^{h-1}}{\sqrt{M}} \right\rfloor} \times \\ \times \left(2^{h-1} - \left\lfloor \frac{i2^{h-1}}{\sqrt{M}} + \frac{1}{2} \right\rfloor\right) Q\left((2i+1)\sqrt{\frac{3\gamma_T}{(M-1)}}\right) \quad \text{(C.1)}$$

Since (C.1) is not invertible, bounds and approximations has gained great attention in the last year. One of the most employed BEP expression is the exponential approximation [96], that results to be easily invertible but not that tight and it is defined as (**A1**):

$$P_{\mathrm{b}}^{(A1)}(e|\gamma_{\mathrm{T}}) \approx 0.2 \exp\left[\frac{-1.6\gamma_{\mathrm{T}}}{M-1}\right]. \quad \text{(C.2)}$$

A more tight approximation but not that easy to invert is the one introduced in [113] (**A2**):

$$P_{\mathrm{b}}^{(A2)}(e|\gamma_{\mathrm{T}}) \approx \frac{A_M}{\log_2 M} \sum_{i=1}^{\sqrt{M}/2} \mathrm{erfc}\left[(2i-1)\sqrt{B_M \gamma_{\mathrm{T}}}\right], \tag{C.3}$$

where $A_M = 2[1-(1/\sqrt{M})]$ and $B_M = [3/2(M-1)]$. Finally, a classical approach is to obtain the BEP expression dividing the symbol-error probability (SEP) by the number of bits per symbols. The BEP derived is (**A3**) [107]

$$P_{\mathrm{b}}^{(A3)}(e|\gamma_{\mathrm{T}}) \approx \frac{A_M}{\log_2 M}\mathrm{erfc}(\sqrt{B_M \gamma_{\mathrm{T}}}) \left[1 - \frac{A_M}{4}\mathrm{erfc}(\sqrt{B_M \gamma_{\mathrm{T}}})\right] \tag{C.4}$$

where A_M and B_M were already defined above.

The three approximations and the exact BEP are reported in Fig. C.1, where the BEP performance for a 4-QAM and 1024-QAM are provided. It can be observed as both (A2) and (A3) are tight approximations, while the exponential approximations get more rough with the increasing of the modulation level.

C.2 Mean BEP

Since in SAM systems, SNR thresholds are evaluated from the averaged BEP, an approximation on this expression leads to an error in the SNR thresholds. The exact BEP in an averged case, can be derived from (C.1):

$$\begin{aligned} P_{\mathrm{b}}(\overline{\gamma}) &= \int_0^{\infty} P_{\mathrm{b}}(e|\gamma_{\mathrm{T}}) f_{\gamma_{\mathrm{T}}|\overline{\gamma}}(\xi) d\xi = \\ &= \frac{2}{\sqrt{M}\log_2(\sqrt{M})} \sum_{h=1}^{\log_2(\sqrt{M})} \sum_{i=0}^{(1-2^{-h})\sqrt{M}-1} (-1)^{\left\lfloor \frac{i2^{h-1}}{\sqrt{M}} \right\rfloor} \times \\ &\times \left(2^{h-1} - \left\lfloor \frac{i2^{h-1}}{\sqrt{M}} + \frac{1}{2} \right\rfloor\right) \int_0^{\infty} Q\left((2i+1)\sqrt{\frac{3\gamma_{\mathrm{T}}}{(M-1)}}\right) f_{\gamma_{\mathrm{T}}|\overline{\gamma}}(\xi) d\xi \end{aligned} \tag{C.5}$$

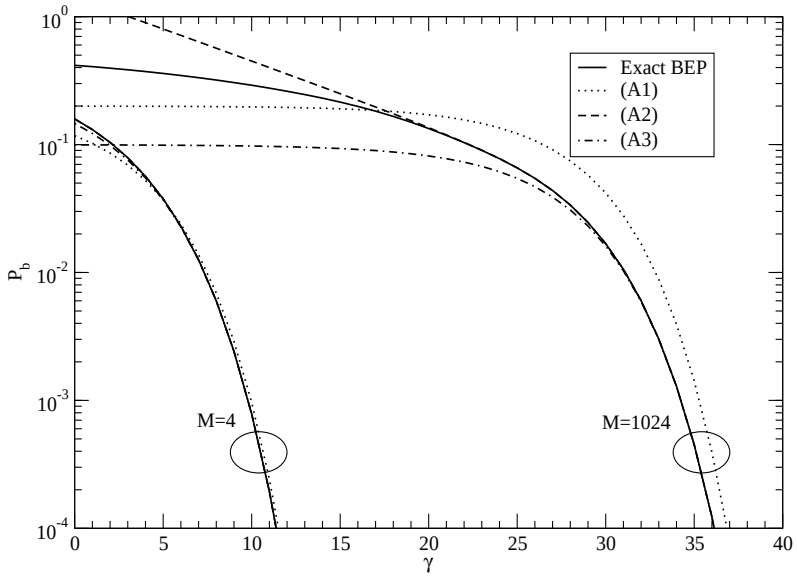

Figure C.1: Exact and approximated BEP vs. instantaneous SNR for a 4-QAM and 1024-QAM system.

Simplifying the integral and considering the canonical expression derived from the virtual branch technique for H-S/MRC [19], the (C.5) can be simplified as [6]

$$P_{\mathrm{b}}(\overline{\gamma}) = \frac{2}{\sqrt{M}\log_2(\sqrt{M})} \sum_{h=1}^{\log 2(\sqrt{M})} \sum_{i=0}^{(1-2^{-h})\sqrt{M}-1} (-1)^{\left\lfloor \frac{i2^{h-1}}{\sqrt{M}} \right\rfloor} \times \\ \times \left(2^{h-1} - \left\lfloor \frac{i2^{h-1}}{\sqrt{M}} + \frac{1}{2} \right\rfloor\right) \Im\left(\frac{3(2i+1)^2}{2(M-1)}\widetilde{b}_n\right) \qquad \text{(C.6)}$$

where

$$\Im(x) = \sum_{n=1}^{\widetilde{N}} \sum_{k=1}^{\mu_n} A_{n,k} I_k(x),$$

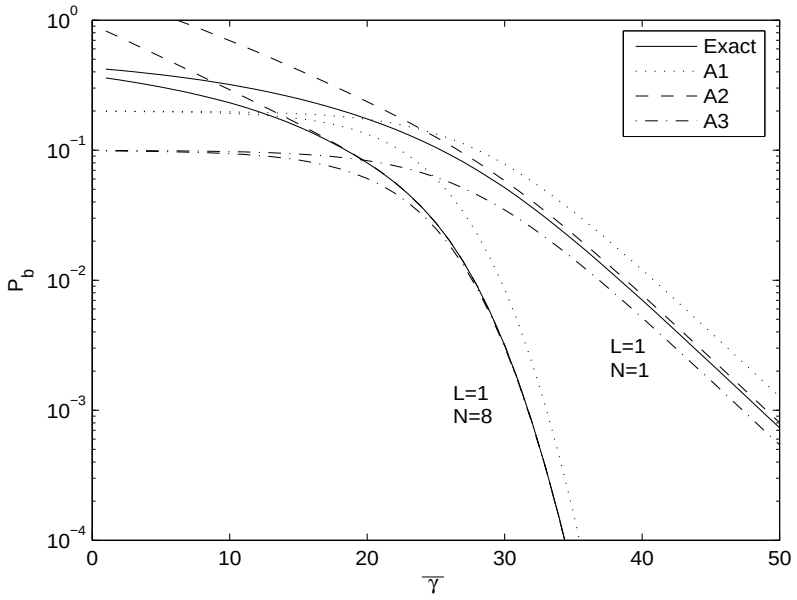

Figure C.2: Exact and approximated BEP vs. averaged SNR for 1024-QAM system.

and $I_k(x) = \frac{1}{\pi}\int_0^{\pi/2}\left(\frac{sin^2\theta}{x+sin^2\theta}\right)^k d\theta$. Similarly, from (C.2), the averaged BEP expression in the exponential expression can be derived

$$\begin{aligned} P_{\mathrm{b}}^{(\mathrm{A1})}(\overline{\gamma}) &= \int_0^{\infty} P_{\mathrm{b}}^{(\mathrm{A1})}(e|\gamma_{\mathrm{T}}) f_{\gamma_{\mathrm{T}}|\overline{\gamma}}(\xi) d\xi = \\ &= 0.2\mathbb{E}_{\gamma_{\mathrm{T}}}\left\{\exp\left[-\frac{1.6}{M-1}\gamma_{\mathrm{T}}\right]\right\} = \\ &= 0.2\sum_{n=1}^{\widetilde{N}}\sum_{k=1}^{\mu_n} A_{n,k}\left[\frac{1}{1+\frac{1.6}{M-1}\widetilde{b}_n}\right]^k \end{aligned} \tag{C.7}$$

where $\mathbb{E}_X$ is the statistical expectation with respect to the random variable X. In the case of MRC receiver, the exponential approximation is given by (C.7). The approximation (A2) for the averaged BEP can be

expressed as:

$$P_{\mathrm{b}}^{(\mathrm{A2})}(\overline{\gamma}) = \int_0^{\infty} P_{\mathrm{b}}^{(\mathrm{A2})}(e|\gamma_{\mathrm{T}}) f_{\gamma_{\mathrm{T}}|\overline{\gamma}}(\xi) d\xi =$$
$$= \frac{2A_M}{\log_2 M} \sum_{i=1}^{\sqrt{M}/2} \frac{1}{\pi} \int_0^{\pi/2} \mathbb{E}_{\gamma_{\mathrm{T}}} \left\{ \exp\left[-\frac{(2i-1)^2 B_M \gamma_{\mathrm{T}}}{sin^2\theta} \right] \right\} d\theta =$$
$$= \frac{2A_M}{\log_2 M} \sum_{i=1}^{\sqrt{M}/2} \sum_{n=1}^{\widetilde{N}} \sum_{k=1}^{\mu_n} A_{n,k} I_k \left[(2i-1)^2 B_M \widetilde{b}_n \right]. \quad \text{(C.8)}$$

Thus, in the case of MRc receiver, the approximation (A2) becomes (C.8). Finally, the third approximation can be derived as

$$P_{\mathrm{b}}^{(\mathrm{A3})}(\overline{\gamma}) = \int_0^{\infty} P_{\mathrm{b}}^{(\mathrm{A3})}(e|\gamma_{\mathrm{T}}) f_{\gamma_{\mathrm{T}}|\overline{\gamma}}(\xi) d\xi =$$
$$= \int_0^{\infty} \frac{2A_M}{\log_2 M} Q\left(\sqrt{2B_M \gamma_T} \right) \left[1 - \frac{A_M}{2} Q\left(\sqrt{2B_M \gamma_T} \right) \right] f_{\gamma_{\mathrm{T}}|\overline{\gamma}}(\xi) d\xi \quad \text{(C.9)}$$

In order to solve the integral, we need to recall that [9]

$$Q^2(x) = \frac{1}{\pi} \int_0^{\pi/4} \exp\left[-\frac{x^2}{2\ \sin^2\theta} \right] d\theta. \quad \text{(C.10)}$$

Substituting (C.10) in (C.9), the BEP becomes

$$P_{\mathrm{b}}^{(\mathrm{A3})}(\overline{\gamma}) = \frac{2A_M}{\log_2 M} \frac{1}{\pi} \int_0^{\pi/2} \mathbb{E}_{\gamma_{\mathrm{T}}} \left\{ \exp\left[-\frac{B_M \gamma_{\mathrm{T}}}{\sin^2\theta} \right] \right\} d\theta -$$
$$- \frac{A_M^2}{\log_2 M} \frac{1}{\pi} \int_0^{\pi/4} \mathbb{E}_{\gamma_{\mathrm{T}}} \left\{ \exp\left[-\frac{B_M \gamma_T}{\sin^2\theta} \right] d\theta \right\} =$$
$$= \frac{2A_M}{\log_2 M} \sum_{n=1}^{\widetilde{N}} \sum_{k=1}^{\mu_n} A_{n,k} I_k \left(B_M \widetilde{b}_n \right) -$$
$$- \frac{A_M^2}{\log_2 M} \frac{1}{\pi} \sum_{n=1}^{\widetilde{N}} \sum_{k=1}^{\mu_n} A_{n,k} \int_0^{\pi/4} \left(\frac{\sin^2\theta}{B_M \widetilde{b}_n + \sin^2\theta} \right)^k d\theta. \quad \text{(C.11)}$$

It is easy to demonstrate that, for a MRC systems, the approximation (A3) is given by (C.11)

The approximated BEP expression and the exact one for different diversity orders are reported in Fig. C.2. We recall that N is the number of branches before the re-order of the HS/MRC and L are the most powerful branches processed by the MRC.

Appendix D

Co Channel Interference

In this appendix, we derive the bit error probability of M-QAM systems in the presence of co-channel interference. We consider N antennas at the receiver, and we assume a fading rate much slower than the signal rate [114]. The received signal on each branch after the matched filtering and the sampling at the symbol rate is denoted by $z_i(k) = z_i^{(P)}(k) + jz_i^{(Q)}(k)$, where k represents the time index. The vector output $\mathbf{z}(k) = [z_1(k), \ldots, z_N(k)]$ can be written as[1](D.1)

$$\begin{aligned}\mathbf{z}(k) &= \mathbf{z}^{(P)}(k) + j\mathbf{z}^{(Q)}(k) \\ &= \sqrt{E_{\mathrm{S}}}\mathbf{h}b_0(k) + \sqrt{E_{\mathrm{I}}}\sum_{n=1}^{N_{\mathrm{I}}}\mathbf{h}_{\mathrm{I},n}b_{\mathrm{I},n}(k) + \mathbf{n}(k), \end{aligned} \tag{D.1}$$

where E_{I} is the mean symbol energy transmitted of each interfering signals; $b_0(k) = b_0^{(P)}(k) + jb_0^{(Q)}(k)$ is the desired signal sample and $b_{\mathrm{I},n}(k) = b_{\mathrm{I},n}^{(P)}(k) + jb_{\mathrm{I},n}^{(Q)}(k)$ is the interfering signal sample of the n-th interferer. Since we assume a slow frequency flat Rayleigh distributed fading, the vectors $\mathbf{h}$ and $\mathbf{h}_{\mathrm{I},n}, n = 1, \ldots, N_{\mathrm{I}}$ have distribution $\mathcal{CN}(0, \mathbf{I}_N)$, and we denote by $\mathbf{H}_{\mathrm{I}} = \{\mathbf{h}_{\mathrm{I,j}}\}_{j=1,\ldots,N_{\mathrm{I}}}$ the interference channel matrix. Being the desired signal affected by fading, the Gaussian approximation for the interferers is justified [115]. Thus, $b_1(k), \ldots, b_{N_{\mathrm{I}}}(k)$ are independent zero-mean complex Gaussian random variables, each with variance one because of the normalization. Following the steps in [114], we derive the

[1]Note that the subscript I represents the interference symbols, while the superscript I is used to indicate the in-phase symbols.

bit error probability as a function of the averaged signal-to-interference-plus-noise ratio (SINR) for a M-QAM system with optimum combining at the receiver. The optimum weight vector that maximizes the SINR is $\mathbf{w} = \alpha \mathbf{R}^{-1}\mathbf{c}_D$, where α is an arbitrary constant and $\mathbf{R}$ the covariance matrix, expressed as

$$\begin{aligned}\mathbf{R} &= \mathbb{E}_{\mathbf{n}(k),b_j(k)} \left\{ \left[\sqrt{E_{\mathrm{I}}} \sum_{n=1}^{N_{\mathrm{I}}} \mathbf{h}_{\mathrm{I},n} b_{\mathrm{I},n}(k) + \mathbf{n}(k) \right] \left[\sqrt{E_{\mathrm{I}}} \sum_{n=1}^{N_{\mathrm{I}}} \mathbf{h}_{\mathrm{I},n} b_{\mathrm{I},n}(k) + \mathbf{n}(k) \right]^H \right\} \\ &= E_{\mathrm{I}} \underbrace{\sum_{j=1}^{N_{\mathrm{I}}} \mathbf{h}_{\mathrm{I},j} \mathbf{h}_{\mathrm{I},j}^H}_{\mathbf{R}_I} + N_0 \mathbf{I}_N, \end{aligned} \tag{D.2}$$

where the last equality holds because the desired signal, the interference and the noise are assumed independent from each other. As observed in [114], considering an overloaded system (i.e., $N_I \geq N$) the SINR of the output at the combiner can be written as $\gamma = E_S \mathbf{h}_S^H \mathbf{R}^{-1} \mathbf{h}_S$. The matrix $\mathbf{R}^{-1}$ can be written as $\mathbf{U}\mathbf{\Lambda}\mathbf{U}^H$, where $\mathbf{U}$ is a unitary matrix with elements $\mathbf{c}_1, \ldots, \mathbf{c}_N$, and $\mathbf{\Lambda}$ is a diagonal matrix whose elements on the principal diagonal are the eigenvalues of $\mathbf{R}$, denoted by $\widetilde{\lambda}_1, \ldots, \widetilde{\lambda}_N$. The SINR can be rewritten as

$$\gamma = E_S \mathbf{h}_S^H \mathbf{U}\mathbf{\Lambda}\mathbf{U}^H \mathbf{h}_S = \sum_{i=1}^{N} \frac{E_D \left| \mathbf{c}_D^H \mathbf{u}_i \right|^2}{E_I \lambda_i + N_0}, \tag{D.3}$$

where $\mathbf{c}_D^H \mathbf{u}_1, \ldots, \mathbf{c}_D^H \mathbf{u}_N$ have the same distribution of $\mathbf{c}_D$, being $\mathbf{U}$ a unitary transformation, and the eigenvalues of $\mathbf{R}$ have been written in terms of the eigenvalues of $\mathbf{R}_{\mathrm{I}}$,

$$\widetilde{\lambda}_i = E_{\mathrm{I}} \lambda_{\mathrm{I}} + N_0, \qquad i = 1, \ldots, N.$$

Since H_{I} is a matrix whose elements are complex values normal distributed $\mathcal{CN}(0,1)$, then the matrix $\mathcal{W} = H_{\mathrm{I}} H_{\mathrm{I}}^H = \mathbf{R}_{\mathrm{I}}$ is called central Wishart matrix [116], and the distribution of the eigenvalues of a central Wishart matrix is given by

$$f_{\boldsymbol{\lambda}}(x1, \ldots, x_N) = \frac{1}{N!} \prod_{i=1}^{N} \frac{x_i^{N_{\mathrm{I}}-N} e^{-x_i}}{(N-i)!(N_{\mathrm{I}}-i)!} \prod_{i<j}^{N} (x_i - x_j)^2. \tag{D.4}$$

Starting from the instantaneous exact bit error probability (C.1), the mean BEP for M-QAM systems can be derived averaging over the SNIR:

$$\begin{aligned} P_{\mathrm{b}} &= \int P(e|\gamma) f_{\gamma}(\xi) d\xi \\ &= \frac{2}{\sqrt{M}\log_2(\sqrt{M})} \sum_{h=1}^{\log 2(\sqrt{M})} \sum_{n=0}^{(1-2^{-h})\sqrt{M}-1} (-1)^{\lfloor \frac{n2^{h-1}}{\sqrt{M}} \rfloor} \times \\ &\times \left(2^{h-1} - \left\lfloor \frac{n2^{h-1}}{\sqrt{M}} + \frac{1}{2} \right\rfloor \right) \underbrace{\frac{1}{\pi} \int_0^{\pi/2} \Psi_{\gamma} \left\{ -\frac{3(2n+1)^2}{2(M-1)\sin^2\theta} \right\} d\theta}_{\zeta_n(\gamma_{\mathrm{T}})}, \end{aligned} \tag{D.5}$$

where the last equality is due to the use of the Craig's formula of the Gaussian Q function [9]. Using the chain rule of conditional expectation, we obtain

$$\zeta_n(\gamma_{\mathrm{T}}) = \int_0^{\pi/2} \int_0^{\infty} \cdots \int_0^{\infty} \Psi_{\gamma_{\mathrm{T}}|\boldsymbol{\lambda}} \left\{ -\frac{c_{M,n}}{\sin^2\theta} \right\} f_{\boldsymbol{\lambda}}(\mathbf{x}) d\theta d\mathbf{x}. \tag{D.6}$$

where $c_{M,n} = \frac{3(2n+1)^2}{2(M-1)}$.

Since the vector $[\mathbf{c}_D^H \mathbf{u}_1, \ldots, \mathbf{c}_D^H \mathbf{u}_N]$ is Gaussian with i.i.d. elements, the conditional characteristic function of γ is given by

$$\Psi_{\gamma|\boldsymbol{\lambda}}(j\nu) = \prod_{i=1}^{N} \left(1 - j\nu \frac{E_D}{E_I \lambda_i + N_0} \right)^{-1} \tag{D.7}$$

Substituting (D.7) in (D.6), we obtain

$$\begin{aligned} \zeta_n(\gamma_{\mathrm{T}}) &= \frac{1}{\pi N!} \frac{1}{\prod_{i=1}^{N} (N-i)!(N_{\mathrm{I}}-i)!} \\ &\times \int_0^{\pi/2} \int_0^{\infty} \cdots \int_0^{\infty} |\mathbf{V}_1(\mathbf{x})|^2 \prod_{i=1}^{N} \frac{\sin^2\theta}{\sin^2\theta + c_{M,n} \frac{E_D}{E_I x_i + N_0}} e^{-x_i} x_i^{N_{\mathrm{I}}-N} \end{aligned} \tag{D.8}$$

where $\mathbf{V}_1(\mathbf{x})$ is the Vandermonde matrix and $|\mathbf{V}_1(\mathbf{x})|^2 = \prod_{i<j}^{N} (x_i - x_j)^2$. Recalling the Lemma 1 in [114]

$$\begin{aligned} &\int_0^{\infty} \cdots \int_0^{\infty} |\boldsymbol{\Psi}(\mathbf{x})||\boldsymbol{\Phi}(\mathbf{x})| \prod_{k=1}^{K} \xi(x_i) dx_1 \ldots dx_K \\ &= K! \det \left(\left\{ \int_0^{\infty} \Phi_i(x) \Psi_j(x) \xi(x) dx \right\}_{k,j=1,\ldots,K} \right) \end{aligned} \tag{D.9}$$

considering $|\mathbf{\Psi}(\mathbf{x})| = |\mathbf{\Phi}(\mathbf{x})| = |\mathbf{V}_1(\mathbf{x})|$, $K = N$ and

$$\xi(x) = \frac{\sin^2\theta}{\sin^2\theta + c_{M,n}\frac{E_\mathrm{D}}{E_\mathrm{I}x_i+N_0}} \quad e^{-x_i}x_i^{N_\mathrm{I}-N}$$

we obtain

$$\zeta_n(\gamma_\mathrm{T}) = \frac{1}{\pi}\frac{1}{\prod_{i=1}^{N}(N-i)!(N_\mathrm{I}-i)!} \times \int_0^{\pi/2} \det\left(\left\{\int_0^\infty e^{-x}x^{N_\mathrm{I}-N+j+i-2}\left(c_{M,n}\frac{E_\mathrm{D}}{E_\mathrm{I}x_i+N_0}\right)dx\right\}_{i,j=1,\ldots,N}\right)d\theta. \tag{D.10}$$

Considering the following identity [110, eq. (16)]

$$\int_0^\infty e^{-x}x^n\frac{x+a}{x+b}dx = b^n e^b n![b(1+n)\Gamma(-1-n,b) + a\Gamma(-n,b)], \tag{D.11}$$

where

$$\begin{aligned} a &= \frac{N_0}{E_\mathrm{I}} = \frac{N_\mathrm{I}}{\overline{\gamma}_\mathrm{I}}, \\ b &= \frac{E_\mathrm{D}}{N_0} + \frac{E_\mathrm{d}}{E_\mathrm{I}}\frac{c_{M,n}}{\sin^2\theta} = \frac{N_\mathrm{I}}{\overline{\gamma}_\mathrm{I}} + \frac{N_\mathrm{I}\overline{\gamma}}{\overline{\gamma}_\mathrm{I}}\frac{c_{M,n}}{\sin^2\theta} \\ n &= N_\mathrm{I} - N + i + j - 2, \end{aligned}$$

(D.10) can be expressed as

$$\begin{aligned} \zeta_n(\gamma_\mathrm{T}) = \frac{1}{\pi}\frac{1}{\prod_{i=1}^{N}(N-i)!(N_\mathrm{I}-i)!}\int_0^{\pi/2} \det\big(\big\{&b^{(i+j+N_\mathrm{I}-N)}e^b(i+j+N_\mathrm{I}-N)! \\ &\times [b(1+(i+j+N_\mathrm{I}-N))\Gamma(-1-i-j-N_\mathrm{I}+N,b) \\ &+ a\Gamma(-(i+j+N_\mathrm{I}-N),b)]\big\}_{i,j=0,\ldots,N-1}\big)\,d\theta. \end{aligned} \tag{D.12}$$

Substituting (D.12) in (D.5), the mean BEP expression is given by the equation (5.12).

When an underloaded system is considered, i.e., $N_\mathrm{I} < N$, the conditional characteristic function of γ is given by

$$\Psi_{\gamma|\boldsymbol{\lambda}}(j\nu) = \left(1 - j\nu\frac{E_\mathrm{D}}{N_0}\right)^{-(N-N_\mathrm{I})} \prod_{i=1}^{N_\mathrm{I}}\left(1 - j\nu\frac{E_D}{E_I\lambda_i + N_0}\right)^{-1} \tag{D.13}$$

and the Wishart matrix is equal to $\mathcal{W} = \mathbf{H}_{\mathrm{I}}^{H}\mathbf{H}_{\mathrm{I}}$. Being the pdf of the eigenvalues $\boldsymbol{\lambda}$ is expressed as [116]

$$f_{\boldsymbol{\lambda}}(x1,\ldots,x_N) = \frac{1}{N_{\mathrm{I}}!}\prod_{i=1}^{N_{\mathrm{I}}}\frac{x_i^{N-N_{\mathrm{I}}}e^{-x_i}}{(N-i)!(N_{\mathrm{I}}-i)!}\underbrace{\prod_{i<j}^{N_{\mathrm{I}}}(x_i-x_j)^2}_{|\mathbf{V}_1((x))|^2}, \tag{D.14}$$

considering the Lemma 1 (D.9) and the identity (D.11), with similar step to the overloaded case, it can be derived that (D.12) become

$$\begin{aligned}\zeta_n(\gamma_{\mathrm{T}}) = \frac{1}{\pi}\frac{1}{\prod_{i=1}^{N}(N-i)!(N_{\mathrm{I}}-i)!}\int_0^{\pi/2}\left(\frac{\sin^2\theta}{\sin^2\theta + c_{M,n}\overline{\gamma}}\right)^{N-N_{\mathrm{I}}} \\ \det\left(\left\{\frac{N_{\mathrm{I}}}{\overline{\gamma}_{\mathrm{I}}} + \frac{N_{\mathrm{I}}\overline{\gamma}}{\overline{\gamma}_{\mathrm{I}}}\frac{c_{M,n}}{\sin^2\theta}^{\,k}\exp\left[\frac{N_{\mathrm{I}}}{\overline{\gamma}_{\mathrm{I}}} + \frac{N_{\mathrm{I}}\overline{\gamma}}{\overline{\gamma}_{\mathrm{I}}}\frac{c_{M,n}}{\sin^2\theta}\right]k!\right. \\ \times\left[\frac{N_{\mathrm{I}}}{\overline{\gamma}_{\mathrm{I}}} + \frac{N_{\mathrm{I}}\overline{\gamma}}{\overline{\gamma}_{\mathrm{I}}}\frac{c_{M,n}}{\sin^2\theta}(1+k)\Gamma\left(-1-k, \frac{N_{\mathrm{I}}}{\overline{\gamma}_{\mathrm{I}}} + \frac{N_{\mathrm{I}}\overline{\gamma}}{\overline{\gamma}_{\mathrm{I}}}\frac{c_{M,n}}{\sin^2\theta}\right)\right. \\ \left.\left. + \; a\Gamma\left(-k, \frac{N_{\mathrm{I}}}{\overline{\gamma}_{\mathrm{I}}} + \frac{N_{\mathrm{I}}\overline{\gamma}}{\overline{\gamma}_{\mathrm{I}}}\frac{c_{M,n}}{\sin^2\theta}\right)\right]\right\}_{i,j=0,\ldots,N-1}\Bigg)\,d\theta.\end{aligned} \tag{D.15}$$

where $k = i + j + N - N_{\mathrm{I}}$. Thus, the mean BEP expression for an underloaded system can be derived, substituting (D.15) in (D.5).

Bibliography

[1] A. Said and W. A. Pearlman, "A new, fast, and efficient image codec based on set partitioning in hierarchical trees," *IEEE Trans. Circuits Syst. Video Technol.*, vol. 6, pp. 243–249, Jun. 1996.

[2] V. K. Goyal, "Multiple description coding: Compression meets the network," *IEEE Signal Processing Mag.*, vol. 18, no. 5, pp. 74–93, Sept. 2001.

[3] V. M. Stankovic, R. Hamzaoui, Y. Charfi, and Z. Xiong, "Real-time unequal error protection algorithms for progressive image transmission," *IEEE J. Select. Areas Commun.*, vol. 21, no. 10, pp. 1526–1535, Dec. 2003.

[4] V. M. Stankovic, R. Hamzaoui, and Z. Xiong, "Efficient channel code rate selection algorithms for forward error correction of packetized multimedia bitstreams in varying channels," *IEEE Trans. Multimedia*, vol. 6, no. 2, pp. 240–248, Apr. 2004.

[5] A. J. Goldsmith and S.-G. Chua, "Variable-rate variable-power MQAM for fading channel," *IEEE Trans. Commun.*, vol. 45, no. 10, pp. 1218–1230, Oct. 1997.

[6] A. Conti, M. Z. Win, and M. Chiani, "Slow adaptive M-QAM with diversity in fast fading and shadowing," *IEEE Trans. Commun.*, vol. 55, no. 5, pp. 895–905, May 2007.

[7] D. L. Goeckel, "Adaptive coding for time-varying channels using outdated fading estimates," *IEEE Trans. Commun.*, vol. 47, no. 6, pp. 844–855, June 1999.

[8] J. N. Laneman, E. Martinian, G. W. Wornell, J. G. Apostolopoulos, and S. J. Wee, "Comparing application- and physical-layer approaches to diversity on wireless channels," in *Proc. ICC*, Anchorage, Alaska, May 2003, vol. 4, pp. 2678 – 2682.

[9] M. K. Simon and M.-S. Alouini, *Digital Communication over Fading Channels: A Unified Approach to Performance Analysis*, John Wiley & Sons, Inc., New York, NY, 10158, first edition, 2000.

[10] J. G. Proakis, *Digital Communications*, McGraw-Hill, Inc., New York, NY, 10020, third edition, 1995.

[11] G. L. Stuber, *Principles of Mobile Communication*, Kluwer Academic Publishers, Norwell, MA 02061, second edition, 2001.

[12] A. Goldsmith, *Wireless Communications*, John Wiley & Sons, Inc., New York, NY 10011-4211,USA, 2002.

[13] R. H. Clarke, "A statistical theory of mobile-radio reception," *Bell Syst. Tech. J.*, pp. 957–1000, Jul-Aug 1968.

[14] W. C. Jakes, *Microwave Mobile Communications*, Wiley, John and Sons, 1994.

[15] Y. R. Zheng and C. Xiao, "Simulation models with correct statistical properties for rayleigh fading channels," *IEEE Trans. Commun.*, vol. 51, no. 6, pp. 920–928, June 2003.

[16] D. Gesbert, M. Shafi D.-S. Shiu, P. J. Smith, and A. Naguib, "From theory to practice: an overview of MIMO space-time coded wireless systems," *IEEE J. Select. Areas Commun.*, vol. 21, no. 3, pp. 281–302, Apr 2003.

[17] T. Eng, N. Kong, and L. B. Milstein, "Comparison of diversity combining techniques for rayleigh-fading channels," *IEEE Trans. Commun.*, vol. 44, no. 9, pp. 1117–1129, Sep 1996.

[18] J. Winters, "Optimum combining in digital mobile radio with cochannel interference," *IEEE J. Select. Areas Commun.*, vol. 2, no. 4, pp. 528–539, Jul 1984.

[19] M. Z. Win and J. H. Winters, "Virtual branch analysis of symbol error probability for hybrid selection/maximal-ratio combining in rayleigh fading," *IEEE Trans. Commun.*, vol. 49, no. 11, pp. 1926–1934, Nov. 2001.

[20] P. G. Sherwood and K. Zeger, "Progressive image coding for noisy channels," *IEEE Signal Processing Lett.*, vol. 4, no. 7, pp. 191–198, July 1997.

[21] P. Cosman, J. Rogers, P. G. Sherwood, and K. Zeger, "Combined forward error control and packetized zerotree wavelet encoding for transmission of images over varying channels," *IEEE Trans. Image Processing*, vol. 9, pp. 132–140, Jun. 2000.

[22] P. G. Sherwood and K. Zeger, "Error protection for progressive image transmission over memoryless and fading channels," *IEEE Trans. Commun.*, vol. 46, no. 12, Dec. 1998.

[23] A. Albanese, J. Blomer, J. Edmonds, M. Luby, and M. Sudan, "Priority encoded transmission," *IEEE Trans. Inform. Theory*, vol. 46, no. 6, pp. 1737–1744, Nov. 1996.

[24] A. E. Mohr, E. A. Riskin, and R. E. Ladner, "Graceful degradation over packet erasure channels through forward error correction," in *Proc. IEEE Data Compression Conference*, Snowbird, UT, March 1999, pp. 92–101.

[25] R. Puri, K.-W. Lee, K. Ramchandran, and V. Bharghavan, "An integrated source transcoding and congestion control paradigm for video streaming in the Internet," *IEEE Trans. Multimedia*, vol. 3, no. 1, pp. 18–32, Mar. 2001.

[26] D. G. Sachs, R. Anand, and K. Ramchandran, "Wireless image transmission using multiple-description based concatenated codes," in *Proc. SPIE*, San Jose, CA, Jan. 2000, vol. 3974, pp. 300–311.

[27] Y. S. Chan, P. C. Cosman, and L. B. Milstein, "A cross-layer diversity technique for multi-carrier OFDM multimedia networks," *IEEE Trans. Image Processing*, vol. 15, no. 4, pp. 833–847, Apr. 2006.

[28] Y. Li, Jr. L.J. Cimini, and N.R. Sollenberger, "Robust channel estimation for ofdm systems with rapid dispersive fading channels," *IEEE Trans. Commun.*, vol. 46, no. 7, pp. 902–915, Jul. 1998.

[29] Ye Li, "Pilot-symbol-aided channel estimation for OFDM in wireless systems," *IEEE Trans. Veh. Technol.*, vol. 49, no. 4, pp. 1207–1215, Jun. 2000.

[30] X. Cai and G.B. Giannakis, "Adaptive PSAM accounting for channel estimation and prediction errors," *IEEE Trans. Wireless Commun.*, vol. 4, no. 1, pp. 246–256, Jan. 2005.

[31] A. Stefanov and T. M. Duman, "Turbo-coded modulation for systems with transmit and receive antenna diversity over block fading channels: system model, decoding approaches and practical considerations," *IEEE J. Select. Areas Commun.*, vol. 19, no. 5, pp. 958–968, 2001.

[32] R. M. Buehrer and N. A. Kumar, "The impact of channel estimation error on space-time block codes," in *Proc. VTC*, Vancouver, British Columbia, Canada, Sep. 2002, vol. 3, pp. 1921–1925.

[33] V. Tarokh, N. Seshadri A. Naguib, and A. R. Calderbank, "Space-time codes for high data rate wireless communication: performance criteria in the presence of channel estimation errors, mobility, and multiple paths," *IEEE Trans. Commun.*, vol. 47, no. 2, pp. 199–207, 1999.

[34] J. Song and K. J. R. Liu, "Robust progressive image transmission over OFDM systems using space-time block code," *IEEE Trans. Multimedia*, vol. 4, no. 3, pp. 394–406, Sept. 2002.

[35] Y. Sun, Z. Xiong, and X. Wang, "Scalable image transmission over differentially space-time coded OFDM systems," in *Proc. GlobeCom*, Taipei, Taiwan, Nov. 2002, vol. 1, pp. 379 – 383.

[36] F. Masoud, S. Cho, and W. A. Pearlman, "Robust image transmission using a new joint source channel coding algorithm and dual adaptive OFDM," in *Proc. GlobeCom*, San Jose, CA, U.S.A., Jan. 2004, vol. 5308, pp. 636–646.

[37] J. M. Shapiro, "Embedded image coding using zerotrees of wavelet coefficients," *IEEE Trans. Signal Processing*, vol. 41, no. 12, pp. 3445–3462, Dec 1993.

[38] R. J. McEliece and W. E. Stark, "Channels with block interference," *IEEE Trans. Inform. Theory*, vol. IT-30, no. 1, pp. 44–53, Jan. 1984.

[39] Y. R. Zheng and C. Xiao, "Simulation models with correct statistical properties for Rayleigh fading channels," *IEEE Trans. Commun.*, vol. 51, no. 6, pp. 920–928, Jun. 2003.

[40] T. S. Rappaport, *Wireless Communications: Principles & Practice*, Prentice Hall, Upper Saddle River, NJ, 1996.

[41] M. Russell and G.L. Stuber, "Interchannel interference analysis of OFDM in a mobile environment," in *Proc. VTC*, Chicago, IL, Jul. 1995, vol. 2, pp. 820–824.

[42] P. Robertson and S. Kaiser, "The effects of doppler spreads in OFDM(A) mobile radio systems," in *Proc. VTC*, Amsterdam, Netherlands, Fall 1999, vol. 1, pp. 329–333.

[43] T. Wang, J.G. Proakis, E. Masry, and J.R. Zeidler, "Performance degradation of ofdm systems due to doppler spreading," *IEEE Trans. Wireless Commun.*, vol. 5, no. 6, pp. 1422–1432, Jun. 2006.

[44] J.K. Cavers, "An analysis of pilot symbol assisted modulation for rayleigh fading channels," *IEEE Trans. Veh. Technol.*, vol. 40, no. 4, pp. 686–693, Nov. 1991.

[45] X. Tang, M.-S. Alouini, and A.J. Goldsmith, "Effect of channel estimation error on M-QAM BER performance in rayleigh fading," *IEEE Trans. Commun.*, vol. 47, no. 12, pp. 1856–1864, Dec. 1999.

[46] R. Negi and J. Cioffi, "Pilot tone selection for channel estimation in a mobile OFDM system," *IEEE Trans. on Consumer Electronics*, vol. 44, no. 3, pp. 1122–1128, Aug. 1998.

[47] M.-A.R. Baissas and A.M. Sayeed, "Pilot-based estimation of time-varying multipath channels for coherent cdma receivers," *IEEE Trans. Signal Processing*, vol. 50, no. 8, pp. 2037–2049, Aug. 2002.

[48] M. Dong, L. Tong, and B.M. Sadler, "Optimal insertion of pilot symbols for transmissions over time-varying flat fading channels," *IEEE Trans. Signal Processing*, vol. 52, no. 5, pp. 1403–1418, May. 2004.

[49] S. M. Kay, *Fundamentals of Statistical Processing, Volume I: Estimation Theory*, Upper Saddle River, NJ: Prentice-Hall,, 1993.

[50] S.-S. Tan, M. Rim, P.C. Cosman, and L.B. Milstein, "Adaptive modulation for OFDM-based multiple description progressive image transmission," in *Proc. GlobeCom*, New Orleans, LA, U.S.A., Nov./Dec. 2008.

[51] P. Frenger, P. Orten, T. Ottosson, and A. Svensson, "Multi-rate convolutional codes, technical report no. 21," Tech. Rep., Department of Information Theory, Chalmers University of Technology, Apr. 1998.

[52] M. Zorzi, R. R. Rao, and L. B. Milstein, "Error statistics in data transmission over fading channels," *IEEE Trans. Commun.*, vol. 46, no. 11, pp. 1468–1477, Nov. 1998.

[53] J. Lai and N.B. Mandayam, "Performance of reed-solomon codes for hybrid-arq over rayleigh fading channels under imperfect interleaving," *IEEE Trans. Commun.*, vol. 48, no. 10, pp. 1650–1659, Oct. 2000.

[54] William C. Jakes, Ed., *Microwave Mobile Communications*, IEEE Press, Piscataway, New Jersey, 08855-1331, classic reissue edition, 1995.

[55] W. Xu and L. B. Milstein, "On the performance of multicarrier RAKE systems," *IEEE Trans. Commun.*, vol. 49, no. 10, pp. 1812–1823, Oct. 2001.

[56] A. J. Goldsmith and S. B. Wicker, "Design challenges for energy-constrained ad hoc wireless networks," *IEEE Trans. on Wireless Commun.*, vol. 9, no. 4, pp. 8–27, Aug. 2002.

[57] Y. Shen, P. C. Cosman, and L. B. Milstein, "Video coding with fixed length pcketization for a tandem channel," *IEEE Trans. on Image Processing*, vol. 15, no. 2, pp. 273–288, Feb. 2006.

[58] Y. Wang and S. Lin, "Error-resilient video coding using multiple description motion compensation," *IEEE Trans. on Circuits and Syst. for Video Tech.*, vol. 12, no. 6.

[59] Y. Liu, P. Salama, Z. Li, and E. J.Delp, "An enhancement of leaky prediction layered video coding," *Circuits and Systems for Video Technology, IEEE Transactions on*, vol. 15, no. 11, pp. 1317–1331, Nov. 2005.

[60] B. Girod, "Efficiency analysis of multihypothesis motion-compensated prediction for video coding," *IEEE Trans. Image Processing*, vol. 9, pp. 173–183, Feb. 2000.

[61] M. van der Schaar and H. Radha, "Adaptive motion-compensation fine-granular-scalability (AMC-FGS) for wireless video," *IEEE Trans. on Circuits and Syst. for Video Tech.*, vol. 12, no. 6, pp. 360–371, Jun 2002.

[62] S. Han and B. Girod, "Robust and efficient scalable video coding with leaky prediction," in *Int. Conf. Image Proccessing*, 2002, pp. 2422–2427, Boston, MA.

[63] D. Fan, Y. S. Chan, X. Yu, and J. W. Modestino, "Network-adaptive transport of motion-compensated fine franularity scalability video using multiple asymmetric paths," in *Intern. Conf. on Image Proc. (ICIP)*, San Diego, CA, Oct. 2008.

[64] F. Wu, S. Li, and Y.-Q. Zhang, "A framework for efficient progressive fine granularity scalable video coding," *IEEE Trans. on Circuits and Syst. for Video Tech.*, vol. 11, no. 3, pp. 332–344, Mar 2001.

[65] W. Li, J. Ohm, M. V. Schaar, H. Jiang, and S. Li, Eds., *MPEG-4 Video Verification Model Version 18.0, ISO/ IEC/ JTC1/ SC29/ WG11/ N3908*, Jan 2001.

[66] "Editor proposed draft text modifications for joint video specification (ITU-T Rec. H.264 — ISO/IEC 14496-10 AVC), Geneva Modification draft 37, Joint Video Team (JVT) of ISO/ IEC MPEG and ITU-T VCEG, JVT-E146d37, geneva, oct. 2002.," .

[67] B. G. Haskell, A. Puri, and A. N. Netravali, Eds., *Digital Video: An Introduction to MPEG-2*, New York: Chapman and Hall, Sept. 1996.

[68] *Generic Coding of Moving Pictures and Associated Audio, Part-2 Video,*, ISO/IEC 13 818-2, 1994.

[69] R. Aravind, M. R. Civanlar, and A. R. Reibman, "Packet loss resilience of MPEG-2 scalable video coding algorithm," *IEEE Trans. on Circuits and Syst. for Video Tech.*, vol. 6.

[70] Y. S. Chan, L. Toni, P. C. Cosman, and L. B. Milstein, "Channel coding for progressive multimedia in a 2-D time-frequency block of an OFDM system," *ACSSC 2007. Forty-First Asilomar Conference on Signals, Systems and Computers, 2007*, pp. 904–908, Nov. 2007.

[71] L. Toni, Y. S. Chan, P. C. Cosman, and L. B. Milstein, "Channel coding for progressive images in a 2-D time-frequency OFDM block with channel estimation errors," *Submitted to IEEE Trans. on Image Proc.*

[72] Y. S. Chan, P. C. Cosman, and L. B. Milstein, "A cross-layer diversity technique for multicarrier OFDM multimedia networks," vol. 15, no. 4, pp. 833–847, Apr. 2006.

[73] M. van der Schaar and H. Radha, "Unequal packet loss resilience for fine-granular-scalability video," vol. 3, no. 4, pp. 381–394, Dec 2001.

[74] Y. S. Chan, P. C. Cosman, and L. B. Milstein, "A multiple description coding and delivery scheme for motion-compensated fine granulatiry scalable video," vol. 17, no. 8, pp. 1353–1367, Aug. 2008.

[75] W. Li, "Overview of fine granularity scalability in MPEG-4 video standard," *IEEE Trans. on Circuits and Syst. for Video Tech.*, vol. 11, no. 3, pp. 301–317, Mar 2001.

[76] G. H. Park and K. Kim, "Adaptive scanning method fpr fine granularity scalable video coding," *ETRI Journal*, vol. 26, no. 4, pp. 332–343, Aug. 2004.

[77] T. Wiegand, G. J. Sullivan, G. Bjøntegaard, and A. Luthra, "Overview of the H.264/AVC video coding standard," *IEEE Trans. on Circuits and Syst. for Video Tech.*, vol. 13, no. 7, pp. 560–576, Jul. 2003.

[78] H.-C. Huang, C.-N. Wang, and T. Chiang, "A robust fine granularity scalability using trellis-based predictive leak," *IEEE Trans. on Circuits and Syst. for Video Tech.*, vol. 12, no. 6, pp. 372–385, Jun 2002.

[79] B. Girod, "The efficiency of motion-compensating prediction for hybrid coding of video sequences," *IEEE J. Select. Areas Commun.*, vol. SAC-5, no. 7, pp. 1140–1154, Aug. 1987.

[80] K.-Y. Chang and R. Donaldson, "Analysis, optimization, and sensitivity study of differential PCM systems operating on noisy communication channels," *IEEE Trans. Commun.*, vol. 20, no. 3, pp. 338–350, Jun 1972.

[81] Y. Liu, Z. Li, P. Salama, and E. J. Delp, "A discussion of leaky prediction based scalable coding," July 2003, vol. 2, pp. II–565–8 vol.2.

[82] V. Vaishampayan and S. John, "Interframe balanced multiple description video compression," in *Proc. Packet Video Workshop*, New York, NY, Apr. 1999.

[83] V. K. Goyal, J. Kovaevic, R. Arean, and M. Vetterli, "Multiple description transform and selective coding images," Oct. 1998, vol. 1, pp. 674–678.

[84] V. Vaishampayan and S. John, "Balanced interframe multiple description video compression," in *Proc. ICIP*, Kobe, Japan, Apr. 1999, pp. 812–816.

[85] A. R. Reibman, L. Bottou, and A. Basso, "Scalable video coding with managed drift," *IEEE Trans. Circuits Syst. Video Technol.*, vol. 13, no. 2, pp. 131–140, Feb. 2003.

[86] A. R. Reibman, H. Jafarkhani, Y. Wang, M. T. Orchard, and R. Puri, "Multiple-description video coding using motion-compensated temporal prediction," *IEEE Trans. Circuits Syst. Video Technol.*, vol. 12, no. 3, pp. 193–204, Mar. 2002.

[87] C.-S. Kim and S.-U. Lee, "Multiple description coding of motion fields for robust video transmission," *IEEE Trans. Circuits Syst. Video Technol.*, vol. 11, no. 9, pp. 999–1010, Sep. 2001.

[88] H. Yang, R. Zhang, and K. Rose, "Optimal end-to-end distortion estimation for drift management in scalable video coding," in *Proc. Packet Video Workshop*, Pittsburgh, PA, Apr. 2002.

[89] C. Mayer, H. Crysandt, and J. R. Ohm, "Bit plane quantization for scalable video coding," in *Proc. SPIE Visual Commun. Image Processing Conf.*, San Jose, CA, U.S.A., Jan. 2002, vol. 4671, pp. 1142–1152.

[90] A. E. Mohr, R. E. Ladner, and E. A. Riskin, "Approximately optimal assignment for unequal loss protection," in *Proc. ICIP*, Sept. 2000, vol. 1, pp. 367–370.

[91] R. Puri, K.-W. Lee, K. Ramchandran, and V. Bharghavan, "An integrated source transcoding and congestion control paradigm for video streaming in the internet," vol. 3, no. 1, pp. 18–32, Mar 2001.

[92] T Stockhammer and C. Buchner, "Progressive texture video streaming for lossy packet network," in *Proc. 11th Packet Video Workshop*, Kyongju, Korea, May 2001.

[93] S. Dumitrescu, X. Wu, and Z. Wang, "Globally optimal uneven error-protected packetization of scalable code streams," *IEEE Trans. Multimedia*, vol. 6, no. 2, pp. 230–239, Apr. 2004.

[94] J. K. Cavers, "Variable-rate transmission for Rayleigh fading channels," *IEEE Trans. Commun.*, vol. COM-20, no. 1, pp. 15–22, Feb. 1972.

[95] W. T. Webb and R. Steele, "Variable rate QAM for mobile radio," *IEEE Trans. Commun.*, vol. 43, no. 7, pp. 2223–2230, July 1995.

[96] S. T. Chung and A. J. Goldsmith, "Degree of Freedom in Adaptive Modulation: A Unified View," *IEEE Trans. Commun.*, vol. 49, no. 9, pp. 1561–1571, Sept. 2001.

[97] M.-S. Alouini and A. J. Goldsmith, "Adaptive modulation over nakagami fading channels," *Wireless Personal Communications Journal*, vol. 13, no. 1-2, pp. 119–143, May 2000.

[98] J. F. Paris, M. C. Aguayo-Torrse, and J. T. Entrambasaguas, "Impact of channel estimation error on adaptive modulation performance in flat fading," *IEEE Trans. Commun.*, vol. 52, no. 5, pp. 716–720, May 2004.

[99] T. Keller and L. Hanzo, "Adaptive modulation techniques for duplex OFDM transmission," *IEEE Trans. on Veh. Technol.*, vol. 49, no. 5, pp. 1893–1906, Sept. 2000.

[100] S. Ye, Rick S. Blum, and Jr. Leonard J. Cimini, "Adaptive OFDM systems with imperfect channel state information," *IEEE Trans. on Wireless Commun.*, vol. 5, no. 11, pp. 3255–3265, Nov. 2006.

[101] S. Zhou and G. B. Giannakis, "How accurate channel prediction needs to be for transmit-beamforming with adaptive modulation over rayleigh MIMO channels?," *IEEE Trans. on Wireless Commun.*, vol. 3, no. 4, pp. 1285–1294, July 2004.

[102] W. M. Gifford, M. Z. Win, and M. Chiani, "Diversity with practical channel estimation," *IEEE Trans. on Wireless Commun.*, vol. 4, no. 4, pp. 1935–1947, July 2005.

[103] A. Conti, M. Z. Win, M. Chiani, and J. H. Winters, "Bit error outage for diversity reception in shadowing environment," *IEEE Commun. Lett.*, vol. 7, no. 1, pp. 15–17, Jan 2003.

[104] A. Conti, M. Z Win., and M. Chiani, "On the inverse symbol-error probability for diversity reception," *IEEE Trans. Commun.*

[105] M. Chiani, A. Conti, and C. Fontana, "Improved performance in td-cdma mobile radio system by optimizing energy partition in channel estimation," *IEEE Trans. on Wireless Commun.*, vol. 51, no. 35, pp. 352–355, Mar. 2003.

[106] W. M. Gifford, M. Z. Win, and M. Chiani, "Antenna subset diversity with non-ideal channel estimation," *IEEE Trans. on Wireless Commun.*, vol. 7, no. 5, pp. 1527–1539, May 2008.

[107] A. Conti, M. Z. Win, and M. Chiani, "Invertible bounds for M-QAM in rayleigh fading," *IEEE Trans. on Wireless Commun.*, vol. 4, no. 5, pp. 1994–2000, 2005.

[108] M. Munster, T. Keller, and L. Hanzo, "Co-channel interference suppression assisted adaptive OFDM in interference limited environments," in *VTC-Fall*, Sept. 1999, pp. 284–288, Amsterdam.

[109] S. Catreux, P. F. Driessen, and L. J. Greenstein, "Attainable throughput of an interference-limited MIMO cellular system," *IEEE Trans. Commun.*, vol. 49, no. 8, pp. 1307–1311, Aug 2001.

[110] L. Toni and A. Conti, "Slow adaptive modulation with diversity in the presence of interference and imperfect thresholds," *Submitted to SPAWC'09.*

[111] L. Toni, A. Conti, and et al., "Slow adaptive modulation with diversity in the presence of interference," *Submitted to IEEE Transaction.*

[112] K. Cho and D. Yoon, "On the general BER expression of one- and two-dimensional amplitude modulations," *IEEE Trans. Commun.*, vol. 50, no. 7, pp. 1074–1080, July 2002.

[113] J. Lu, K. B. Letaief, J. C-I Chuang, and M. L. Liou, "M-PSK and M-QAM BER computation using signal-space concepts," *IEEE Trans. Commun.*, vol. 47, no. 2, pp. 181–184, Feb. 1999.

[114] A. Zanella, M. Chiani, and M. Z. Win, "MMSE reception and successive interference cancellation for MIMO systems with high spectral efficiency," *IEEE Trans. on Wireless Commun.*, vol. 4, no. 3, pp. 1244–1253, May 2005.

[115] A. Giorgetti and M. Chiani, "Influence of fading on the gaussian approximation for BPSK and QPSK with asynchronous cochannel interference," *IEEE Trans. on Wireless Commun.*, vol. 4, no. 2, pp. 384–389, March 2005.

[116] A. T. James, "Distributions of matrix variates and latent roots derived from normal samples," *Ann. Math. Statist.*, vol. 35, pp. 475–501, 1964.

[117] M. Aronowich and R. J. Adler, "Extrema and level crossings of χ^2 processes," *Adv. Appl. Probab.*, vol. 18, no. 4, pp. 901–920, Dec 1986.

[118] A. Papoulis, *Probability, Random Variables and Stochastic Processes*, New York: McGraw Hill, 3rd edition, 1991.

Acknowledgments

The research presented in this thesis would not have been possible without the support and the help of the following people that I would like to warmly thank:

my advisor Prof. Oreste Andrisano and my co-advisor Prof. Andrea Conti, WiLab, University of Bologna, that guided me during my PhD research;

Prof. Larry Milstein and Prof. Pamela Cosman, that gave me the opportunity to spend a training period in their lab at the University of California, San Diego;

all the members of the WiLab, Barbara, Raffaele, Gianni, Flavio, Matteo, Bandy, Virginia, Paolo and all the other FPGA guys, that improve the quality of my research and most importantly of my life during these years;

Yee Sin Chan, who patiently introduced me to the secrets of multimedia coding;

my friends from Bologna, Marco, Giulia, Luca, and Cica, and all the friends I met in San Diego, Anna, Ilenia, Ottaviano, Savaz, Elio, Michele, Massimo, Paolo, Federico, Sheu-Sheu, Ken, Clari, and Claudio. Thank you for the great time we had hanging out together.

Finally, I would like to thank my family that encouraged me all the time. Thanks to mamma, Cesco, papà, and Francesca. A special thank to Giovanni, who has to put up with me all the time.